Progress in Retinal and Eye Research xxx (xxxx) xxx–xxx

Contents lists available at ScienceDirect

Progress in Retinal and Eye Research

journal homepage: www.elsevier.com/locate/preteyeres

Anterior segment optical coherence tomography

Marcus Ang[a,b,c], Mani Baskaran[a,b], René M. Werkmeister[d,e], Jacqueline Chua[a,b], Doreen Schmidl[f], Valentin Aranha dos Santos[d,e], Gerhard Garhöfer[f], Jodhbir S. Mehta[a,b], Leopold Schmetterer[a,b,d,e,f,g,*]

[a] Singapore Eye Research Institute, Singapore National Eye Centre, Singapore
[b] Ophthalmology and Visual Sciences Academic Clinical Program, Duke-NUS Medical School, Singapore
[c] Moorfields Eye Hospital, London, United Kingdom
[d] Center for Medical Physics and Biomedical Engineering, Medical University of Vienna, Austria
[e] Christian Doppler Laboratory for Ocular and Dermal Effects of Thiomers, Medical University of Vienna, Austria
[f] Department of Clinical Pharmacology, Medical University of Vienna, Austria
[g] Department of Ophthalmology, Lee Kong Chian School of Medicine, Nanyang Technological University, Singapore

ARTICLE INFO

Keywords:
Optical coherence tomography
Cornea
Glaucoma
Anterior segment
Angiography

ABSTRACT

Optical coherence tomography (OCT) provides non-contact, rapid *in vivo* imaging of ocular structures, and has become a key part of evaluating the anterior segment of the eye. Over the years, improvements to technology have increased the speed of capture and resolution of images, leading to the increasing impact of anterior segment OCT imaging on clinical practice. In this review, we summarize the historical development of anterior segment OCT, and provide an update on the research and clinical applications of imaging the ocular surface, cornea, anterior chamber structures, aqueous outflow system, and most recently anterior segment vessels. We also describe advancements in anterior segment OCT technology that have improved understanding with greater detail, such as tear film in dry eye disease evaluation, intra-operative real-time imaging for anterior segment surgery, and aqueous outflow with angle assessment for glaucoma. Improvements to image processing and software have also improved the ease and utility of interpreting anterior segment OCT images in everyday clinical practice. Future developments include refinement of assessing vascular networks for the anterior segment, *in vivo* ultra-high resolution anterior segment optical coherence tomography with histology-like detail, en-face image with 3-dimensional reconstruction as well as functional extensions of the technique.

1. Introduction

Optical coherence tomography (OCT) is a modality that uses low-coherence interferometry to enable non-contact, *in vivo* imaging of ocular structures (Huang et al., 1991). Since its introduction, OCT imaging has become a key part of clinical evaluation of the cornea, and the anterior eye segment. As improvements to the technology have increased, e.g. the speed and resolution of the images captured, the impact of anterior segment OCT (AS OCT) imaging on clinical practice, has been rapidly increasing. Furthermore, OCT image-processing software has now allowed for combination of multiple scans, 3-dimensional reconstruction and accurate measurements. This allows for pre-operative diagnosis where direct visualization may be difficult, intra-operative real-time imaging that may affect surgical decisions, as well as postoperative evaluation of disease progression and surgery outcomes. The aim of this review is to summarize the historical and technological development of AS OCT, and the above-mentioned clinical applications of OCT imaging of the ocular surface, cornea, anterior chamber structures, aqueous outflow system, and anterior segment vascular supply. We also introduce novel developments in AS OCT, which may have potential clinical applications in the future.

The OCT generates 2- or 3-dimensional tomographic images by measuring the echo time delay of light backscattered from tissue structures. For this purpose light from a low-coherence light source is split into two paths with a beam splitter directing it into the two arms of an interferometer (Fig. 1). In the reference arm, a mirror reflects the light, while in the sample arm the light is back scattered by the tissue. Optical components in the sample arm define the illumination properties such as shape, depth of focus, and intensity distribution of the beam. In a tissue different structures have different refractive index. Hence, light is backscattered at interfaces between layers of different refractive index. The light returning from the reference and sample arm

* Corresponding author. The Academia, Level 6, 20 College Road, Discovery Tower, 169856, Singapore.
E-mail addresses: leopold.schmetterer@seri.com.sg, leopold.schmetterer@meduniwien.ac.at (L. Schmetterer).

https://doi.org/10.1016/j.preteyeres.2018.04.002
Received 28 September 2017; Received in revised form 20 February 2018; Accepted 4 April 2018

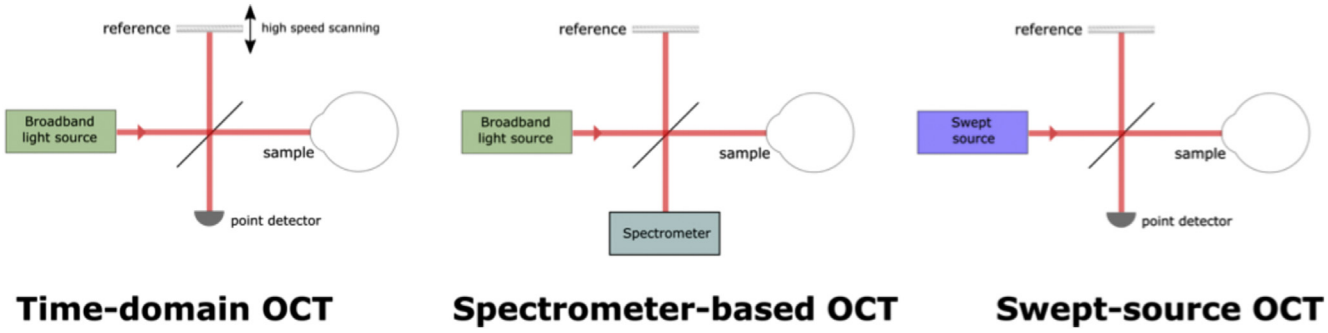

Fig. 1. Figure depicting various set-ups of the time-domain, spectrometer-based and swept-source anterior segment optical coherence tomography.

are recombined at the beam splitter and guided towards the detector. Interferences occur only when the pathway between the two beams is within the coherence length of the light source. For obtaining depth resolution either time-domain (TD) or Fourier-domain (FD) solution have been provided (Fig. 1). In TD OCT a scanning reference delay is used while translating the mirror in the reference arm. The light is collected with a point detector and depth resolution is achieved when the reference mirror is moved at constant velocity. At different positions of the reference mirror different structures within the sample lead to interferences. A complete travel of the reference mirror is called A-scan in analogy to ultrasound technology. Whereas in TD OCT light echoes are detected sequentially FD OCT collects modulations in the source spectrum with all spectral components captured simultaneously. In spectrometer-based FD OCT systems the light is spectrally analyzed by using a spectrometer and a CCD line camera. As such the mirror in the reference arm is static and an A-Scan is obtained with one camera shot leading to higher acquisition rates. Acquisition speed of spectrometer-based systems is therefore limited by the read-out rate of the line sensor. The wave number-dependent signal is transformed into the axial scan information by using an inverse Fourier transform. Another FD OCT technology is based on Swept-Source (SS) technology i.e. with this light source the wavelength is rapidly swept within the laser allowing for the use of a point detector and high acquisition rates up to several MHz.

2. Optical coherence tomography of the anterior segment - history and technical aspects

Soon after the introduction of OCT the technique was applied to the anterior segment of the eye (Izatt et al., 1994). Using a TD system, the authors were able to provide images of the anterior chamber, the chamber angle, and the lens. In comparison with retinal OCT, further refinement of the technique was progressing relatively slow. Whereas early studies were done with custom-built systems, commercial OCT systems designed for retinal imaging were adapted for anterior segment imaging. As such approaches to image the anterior segment of the eye were already done with the Zeiss Stratus OCT (Carl Zeiss Meditec, Dublin, CA, USA) in the early 2000s (Feng et al., 2001; Kalev-Landoy et al., 2007; Leung et al., 2005; Nozaki et al., 2002). In 2001, the measurement of central corneal thickness using a commercially available TD OCT system was reported for the very first time (Bechmann et al., 2001). In the same year, Radhakrishnan and co-workers presented a fourier-domain (FD) OCT system specifically designed for anterior segment imaging, using a frame rate of 8 Hz at 500 A-scans operating at a wavelength of 1310 nm (Radhakrishnan et al., 2001). The system used telecentric scan geometry, allowing scan widths of up to 15 mm and scan depths up to 6 mm thereby enabling for wide-field imaging. Due to an improved speed, real-time imaging of physiological pupillary constriction in response to a light stimulus was made possible. In contrast to retinal imaging, light sources in wavelengths around 1300 nm can be used for anterior segment imaging, because absorption of this wavelength by water is less of a problem. The longer wavelength has the advantage of deeper penetration into the tissue because of lower scattering loss. Moreover, higher light powers can be used in this wavelength range because most of the light is absorbed by the vitreous and does not reach the retina. The first commercial OCT systems specifically designed for anterior segment imaging were the Zeiss Visante OCT™ (Carl Zeiss Meditec, Dublin, CA, USA) and the Slit-Lamp OCT (SL-OCT, Heidelberg Engineering GmbH, Heidelberg, Germany), which were United States Food and Drug Administration (FDA)-approved in 2005 and 2006 respectively. Both systems utilized TD OCT technology and provided axial resolutions between 18 and 25 µm. Since lasers at a central wavelength of 1310 nm are used, the penetration depth is relatively high, which has the advantage of imaging deeper structures such as scleral spur. However, a major drawback of the TD OCT relates to the low A-scan rate (2000 A-scans/second with the Visante OCT system, and 200 A-scans/second with the SL-OCT) and the lower sensitivity when compared to FD OCT (Leitgeb et al., 2003). The Visante OCT system was stand-alone whereas the SL-OCT had to be coupled to a commercial Haag Streit Slit-Lamp.

Soon after the introduction of these systems, FD OCT scanners designed for posterior pole imaging were brought to the market, offering additional lens systems for imaging of the anterior segment. Even though the FD OCT systems offer higher speed than the TD OCT systems ($>$ 25000 A-scans/s), the field of view was considerably smaller. For the RTVue FD OCT (Optovue, Fremont, CA, USA), the cornea anterior module (CAM) was available in two magnifications. Specifically, the CAM-S scans an area of 2 × 2 mm, whereas the CAM-L allows for scanning of 6 × 2 mm, but with lower resolution. The Cirrus HD-OCT (Carl Zeiss Meditec, Dublin, CA, USA) has a built-in anterior segment-imaging module, which uses a 60-diopter lens that allows the scanning of a 3 mm × 1 mm area. Both systems use super luminescent diodes at a wavelength of 840 nm and therefore the penetration depth is markedly lower when compared to the TD systems introduced earlier. Recently, Cirrus HD-OCT version 8 utilised a 15.5 × 5.8 mm angle-to-angle scan, and achieved a scan depth of 5.8 mm in high resolution by overlapping the source and mirror images. Spectralis (Heidelberg Engineering GmbH, Heidelberg, Germany) also utilises an anterior segment module for high definition angle-to-angle scans but to achieve this it sacrifices the part of the corneal image. In the recent years other spectrometer-based OCT system such as Envisu (Bioptigen Inc., Research Triangle Park, NC, USA) and the Copernicus HR (Optopol Technologies SA, Zawiercie, Poland) allowing for anterior segment imaging have also been brought to the market.

In 2008, the first swept-source (SS) FD OCT was brought to the market. The Casia SS OCT (Tomey, Nagoya, Japan) uses a 1310 nm swept-source laser as light source and was specifically designed to scan the anterior segment. The scanning area is as high as 16 × 16 mm with a depth of 6 mm. At an A-scan rate of 30000 per second, this allows for three-dimensional representation of the entire anterior segment of the eye based on 128 radial scans. Casia SS OCT version 2 allows imaging the entire lens as well with automated quantitative analysis of the angle

Table 1
Summary of commercially available anterior segment optical coherence tomography.

OCT Type	Manufacturer	Optical Source	Axial resolution[a] (optical)	Transverse resolution[a]	Scan Speed (A- Scans per second)	Scan Depth	Maximum Scan Width
Visante OCT	Carl Zeiss Meditec, Dublin, CA	SLD 1310 nm	18 μm	60 μm	2000	6 mm	16 mm
Slit Lamp OCT	Heidelberg Engineering, Heidelberg, Germany	SLD 1310 nm	< 25 μm	20-100 μm	200	7 mm	15 mm
Cirrus OCT	Carl Zeiss Meditec, Dublin, CA	SLD 840 nm	5 μm	15 μm	27,000	2 mm	6 mm
Spectralis OCT	Heidelberg Engineering, Heidelberg, Germany	SLD 820 nm	7 μm (optical)	20 μm	40,000	2 mm	6 mm
Optovue iVue	Optovue, Inc, Fremont, CA	SLD 840 nm	5 μm	15 μm	26,000	2–2.3 mm	13 mm
Nidek RS 3000	Nidek, Gamagori, Japan	SLD 880 nm	7 μm	15 μm	53,000	2 mm	8 mm
Revo NX	Optopol, Zawiercie, Poland	SLD 830 nm	5 μm	18 μm	110,000	2.4 mm	16 mm
CASIA SS-1000 OCT	Tomey Corporation, Nagoya, Japan	SS laser 1310 nm	10 μm	30 μm	30,000	6 mm	16 mm
Triton OCT	Topcon Corporation, Tokyo, Japan	SS laser 1310 nm	8 μm	30 μm	100,000	6 mm	12 mm

OCT- Optical Coherence Tomography; SLD – Superluminescent Diode; SS – Swept source.
[a] Specific for posterior segment, which may vary for anterior segment scans.

and other parameters. Imaging of the anterior segment is also made possible with the Triton SS OCT (Topcon, Tokyo, Japan), which is designed for posterior segment imaging. As such, an external add-on lens needs to be attached to the existing system. The Triton SS OCT system offers a high A-scan rate of 100 kHz but a scan depth of only 3 mm. We have summarized the technical specifications of various commercially available OCT systems for the anterior segment in Table 1.

The following key characteristics need to be considered when employing an OCT system to image the structures of the anterior segment. As mentioned above, there are broadly two principle approaches for the OCT i.e. the TD and FD systems. The FD systems can be further divided into systems that use a spectrometer-based detection and SS OCT systems. The first OCT system was based on TD technology, but this approach has lost importance because of lower scanning speed, related to the need of mechanically moving a mirror in the sample arm and lower sensitivity (Leitgeb et al., 2003). Low scanning speed makes the imaging sensitive to motion and limits the number of B-scans that can be acquired within a reasonable measurement time. Low sensitivity reduces signal-to-noise ratio and as such does not allow for visualization of structures with low contrast. Spectrometer-based FD OCT does not require any moving parts, but rather a more sophisticated detection unit including a spectrometer with a diffraction grating, a collimator and a high-speed line camera. Using state of the art charge-coupled-device (CCD) cameras or complementary metal–oxide–semiconductor (CMOS) cameras, maximum A-scan rates in the order of 100 kHz can be obtained, although systems operating at more than 300 kHz have been realized (Potsaid et al., 2008). Swept-source OCT uses a light source with a narrow bandwidth that is swept in frequency. As compared to superluminescent diodes used in TD OCT and spectrometer-based FD OCT, these light sources are nowadays considerably more expensive. The detection unit is, however, cheaper requiring only a single-point photodetector. A major advantage of the technology is that ultrafast systems can be developed, which nowadays can reach 2 million A-scans per second and more (Huo et al., 2015; Kolb et al., 2015; Zhi et al., 2015). Moreover, SS OCT provides greater depth range with significantly reduced sensitivity roll-off and is less sensitive to motion artifacts due to higher speed (Gora et al., 2009).

Another important feature of OCT relates to the resolution of the system. Unlike in conventional microscopy, the axial (Δz) and the transversal resolution (Δx,y) in OCT are independent. The axial resolution is determined by the coherence length (l_c), which is a function of the bandwidth (Δλ) and the central wavelength (λ) of the light source:

$$\Delta z = \frac{2 \ln 2}{\pi} \frac{\lambda^2}{\Delta\lambda}$$

Fig. 2 depicts the axial resolution as a function of the bandwidth for three different wavelengths used for anterior segment OCT imaging (840 nm, 1060 nm and 1310 nm). To date, the best axial resolution that can be achieved in prototype systems is in the order of 1 μm (Ishida and Nishizawa, 2012; Lim et al., 2005; Moon and Kim, 2006; Nishizawa et al., 2004). The transversal resolution is dependent on the numerical aperture of the OCT system:

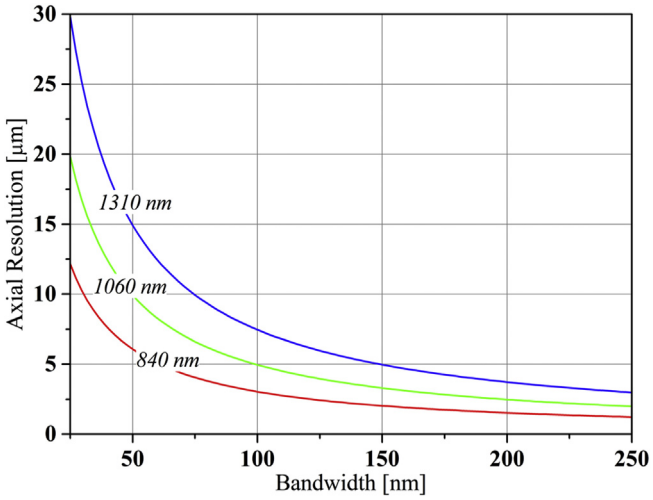

Fig. 2. Axial resolution vs. bandwidth for the typical optical coherence tomography light source center wavelengths of 840, 1060, and 1310 nm.

$$\Delta x = \frac{4\lambda}{\pi} \frac{f}{d}$$

In equation (2), f is the focal length of the objective lens and d is the diameter of laser beam at the lens. As such, systems with shorter wavelength provide better transversal resolution, considering the rest of the optical setup to be identical. In addition, there are two potential ways to improve Δx,y, either by increasing the diameter of the beam or by reducing the focal length of the objective lens. When increasing the numerical aperture, one does, however, limit the depth of field similarly to conventional microscopy. Hence, OCT imaging with low Δx,y is more suitable for en face imaging than for 3-dimensional imaging of tissues.

In retinal imaging, the transversal resolution is determined by the imperfections of the optical media and spot sizes below 15–20 μm cannot be reached using conventional optics. As such, OCT systems designed for the posterior pole usually have low numerical aperture, which importantly does not influence axial resolution. In order to improve Δx,y, it is a requirement to combine OCT with adaptive optics

(AO), thereby correcting for these errors (Jonnal et al., 2016; Polans et al., 2017). In anterior segment imaging, the transverse resolution can be directly influenced by the numerical aperture. During scanning, eye movements can limit Δx,y. Little work has been focused on optimization of Δx,y for en face imaging of corneal layers or for visualization of aqueous outflow structures. When Δz gets very low, such as in spectrometer-based FD OCT systems, the depth of field may be dependent on the number of pixels on the camera. For a detailed description on the principles of OCT imaging, the reader can be referred to a recent textbook (Drexler and Fujimoto, 2015).

3. Optical coherence tomography for the cornea

The cornea is part of the refractive system of the eye and contributes approximately two thirds of the optical power of the human eye. Since the cornea is transparent it does not contain any blood vessels and oxygenation is entirely provided via diffusion. The cornea is richly innervated and the unmyelinated nerve endings are sensitive to mechanical stress, temperature and chemicals. In humans, the healthy cornea has a thickness of 500–800 μm and a radius of 11–12 mm. The border between the cornea and the adjacent sclera is called corneal limbus. The human cornea has five layers: epithelium, Bowman's layer, corneal stroma, Descemet's membrane, and endothelium. The corneal epithelium is covered by the pre-corneal tear film, which ensures nutrition of the anterior surface of the cornea. The epithelium is a multicellular tissue layer that continues with the conjunctival epithelium. Bowman's layer consists of heparan sulfate proteoglycans organized mainly of collagen fibrils thereby protecting the stroma. The stroma is the thickest layer of the cornea consisting of collagen fibres and interconnected keratocytes. Descemet's membrane is the acellular basement membrane of the corneal endothelium mainly containing type IV collagen. The corneal endothelium is a monolayer that regulates fluid transport from the aqueous humour. Unlike the corneal epithelium the corneal endothelium does not regenerate.

Already soon after the introduction of AS OCT, the clinical potential of the technique in evaluating the cornea had been realized (Akiba et al., 2007; Christopoulos et al., 2007; Gotzinger et al., 2004; Hirano et al., 2001; Kaluzny et al., 2006; Reddy et al., 2007). As already mentioned in the prior section, recent technological developments in OCT have greatly increased imaging capabilities in terms of resolution. Specific to the cornea, this now allows us to image corneal layers and structures in greater detail i.e. epithelium, Bowman's layer, stroma, Descemet membrane and endothelium (Moutsouris et al., 2011). Nonetheless, in the cornea there is still a role for TD OCT such as the Visante OCT (Carl Zeiss Meditec, Dublin, CA, USA), which uses a longer wavelength of light that reduces scattering and allows deeper penetration through corneal opacities or sclera. Moreover, the TD OCT has a wider field of imaging compared to a smaller field by the FD OCT albeit with higher resolution and detail – Fig. 3. In combination with specific image processing improved contrast in corneal OCT images can be observed (Girard et al., 2015).

3.1. Diagnosis of corneal pathologies

There are now a wide variety of clinical applications of AS OCT for the diagnosis of corneal pathologies from the superficial to deeper layers of the cornea – Fig. 4. For example, on the ocular surface, OCT imaging distinguishes pterygium from pseudo-pterygium, as the subepithelial hyperreflective layer is not really attached to the underlying Bowman's layer or corneal stroma in the latter (Nanji et al., 2015). AS OCT has become an important tool in the clinical evaluation of pterygium and histopathological correlates of anomalous hyperreflectivity of the OCT pattern have been reported(Gasser et al., 2017; Lluch et al., 2016). In ocular surface neoplasia, OCT reveals hyperreflective, thickened epithelium with abrupt transitions from normal to abnormal epithelium (Nanji et al., 2015) and can assist diagnosis and management guidance (Nanji et al., 2015; Ong et al., 2016; Sayed-Ahmed et al., 2017; Shousha et al., 2011).

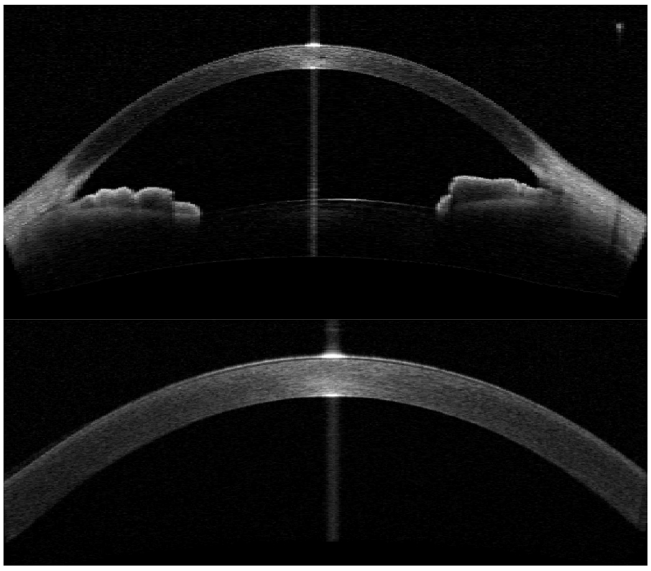

Fig. 3. Example of anterior segment optical coherence tomography (OCT) scan of a normal cornea with a wider field anterior segment scan (top) and high-resolution cornea scan (bottom) using the Visante OCT.

The AS OCT is also extremely useful in studying anterior segment pathology through an edematous cornea such as in Descemet membrane detachments. In the corneal stroma itself, corneal infiltrates secondary to infectious keratitis, may be measured and monitored, as the area of infiltration or thinning may not be easy to evaluate using the slit-lamp microscopy alone (Konstantopoulos et al., 2008). Furthermore, the AS OCT is useful for assessment of the area of corneal thinning and actual corneal thickness in cases of impending perforation. Another useful clinical application is in patients with keratoconus, OCT features such as increased epithelial thickness; anterior hyperreflection at the Bowman's layer and stromal thinning at the cone may be associated with increased risk of corneal hydrops(Fuentes et al., 2015; Li et al., 2012c, 2016c; Ortiz et al., 2012; Pahuja et al., 2017; Sandali et al., 2013; Su et al., 2015). As compared to Placido-Scheimpflug imaging AS OCT offers the advantage of improved reproducibility for central corneal thickness and keratometry parameters(Chan et al., 2017). A longitudinal study also showed that the technique is capable of monitoring keratoconus progression (Fujimoto et al., 2016). Recently, keratometry and wavefront aberration of the anterior corneal surface and epithelium-Bowman's layer interface were presented yielding higher values in patients with keratoconus than in healthy controls(Matalia et al., 2017). Further studies are required to fully understand the potential of this technique in the early diagnosis of keratoconus. Corneal dystrophies are classified according to the IC3D classification and AS OCT has become an important tool for differential diagnosis in addition to slit lamp examination and genetic testing (Siebelmann et al., 2017). Several studies have looked into the depth, size, and position of the structural changes with different dystrophies.

3.2. Role of optical coherence tomography in cornea surgeries

The role of AS OCT is also important in pre-operative, intra-operative and post-operative assessment of patients requiring corneal surgeries(Szalai et al., 2017). As corneal diseases are the second most common cause of non-refractive vision loss (Whitcher et al., 2001), corneal transplantation still remains the main method for restoring vision(Tan et al., 2012). Recent developments in surgical techniques have enabled surgeons to perform selective replacement of the diseased layer of the cornea – which may lead to improved corneal graft survival

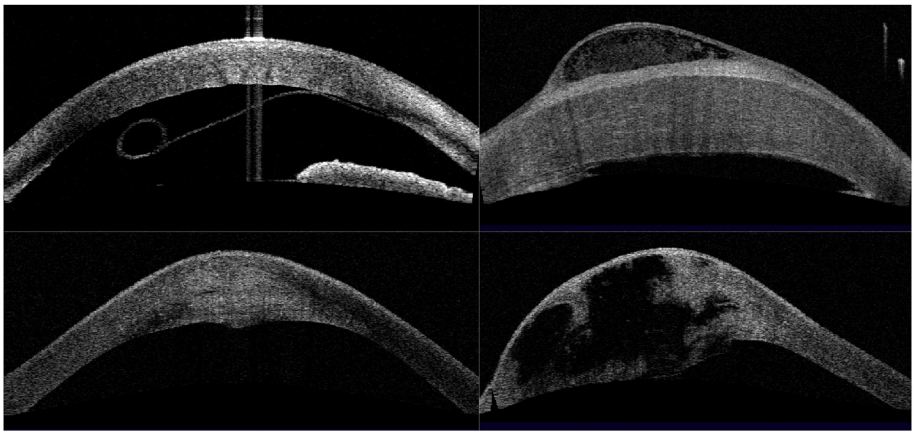

Fig. 4. Example of clinical applications of optical coherence tomography (OCT) for the cornea using the Visante OCT. Diagnosis of Descemet membrane detachment in the presence of corneal edema (top left). Intra-epithelial collection of fluid in bullous keratopathy with secondary bacterial infection (top right). Intra-stromal lesion in infective keratitis (bottom left). Hydrops in keratoconus demonstrating a break in the Descemet membrane (bottom right).

and surgical outcomes(Fuest et al., 2017). In particular, selective replacement of the endothelial layer (Ang et al., 2012b), or the stromal layer, may confer advantages such as tectonic stability or a rapid visual recovery (Ang et al., 2012c), compared to replacing the entire cornea during transplantation(Bose et al., 2013). Thus, the role of imaging to delineate corneal layers is becoming increasingly important. AS OCT may also play a role in clinical decisions for surgical techniques to remove corneal debris and scar tissues in eyes with corneal dystrophy (Kim et al., 2010; Lim et al., 2008). Postoperatively, AS OCT is able to detect early graft detachment after Descemet membrane endothelial keratoplasty, with a potential predictive value for long-term graft adherence(Yeh et al., 2013). Furthermore, in other corneal transplantation techniques such as keratoprosthesis with limited postoperative visualization, AS OCT is useful to detect complications such as interface gape and angle closure(Zarei-Ghanavati et al., 2015).

There is also an important role of AS OCT in other corneal surgeries such as refractive surgery often requiring accurate preoperative measurements to reduce risk of corneal ectasia, and postoperative assessment of complications such as interface fluid syndrome or inflammation (Li et al., 2007). High-resolution AS OCT is now useful to aid more accurate measurements of flap thickness, assess flap interface, and minor flap displacements(Rosas Salaroli et al., 2009). Newer refractive surgeries such as refractive lenticule extraction (Ang et al., 2014), may also benefit from AS OCT imaging and assessment of outcomes(Tay et al., 2012). After femtosecond-assisted laser refractive surgery and photorefractive keratectomy it is capable of characterizing the forward protrusion of the posterior cornea (Chan et al., 2015b), and the change in corneal power(McNabb et al., 2015). As compared to Scheimpflug imaging AS OCT provides higher reliability in terms of corneal thickness and keratometry measurements of the cornea after laser in situ keratomileusis(Chan et al., 2015a). Measuring the curvatures of the stromal layers may provide insight into the remodelling of the epithelium and stroma after photorefractive keratectomy(Chandapura et al., 2018). Using signal processing techniques, volume rendering and maximum intensity projections it was recently possible to provide 3-dimensional images of corneal nerves(Shin et al., 2017). This may have potential in minimizing nerve injury during surgical procedures.

AS OCT has also an important role in refractive outcomes of cataract surgery, such as pre-operative corneal evaluation in corneas with high astigmatism and post-operative position of toric intraocular lenses (Hoffmann et al., 2014; Lucisano et al., 2017). Using whole eye scanning a correlation between crystalline lens tilt and intraocular lens tilt was reported indicating that preoperative tilt is predictive for intraocular lens tilt after surgery(Hirnschall et al., 2017). Likewise, it has been shown that toric and non-toric implantable collamer lens implantation leads to a reduction in the iridocorneal angle(Garcia-De la Rosa et al., 2017). AS OCT imaging can also monitor changes in corneal epithelial and stromal thickness after procedures such as collagen cross-linking used for the stabilization in patients with keratoconus – and may have a role in evaluating the demarcation line which correlates to the effective depth of the treatment(Bata et al., 2016; Rocha et al., 2014).

3.3. Intra-operative applications of optical coherence tomography for the cornea

The advent of lamellar corneal transplantation techniques has increased the role for intra-operative AS OCT as more precision is required to achieve selective replacement of corneal layers(Ehlers et al., 2014a). However, even in penetrating keratoplasty, intraoperative OCT aids in visualisation of anterior segment abnormalities through a hazy cornea, and proper graft-donor apposition during suturing(Ehlers et al., 2015). For anterior lamellar surgery, preserving an intact Descemet membrane with the least amount of residual stroma is the key to successful deep anterior lamellar keratoplasty, which can be achieved manually or with a big-bubble(Scorcia et al., 2013). Intraoperative OCT may improve the success of achieving a big bubble by helping to assess the cornea stroma thickness and the depth of needle insertion(Au et al., 2015). In cases with irregular corneal scarring and thinning, the AS OCT can help decide the initial trephination depth to avoid a perforation (Steven et al., 2014), and to achieve a good manual dissection during deep anterior lamellar keratoplasty(De Benito-Llopis et al., 2014). However, current surgical instruments for lamellar dissection are metal that cast an optical shadow affecting the visualization of the underlying cornea or structures during intraoperative OCT. Thus, instruments need to be removed from the surgical field from time to time during layer-by-layer dissection(Au et al., 2015).

Intraoperative OCT imaging is now routinely used in all femtosecond cataract surgery systems in order to estimate the anatomical landmarks of the cataract, anterior to posterior capsular boundaries, and to determine the placement of corneal incisions(Grewal et al., 2016). Although intraoperative OCT helps visualization of the corneal wounds, depth of phacoemulsification during surgery and status of the posterior capsule, more studies are required to establish that this reduces complications associated with cataract surgery(Nguyen and Chopra, 2013). Real-time intra-operative AS OCT systems have also been shown to be useful during Descemet stripping automated endothelial keratoplasty (DSAEK) to detect the presence of interface fluid and assess the effect of the procedure and air tamponade on graft thickness – Fig. 5(Sng et al., 2012a). Thus, intraoperative OCT used during DSAEK could help with surgical decisions to reduce surgical duration and complications such as donor dislocations(Titiyal et al., 2016). The main advantage of intraoperative OCT in DSAEK is especially in complex anterior segment cases with cornea edema and poor visibility, where anterior chamber anatomy is disrupted and graft insertion and manipulation may be challenging without visualisation.

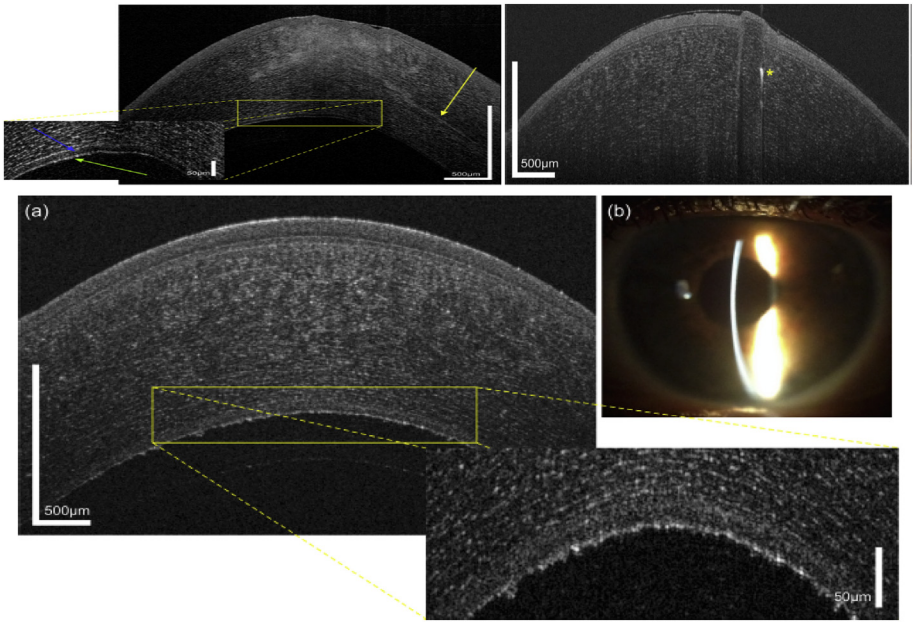

Fig. 5. Imaging of corneal pathology with a custom built optical coherence tomography system with an axial resolution of approximately 1.3 mm in air. Left upper panel: Cross-sectional image in a patient with acanthamoeba keratitis reveals radial keratoneuritis with a thickened corneal nerve (yellow arrow) and a hyporeflective space (blue arrow) above the double banded structure of the epithelium. Right upper panel: Intrastromal foreign body in a 43 year old male patient who wore glasses during an accident. lower panel: Fuchs' endothelial dystrophy in a 60 year old female patient, (a) optical coherence tomography image, (b) corresponding slit lamp photograph(with permission from Werkmeister et al., 2017b).

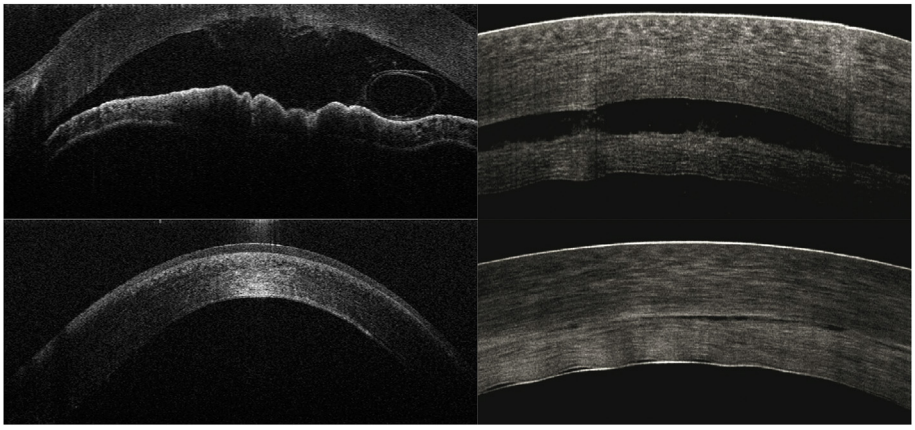

Fig. 6. Example of intraoperative optical coherence tomography (OCT) during Descemet membrane endothelial keratoplasty (DMEK) showing a graft single scroll configuration (top left) and successful graft adhesion after air bubble injection (bottom left). Intraoperative OCT during Descemet stripping automated endothelial keratoplasty (DSAEK) shows interface fluid between the donor and recipient (top right) with eventual graft adhesion and reduction of interface fluid after air tamponade (bottom right).

Another useful application of intraoperative OCT is in Descemet membrane endothelial keratoplasty (DMEK) as its increasingly being performed (Ang et al., 2016e), because it has been described to aid in determining graft orientation – Fig. 5(Ang et al., 2015b; Steven et al., 2013). However, limitations with scan speed and axial resolution currently affect the quality of image capture and field of view, which may improve with further development of intraoperative OCT technology (see Fig. 6).

3.4. Recent advances in optical coherence tomography for the cornea

Existing commercial AS OCT systems obtain cross-sections of the cornea with 5–20 μm axial resolution, at a variety of widths (6–16 mm) and depths (2–6 mm) (Ang et al., 2012a). High-resolution AS OCT uses a light source with a broad bandwidth of more than 100 μm and a spectrometer, to improve the axial resolution to 1–4 μm, with scan width of 5–12 mm(Bizheva et al., 2011, 2016, 2017a; Hutchings et al., 2010; Karimi et al., 2011; Lawman et al., 2016; Wang et al., 2011; Werkmeister et al., 2017b; Wu et al., 2014). Examples of *in vivo* corneal imaging using OCT systems with an axial resolution close to 1 μm are presented in Fig. 5. The role of high-resolution AS OCT for assessing the ocular surface and tear film will be discussed in greater detail in section 6 of this review article. Recently, a conical scan pattern was proposed for imaging of the cornea resulting in improved image quality in the peripheral cornea(Beer et al., 2017). This overcomes a common problem with conventional AS-OCT systems using telecentric illumination where the angle of incidence strongly deviates from 90° resulting in low image intensity. In contrast to retinal OCT 1–2 μm spatial resolution can be obtained; a technique termed micro-OCT (μOCT) that has been introduced in an attempt to achieve cellular level imaging (2 μm × 2 μm x 1 μm resolution in tissue) *in vitro*. This may enable imaging of corneal cells or even delineation of micro-vascular structures, which had previously only been possible with laser scanning *in vivo* confocal microscopy or histopathology(Ang et al., 2016c). However, the disadvantages of high resolution μOCT for the cornea include the trade-off between lateral resolution and depth of focus, limited axial imaging range, imaging speed and the high sensitivity to movement(Liu et al., 2011a). As such it is doubtful whether μOCT is a feasible approach to *in vivo* imaging of the cornea. The potential clinical applications of *in vivo* imaging of the corneal endothelial cells are, however, wide include monitoring corneal endothelial cell count and morphology to guide surgery, or improving corneal endothelial cell imaging to compare endothelial keratoplasty techniques(Liu et al., 2014).

Newer combined AS OCT and Scheimpflug camera devices offer real-time, cross-sectional imaging of the anterior and posterior cornea, as well as corneal topography and tomography measurements(Mi et al., 2015). They have gained popularity due to their rapid, non-contact nature and superior accuracy over other modalities such as slit-

scanning topography. Their precise topographic measurements and high-resolution images have allowed assessment of pre-operative evaluation of post-operative complications, outcomes and management of surgeries such as DSAEK. Furthermore, en face OCT imaging now allows for rapid, non-contact visualization of ocular surface or corneal lesions not obvious on B scan or cross-sectional scans – a larger field of view albeit with less detail compared to *in vivo* confocal microscopy. Automated analysis programs are also emerging for AS OCT images to provide rapid quantification of corneal parameters with high repeatability(Ang et al., 2013). Corneal parameters such as central corneal thickness, anterior and posterior corneal curvature as well as novel parameters such as posterior corneal arc length are automatically derived after identifying the scleral spur. These corneal parameters are then used for surgical planning such as sizing of corneal donor graft size.

4. Optical coherence tomography of the aqueous outflow system

The aqueous outflow system is an important component in the maintenance of intraocular pressure (IOP). Aqueous humor is produced from plasma within the capillaries of the ciliary processes by three distinct mechanisms: diffusion, ultrafiltration and secretion. Aqueous humor then flows through the pupil from the posterior chamber into the anterior chamber. From the anterior chamber, aqueous then drains via the trabecular and the uveoscleral pathway. Under physiological conditions, the trabecular pathway accounts for approximately 90% of the outflow. As part of this route, aqueous humor flows through the trabecular meshwork (TM) towards Schlemm's canal (SC). The trabecular meshwork is a porous structure consisting of laminar beams with a core of elastic and collagenous fibers (Tamm, 2009). Drainage through the TM is passive, virtually acting as a filter. The SC is an endothelium-lined circular vessel that shares many similarities with lymphatic vessels. From the SC, 25 to 35 collector channels anastomose with the aqueous veins, where the aqueous humor is drained. The major site of resistance to flow is not fully known but may include juxtacanalicular tissue region and the inner wall of SC.

In the uveoscleral outflow pathway, aqueous passes through the ciliary body, into the suprachoroidal space and is finally drained by the venous circulation. The IOP is dependent on the dynamic balance between production and outflow of aqueous humor and an increase in outflow resistance will lead to an increase in IOP. In glaucoma, increased IOP is a consequence of elevated outflow resistance associated with changes in the outflow pathway, such as trabeculae thickening, excessive deposit of plaque material within the cribriform layer, and abundance of long spacing collagen (Schmidl et al., 2015a; Stamer and Acott, 2012). In this section, we will focus on the visualization of outflow structures using OCT except of the chamber angle, which is covered in a separate section within this review.

The first OCT image of SC and the TM was presented by Sarunic and co-workers in 2008 using a SS OCT system operating at 1310 nm and proving an axial resolution of approximately 9 mm - Fig. 7. The axial resolution of this system was, however, not good enough to visualize details of this structure or to quantify SC dimensions. The idea of imaging SC by means of OCT was followed up by Kagemann and co-workers from the Pittsburgh group in the following years. The authors used an FD OCT optics engine comprising a superluminescent diode with a centre wavelength of 870 nm and a bandwidth of 200 nm, resulting in a theoretical axial resolution of 1.3 mm in tissue. The authors were able to visualize SC, collector channels and scleral veins (Kagemann et al., 2010) – Fig. 8. Due to its high resolution, the authors were subsequently able to quantify the cross-sectional area of SC and reported values of 10,983 mm^2 and 8308 mm^2 on the nasal and temporal side, respectively. The authors also reported reduced cross-sectional area of SC in patients with glaucoma, but this conclusion was based on measurements in two patients only. In a later publication, it was shown that acute IOP elevation using ophthalmodynamometry

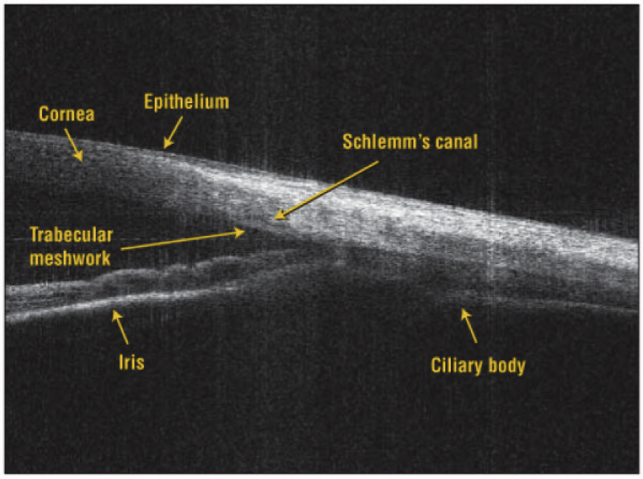

Fig. 7. The first anterior segment optical coherence tomography showing the trabecular meshwork and Schlemm's canal (with permission from Sarunic et al., 2008).

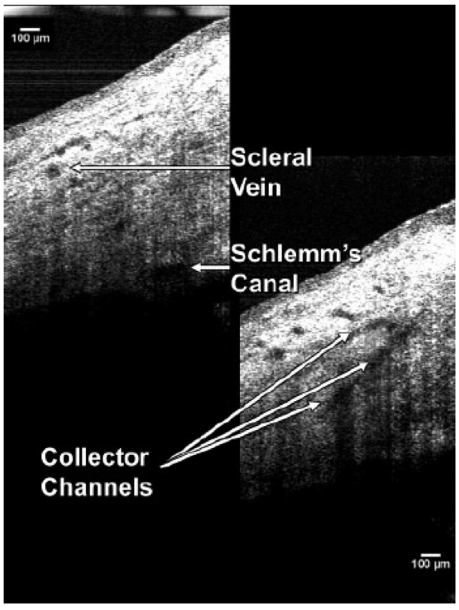

Fig. 8. Imaging of the scleral vein, Schlemm's canal and collector channels using a custom-built optical coherence tomography system with a theoretical axial resolution of 1.3 mm in tissue. (with permission from Kagemann et al., 2010).

significantly decreased SC cross-sectional area in healthy subjects (Kagemann et al., 2014). Using the prototype system as well as a commercially available FD OCT system, the same group later provided 3D virtual castings of SC and more distal outflow structures – Fig. 9 (Fig. 3, Kagemann et al., 2012).

Comparison of OCT images with histology in human cadaver eyes shows that the structure identified in these images is indeed SC (Francis et al., 2012; Usui et al., 2011). Cross-sectional area of SC was measured by several investigators and reported results show considerable differences between studies. Using a custom-built SS OCT with a 1310 nm light source, values of 7766 mm^2 and 8010 mm^2 were reported for the nasal and temporal side, respectively (Shi et al., 2012). Later the same group reported significantly reduced cross-sectional area of SC (3942 mm^2) in patients with primary open angle glaucoma (Wang et al., 2012a). Significantly smaller cross-sectional area of SC was reported in healthy subjects (nasal: 2854 mm^2, temporal: 2862 mm^2) when using the commercial RTVue OCT (Optovue, Inc., Fremont, CA) in

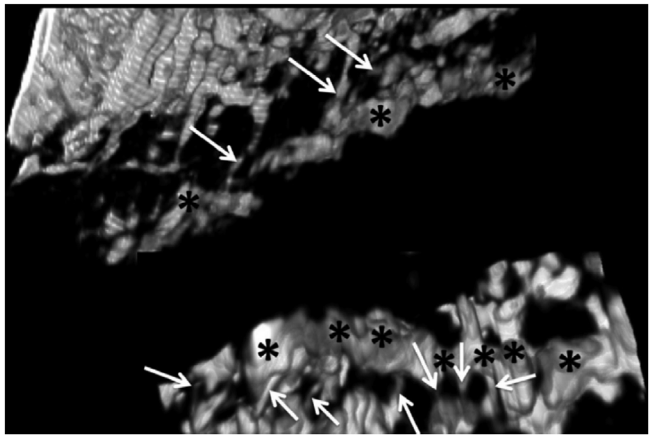

Fig. 9. Imaging of Schlemm's canal produced from volumetric anterior segment scans of the limbus imaged with a commercial Cirrus optical coherence tomography system. Schlemm's canal is marked with asterisks, and locations of connecting collector channels at ostia are marked with arrows. (with permission from Kagemann et al., 2012).

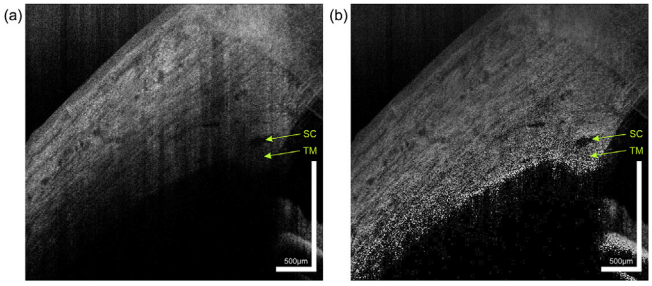

Fig. 10. OCT tomograms of sclero-corneal limbus acquired by ultra-high resolution OCT before (a) and after (b) applying the Corneal Adaptive Compensation (CAC) algorithm. After applying of CAC, the visibility of trabecular meshwork and Schlemm's canal was improved with noticeable visual contrast between Schlemm's canal lumen and its wall. TM: Trabecular meshwork. SC: Schlemm's canal.

combination with the cornea-lens adapter (Chen et al., 2013). Other studies using the same device did, however, report approximately 4 fold larger SC areas with 13,991 mm^2 in healthy subjects and 11,332 mm^2 in patients with newly diagnosed primary open angle glaucoma (Hong et al., 2013). Reduced SC area was also observed in pseudoexfoliation (PEX) glaucoma (4000 mm^2) as compared to healthy subjects (5000 mm^2) again using the same commercial OCT system (Imamoglu et al., 2016). The study did, however, not observe a correlation between IOP and cross-sectional area. In another study of 11 healthy eyes, a wide range of SC cross-sectional area was observed ranging from 1664 to 6007 μm^2 (average 3514 ± 1235 μm^2) showing considerable regional variability. The number of collector channels also varied considerably among subjects, ranging from 5 to 11 with wider SC diameters in areas of higher collector channel density (Li et al., 2017). Using an ultrahigh resolution OCT system, we have recently observed a SC cross-sectional area of 3620 ± 589 μm^2 nasally and 4075 ± 335 μm^2 temporally (Werkmeister, 2016). Visibility of SC was significantly improved when a corneal adaptive compensation (CAC) algorithm was employed – Fig. 10 (Girard et al., 2015, Fig. 4). Using a commercial spectrometer-based FD OCT, SC could be identified in approximately 85% of healthy subgroup of subjects participating in a population-based study (Day et al., 2013). The results of this study did not show an association between the diameter of SC and IOP. It was, however, observed that nasal, but not temporal TM cross-sectional area is negatively correlated to the level of IOP. Other studies did find a significant negative association between SC area and the IOP (Hong et al., 2013).

Recent work was directed towards three-dimensional reconstruction of circumferential aqueous humor outflow using automated detection of SC and first-order collector channels (Huang et al., 2017) based on a commercial FD OCT system. A circumferential scanning pattern around the limbus was used and outflow pathways were re-constructed showing variable diameter of SC at different positions as well as roots of collector channels. Visualization of the conventional outflow system was also achieved in the living mouse. After administration of a Rho-kinase inhibitor, a widening of the TM and significant increases in cross-sectional area of SC were observed (Li et al., 2016a). An en face OCT technology was used to visualize the vasculature of the scleral venous plexus (Uji et al., 2016). The authors were able to visualize post-trabecular aqueous outflow pathway in a single B-scan from SC to the episcleral venous plexus. The observed vessels were running posteriorly and formed anastomoses that drained into the episcleral plexus. A recent innovation is based on OCT imaging via a catheter probe in which the illuminating light is guided by a single mode catheter fibre (Xin et al., 2017). Using a Gradient Index (GRIN) lens to shape the OCT beam, the authors were able to obtain a beam diameter in the order of 20 mm. Human porcine and cadaver eyes were used to evaluate the system using *in vitro* experiments (Fig. 11).

Employing phase-sensitive detection, it is possible to detect TM movement ex vivo and *in vivo*. In isolated monkey eyes mounted in an anterior segment holder different IOP level were set using a perfusion system. During the experiments, IOP was changed at a frequency of 1 Hz with amplitude of 3 mmHg mimicking the ocular pressure pulse. Via phase sensitive detection the authors were able to visualize and quantify the movement of the TM. This movement of TM was most pronounced in the region close to SC endothelium (Li et al., 2012b). The technique was also used to study the dynamic behaviour of SC and the collector channels in human cadaver eyes in response to pressure changes (Xin et al., 2016). When pressure was increased, the widening of SC and the collector channels occurred within 50 ms and the biomechanical properties of the TM could be determined. The technique has considerable potential to identify patients who are at risk to unstable IOP values in the future, but further studies are required to optimize this approach for clinical use (Johnstone, 2004).

Visualizing aqueous outflow pathway may have implications in guiding glaucoma surgery and evaluating treatment success. Patients with glaucoma undergoing canaloplasty showed an increase in SC width and height that was negatively correlated to the change in IOP (Fuest et al., 2016). Likewise, another study showed dilation of SC area that correlated with the IOP decrease as well as a reduction of TM thickness after phacocanaloplasty in patients with primary open angle glaucoma (Paulaviciute-Baikstiene et al., 2016). This is well compatible with other studies showing an increase in SC area that correlated with IOP reduction after trabeculectomy (Hong et al., 2014) and trabeculoplasty (Skaat et al., 2017). In patients undergoing trabeculotomy, opening size did not correlate with IOP reduction, but may be related to anterior chamber depth (Wecker et al., 2017). Dilation of SC was even observed after phacoemulsification surgery and correlated to the decrease in IOP (Zhao et al., 2016). A pronounced increase in SC area was seen after implantation of a Stegman expander (Fig. 12). An increase in mean lumen area from 4,900 μm^2 at a distance 1.5 mm distal to the implant to approx. 3,5100 μm^2 in the region widened by the expander was measured using an ultrahigh resolution OCT system (Werkmeister et al., 2017a).

Dilatation of SC was also seen after pharmacological reduction of IOP. After instillation of 0.004% travoprost, a pronounced increase in SC cross-sectional area of approximately 90% on both the nasal and the temporal side was reported (Chen et al., 2013). Dilation of SC was also observed after topical instillation of pilocarpine hydrochloride (Skaat et al., 2016; Werkmeister, 2016), a nonselective muscarinic receptor agonist that reduces IOP by ciliary muscle contraction and expansion of the juxtacanalicular portion of the TM (Li et al., 2014a). Even though the technique has potential to study the outflow system *in vivo*, it has

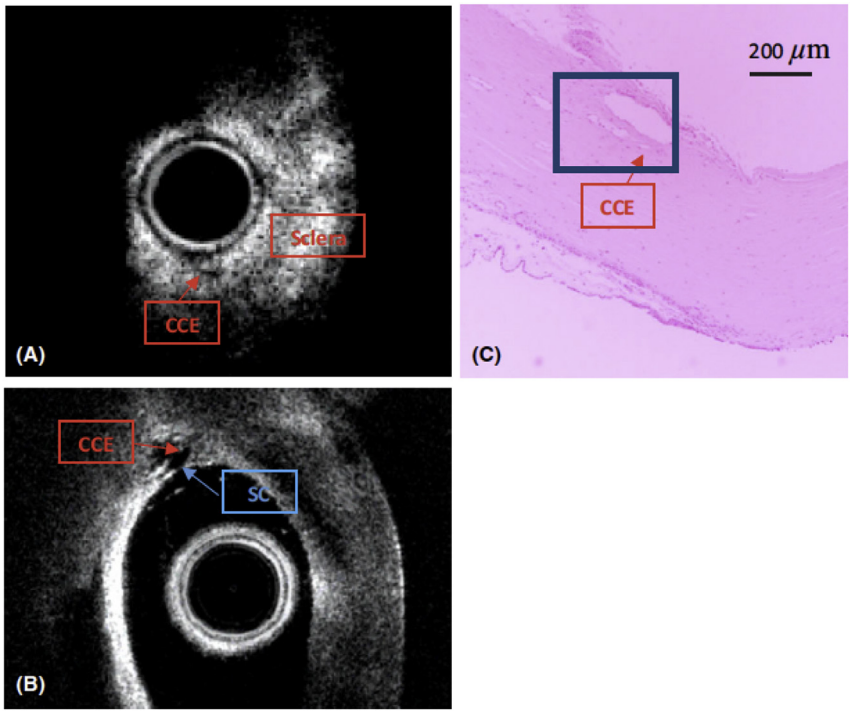

Fig. 11. An optical coherence tomography catheter probe is capable of imaging the aqueous outflow system of a post-mortem human eye. (A) is an optical coherence tomography image of the aqueous outflow system following the placement of the catheter probe in the lumen of Schlemm's canal (SC). The collector channel entrance (CCE) can be identified. (B) is the OCT image of the aqueous outflow system following intracameral placement of the catheter probe. Both SC and CCE can be identified. (C) gives a light microscopy image of the aqueous outflow system. The area marked with thick square shows the approximate region scanned by the optical coherence tomography as shown in A and B (with permission from Xin et al., 2016).

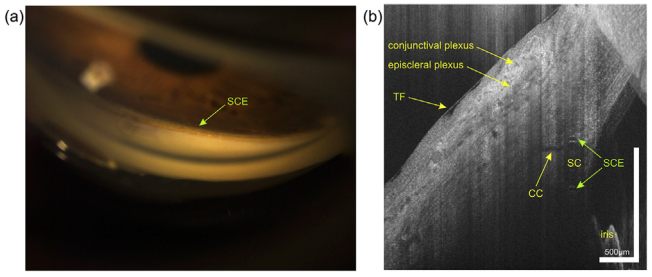

Fig. 12. *In vivo* imaging of Schlemm's canal in a glaucoma patient 9 month after Stegmann Canal Expander implantation (a) Post-surgical gonioscopic view and (b) Ultra-high resolution optical coherence tomography tomogram of sclero-corneal limbus showing the properly positioned Stegmann Canal Expander inside SC 9 month after implantation month after implantation. SC, Schlemm's canal; CC, collector channel; SCE, Stegmann canal expander; TF, tear film.

not yet found its way into clinical praxis. The most obvious application may be related to the optimization of treatment planning in glaucoma surgery. In principle, OCT-guided placement of devices in micro-invasive glaucoma surgery (MIGS) may result in an improvement in the IOP control. However, a randomized clinical trial will be required to prove this hypothesis. Another plausible application may be the testing of pharmacological actions of anti-glaucoma agents. During drug screening, the technique may provide valuable information on the mechanism of action. The technique does, however require further technical refinement for it to be translated into clinical setting. Some important key questions remain unanswered. What is the resolution required to obtain meaningful information on the pathway of the aqueous outflow system? Given the small diameter of collector channels, it appears that an ultrahigh resolution system is required to obtain a full 3-dimensional reconstruction of the outflow system. Furthermore, it remains to be investigated which area of the aqueous humour outflow system needs to be covered. Given the significant local variability, it seems unlikely that a single cross-sectional area measurement of SC will be sufficient.

5. Optical coherence tomography for the anterior chamber and angle

Imaging of the ocular anterior chamber is gaining increasing importance for the diagnosis, management and follow-up of angle closure disease(Leung et al., 2008). The main pathological area in this form of glaucoma is the TM, which is the site for drainage of aqueous humor of the eye. Qualitative and quantitative assessment of anterior chamber angle (ACA), anterior chamber, iris and lens are accomplished with AS OCT. Angle closure with AS OCT is determined by any contact between the iris and the angle wall anterior to the scleral spur whereas for gonioscopy, the quadrant would still be considered open unless the apposition reached the posterior trabecular meshwork. The identification of the scleral spur is an important landmark to be assessed, although the Schwalbe's line (SL) has been proposed as another possible landmark since it has better identification in FD OCT devices(Cheung et al., 2011). Common parameters used to describe features of the ACA include the angle opening distance (AOD), the angle recess area (ARA) and the trabecular-iris space area (TISA) (Fig. 14). These parameters can be measured at varying intervals anterior to the scleral spur, most frequently at 500 or 750 μm anterior to the scleral spur (i.e., AOD500, AOD750)(Console et al., 2008; Smith et al., 2013). The SL-angle opening distance (SL-AOD) was defined as the distance from the SL (termination of the Descemet membrane) to the anterior iris surface perpendicular to the corneal endothelial surface. The SL-trabecular iris space area (SL-TISA) was defined as an area bounded anteriorly by the SL-AOD, posteriorly by a line drawn along the trabecular meshwork at 500 μm from the SL perpendicular to the plane of the inner scleral wall to the opposing iris; superiorly by the inner corneoscleral wall; and inferiorly by the iris surface (Cheung et al., 2011). Very few studies have compared the quantitative results of UBM and AS OCT. Dada et al. analysed 63 eyes using the two methods and concluded that they correlated well and AS OCT scans provided sharper images of the scleral spur. However, there was a tendency towards smaller measurements of angle and slightly higher measurements of the ACD/CCT in AS OCT compared to UBM(Dada et al., 2007).

The ability to capture the entire anterior chamber in a single image using AS OCT allows better assessment of the structures relative to each

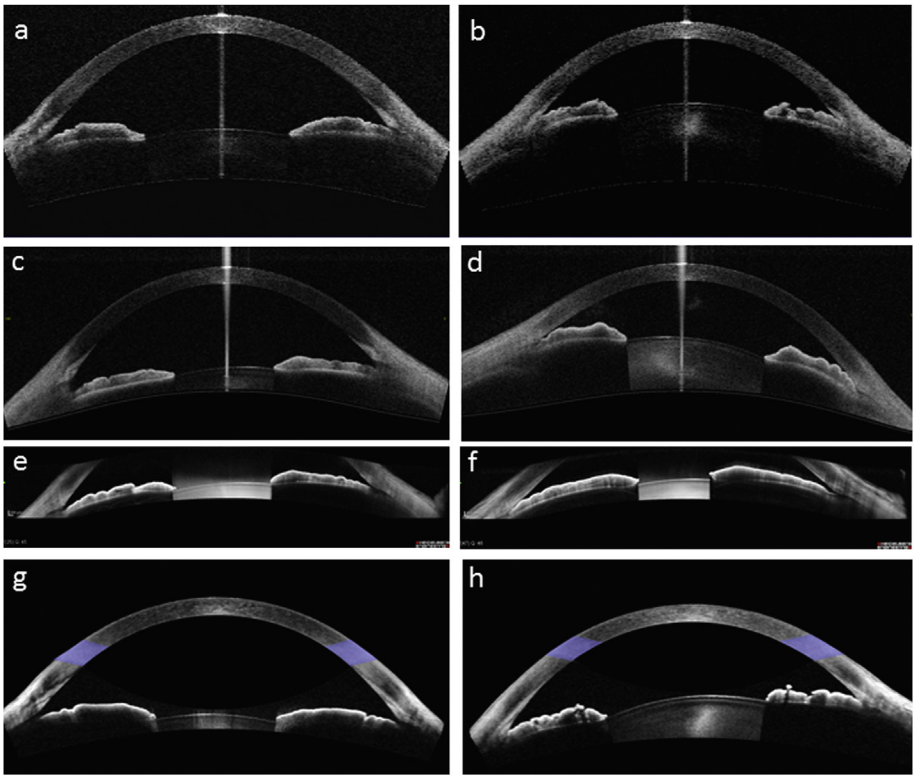

Fig. 13. Open and closed angles imaged using Visante optical coherence tomography (OCT) (a, b), Casia swept-source OCT (c,d), Spectralis spectral-domain OCT (e,f) and Cirrus HD-OCT (g,h) angle-to-angle OCT scans respectively.

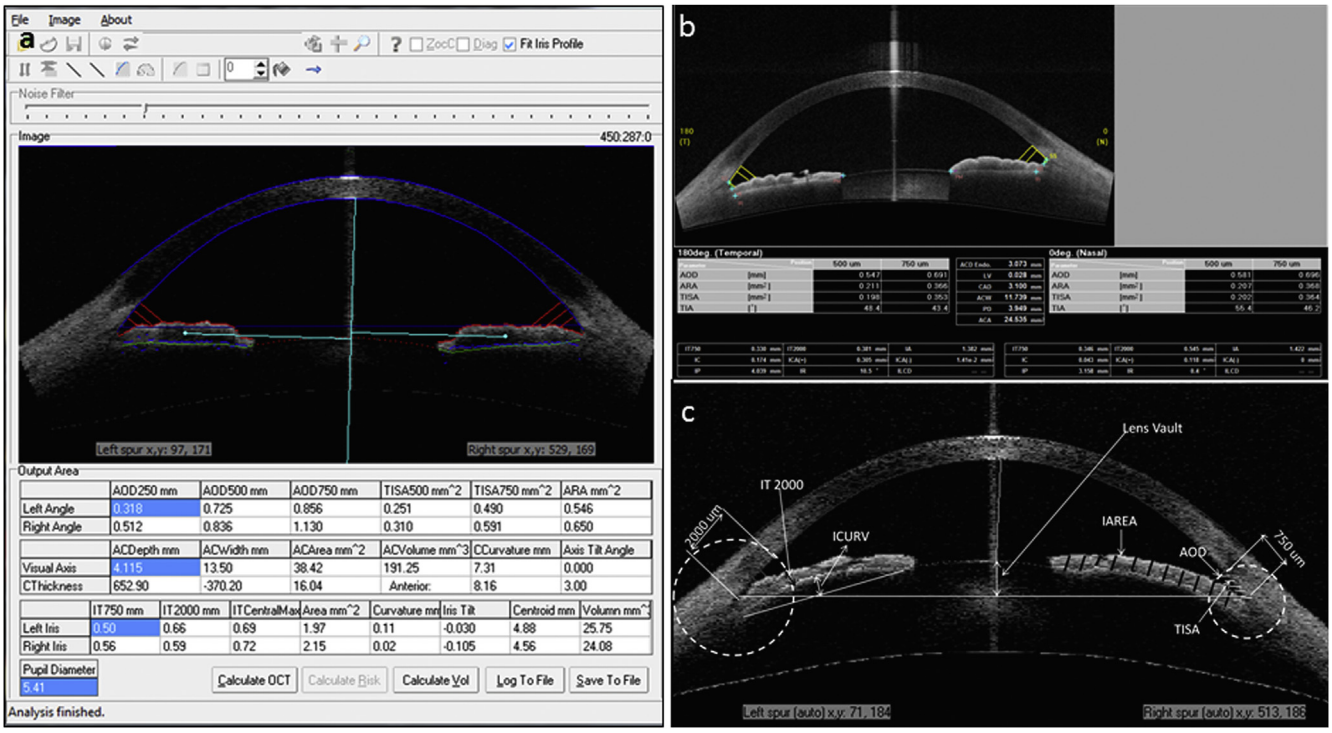

Fig. 14. Quantitative analysis with anterior segment optical coherence tomography (OCT) systems. a: Zhongshan Angle closure Assessment Program for Visante OCT, b: 360° angle analysis software for Casia swept-source OCT volume scan, c: Schematic representation of important parameters measured in customised software for Visante OCT: Angle Opening Distance (AOD, measures the perpendicular length between iris anterior surface and trabecular meshwork at a fixed distance), Trabecular Iris Surface Area (TISA, represents the area enclosed by points on scleral spur, iris and trabecular meshwork at a fixed distance), Lens Vault (LV, represents that portion of the lens in anterior chamber beyond the line of scleral spur) and Iris parameters include Iris curvature (ICURV), Iris thickness (IT 2000 at 2000 μm) and Iris Area (IA).

other (Fig. 13). Customized analysis software like the Zhongshan Angle Assessment Program (ZAAP, Guangzhou, China) (Console et al., 2008) or inbuilt applications (Fig. 14) are used to objectively measure the various anterior segment structures. This program requires manual input for scleral spur and 27% cases suffer from lack of proper landmark (Console et al., 2008; Sakata et al., 2008). Leung et al. devised ACADEMIA program for quantitative analysis of chamber structures; however, this may have some limitations in deep angle recess(Leung et al., 2006). Initial studies by Nolan et al. reported that qualitative AS OCT could determine 98% (of 152/342 eyes) of gonioscopic angle closure eyes, but suggested a higher number of angle closures among gonioscopically open angles (44.6% of 228/342 eyes)(Nolan et al., 2007). A community based screening study suggested an AUC of 0.76, with a low specificity of 62.9%(Lavanya et al., 2008). AOD750 was noted to be the best performer in quantitative analysis in a subgroup of subjects (AUC 0.90 for nasal quadrant and 0.91 for temporal quadrants) (Narayanaswamy et al., 2010). A scoring system based on a combination of six anterior chamber parameters such as anterior chamber volume (ACV), anterior chamber width (ACW), iris thickness (IT), iris area (IA), anterior chamber area (ACA) and lens vault (LV) performed better with an AUC of 0.94(Nongpiur et al., 2013b). In a four-year follow up study, Baskaran and co-workers determined that those angle closure eyes on AS OCT at baseline trended to develop more gonioscopic angle closures at four years(Baskaran et al., 2015). Current commercially available FD OCT devices are inconsistent in determining the scleral spur and have poor visibility of angle recess in many subjects. However, the high definition provided by these devices provided some insights into the location of Schlemms's canal (SC) and its relationship to other anterior segment structures (Fig. 15). While AS OCT could identify all anterior chamber structures, due to absorption by pigments, iris and ciliary body were not visible, in comparison to Ultrasound biomicroscopy (UBM). Iris trabecular index (which provides the circumferential extent of angle closure in percentage) in 360° angle scans was found to have moderate diagnostic performance(Baskaran et al., 2013). Xu et al. established that increased number of scans analysed provided better variability in the anterior segment parameters(Xu et al., 2016). Newer software modifications provide angle-to-angle scans in Cirrus HDOCT, with similar diagnostic performance in angle closure detection(Tun et al., 2017).

Automated algorithms have been developed to provide diagnosis and mechanistic classifications for angle closure using AS OCT images from Visante OCT, Casia SS OCT and Cirrus HD-OCT angle-to-angle scans(Fu et al., 2017; Niwas et al., 2016; Xu et al., 2013). While most of them provide good diagnostic performance against clinician grading of the images, nobody compared them with gonioscopic reference standard. However, it is to be noted that gonioscopy is controversial as a reference standard in determining angle closure due to visible light conditions affecting pupil constriction, while it will remain an undisputed clinical tool for complete evaluation of the angle(Friedman and He, 2008). Apart from diagnostics, several novel anatomical risk parameters have been identified using AS OCT for angle closure such as iris thickness/area, anterior chamber width, lens vault and anterior chamber area/volume(Nongpiur et al., 2010, 2011; Wang et al., 2010a). Dynamic factors associated with angle narrowing under various conditions have been studied(Leung et al., 2007). Iris volume (IV) increase per millimetre of pupil dilation in darkness, was found to be an independent predictor of angle narrowing, more so in fellow eyes of APAC(Aptel and Denis, 2010). Zhang et al. compared the change in IA after physiologic and pharmacologic mydriasis among the spectrum of angle closure disease sub-categorized as pupillary block, plateau iris and thick peripheral iris roll. The study observed that the change in IA was significantly different among groups(Zhang et al., 2015b). It has been proposed that differences in iris connective tissue and permeability of the iris stroma to aqueous may account for the differences in volume change in eyes with closed angles and open angles(Quigley et al., 2009).

Higher lens vault represents the portion of lens in anterior chamber that determines angle crowding better than any other parameter at least in the Chinese ethnicity(Nongpiur et al., 2011). Several other parameters have also been proposed to represent the lens contribution such as anterior lens vault, relative lens vault and others. Subgrouping of the AS OCT images of angle closure identified two to four clusters,

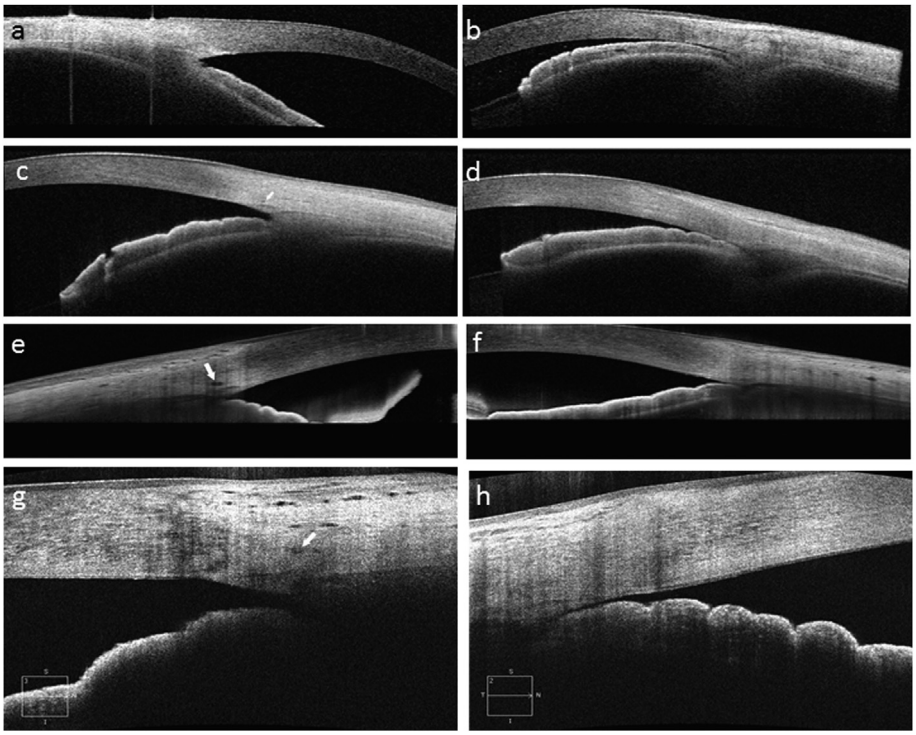

Fig. 15. Open and closed angles imaged with high resolution using Visante optical coherence tomography (OCT) (a, b), Casia swept-source OCT (c,d), Spectralis spectral-domain OCT (e,f) and Cirrus HD-OCT (g,h) angle-to-angle angle scans respectively. Arrow marks refer to Schlemm's canal.

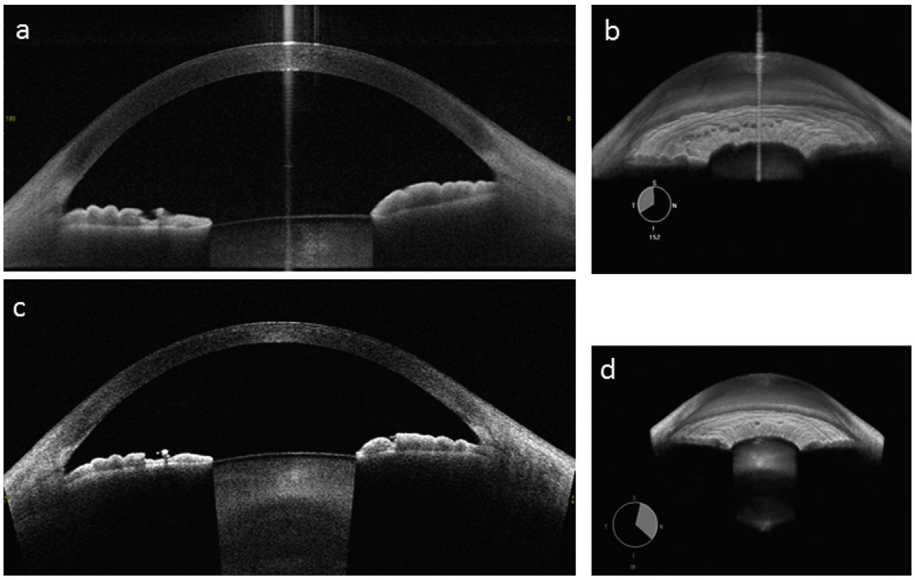

Fig. 16. Casia swept-source optical coherence tomography (SS OCT) versions. a and b: Cross-sectional and 3-dimensional reconstruction images of CASIA 1 SS OCT version showing partial image of central lens, c and d: Cross-sectional and 3-dimensional reconstruction images of CASIA 2 SS OCT version showing full image of central lens.

suggesting that iris, lens or both components may predominate in the mechanism of angle closure(Baek et al., 2013; Niwas et al., 2016; Nongpiur et al., 2013a). Newer version of SS OCT (CASIA 2, Tomey, Japan) can present deeper structures including the entire central lens, enabling lens thickness/volume measurements (Fig. 16).

Few studies have attempted to determine peripheral anterior synechiae patterns in SS OCT; however, none could provide the diagnostic equivalence of indentation gonioscopy(Lai et al., 2013; Tun et al., 2015). Similarly, plateau iris configuration and choroidal effusion are some of the features that cannot be determined directly using AS OCT. Lin and colleagues showed that patients with plateau iris features on gonioscopy/UBM reveal a significant difference in iris thickness compared to pupillary block subjects(Li et al., 2014b). Based on an earlier defined UBM criteria, plateau iris was defined across three pre-defined AS OCT patterns in 210 subjects by Verma et al. The authors could not differentiate plateau iris based on any of the AS OCT patterns, however, an increased peripheral iris thickness in ASOCT was associated with plateau iris likelihood(Verma et al., 2017). Ethnic differences in anterior segment parameters have been reported among Chinese and Caucasians explaining the differences in angle closure prevalence(Lee et al., 2012). Apart from this, AS OCT is used clinically in special situations to visualize angle status when routine slit lamp and gonioscopy cannot establish the angle status (Fig. 17).

Structural changes after procedures such as laser peripheral iridotomy (Jiang et al., 2014; Lee et al., 2013), argon laser iridoplasty (Sng et al., 2014, 2016), goniosynechiolysis and phacoemulsification (Tun et al., 2015) have been reported. Studies have shown a deeper angle recess with increased angle width and flattened iris profile in the short term in PACS but with lesser changes in APAC eyes, especially with greater lens vault. ACA shortened several months post LPI as reported in a couple of studies (Fig. 18). (Jiang et al., 2014; Lee et al., 2013) Lesser successful outcome after LPI was determined by a baseline narrower angle width, thicker iris and greater lens vault(Ang and Wells, 2011). AS OCT can provide diagnostic, mechanistic and prognostic aid in angle closure eyes. However, lack of easier interpretation, cost and agreement issues with gonioscopy preclude its widespread use by clinicians. The research insights provided by AS OCT have added much to the existing literature on angle closure glaucoma. Further work on automated diagnostic applications, higher resolution AS OCT, *in vivo* dynamic imaging and longitudinal studies might throw more light into angle closure diagnostics, aqueous humour dynamics, trabecular biomechanics and residual angle closure mechanisms.

Determination of the feasibility of Intraoperative Spectral domain microscope Combined/integrated OCT Visualisation during Enface Retinal and Ophthalmic surgery (DISCOVER) study, represents the results of intraoperative OCT (iOCT, e.g. Carl Zeiss Meditec RESCAN 700, Cole Eye Institute/Haag-Streit iOCT prototype) systems. The instant feedback regarding the interaction of instrument to tissues in anterior and posterior segment surgeries can be very useful in establishing guidelines and providing inputs to innovative surgical approaches. Currently such systems are used in evaluating vitro-macular traction, epiretinal membrane surgery and deep anterior lamellar keratoplasty.

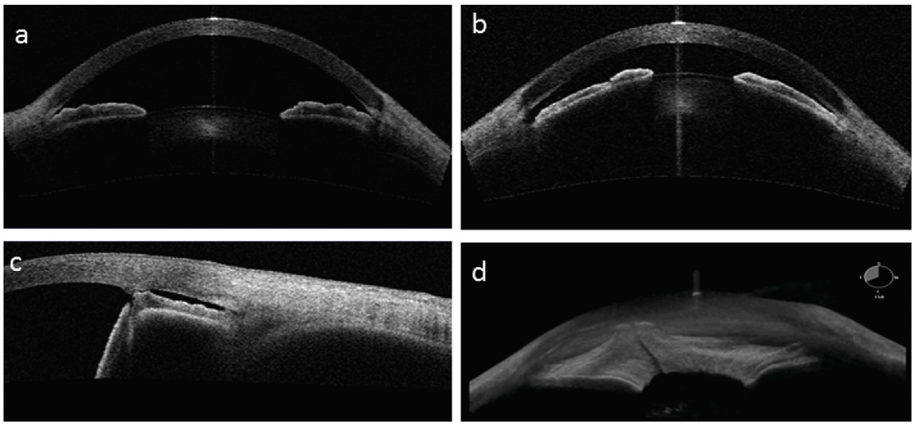

Fig. 17. Examples of clinical application using optical coherence tomography (OCT). a: Plateau iris (Visante OCT) with peripheral scroll of iris and central normal anterior chamber depth, b: Large lens vault in angle closure (Visante OCT), c: Adherent leukoma with slit open angle (Visante high definition OCT), d: Demonstration of peripheral anterior synechiae using reconstructed 3-dimensional image (Casia swept source OCT).

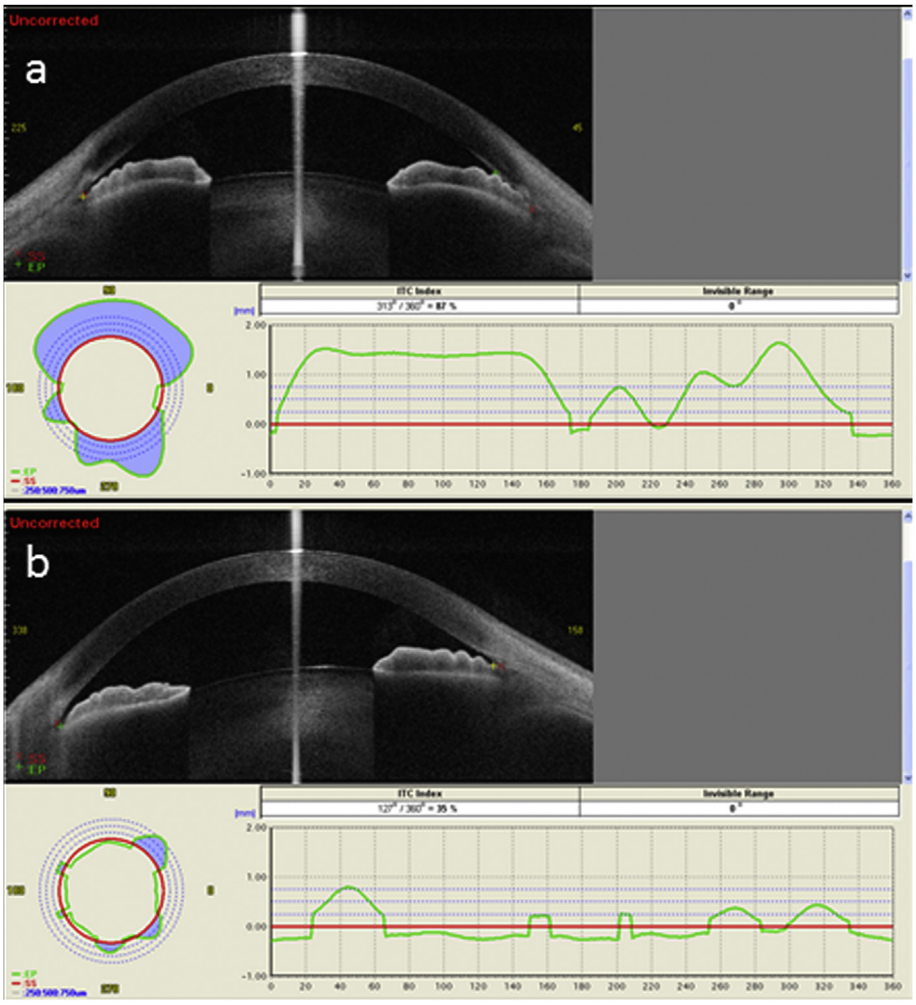

Fig. 18. Pre and post laser peripheral iridotomy Casia swept-source optical coherence tomography images (a and b respectively) with respective iris trabecular index quantification using 16 scans, respectively (angle closure reduced from 87% to 35%).

There are more areas that need to be explored, including angle surgeries, such as the various stents for glaucoma using this innovative technology(Ehlers et al., 2014b, 2014c).

6. Optical coherence tomography for ocular surface and dry eye disease

When the eye is opened after blinking, a thin liquid film called precorneal tear film covers the cornea and sclera. Although the TF is only few μm in thickness, its composition is complex and it plays a key role in protecting and nourishing the cornea. When the eye is kept open, the TF thins over time till it breaks up (break up time, BUT), requiring a blink to refresh the ocular surface. Thinning of the TF between blinks involves a variety of mechanisms including evaporation, osmotic flow through the cornea and conjunctiva, tangential flow of aqueous tears and diffusion of tear solutes (Braun et al., 2015).

The TF has three distinct layers. Beginning from the outermost surface, the lipid layer provides a hydrophobic barrier reducing surface tension and helps to re-spreads the tears after each blink. Although, the thickness of the lipid layer is virtually a few nm, it has a two-layer structure: an extremely thin, potentially monomolecular layer of polar lipids residing at the water as well as a lipid interface covered by a layer of non-polar lipids which forms the outermost eye–air interface (Cwiklik, 2016). The aqueous layer is the thickest part of the TF and promotes spreading of the tear film and osmotic regulation. It plays an important role in oxygenation of the cornea as well as providing the defence system against infection. The aqueous phase of the TF contains a wide variety of metabolites as well as electrolytes and proteins. The innermost layer of the TF is the mucin layer (Ablamowicz and Nichols, 2016). The mucin layer compensates for corneal unevenness, reduces friction during blinking and plays a role in debris removal.

Dry eye disease (DED) is a highly prevalent ocular condition, with a variety of clinical consequences such as visual disturbance, ocular discomfort and in severe cases damage of the ocular surface. Approaches to visualize alterations in patients with DED using anterior segment OCT can be divided into two categories - visualization of anatomical structures that are affected by the disease as well as the direct visualization of the TF. Among the anatomical structures that have been visualized, apart from the cornea, are lid-parallel conjunctival folds (LIPCOFs) allowing for objective grading of DED related alterations (Veres et al., 2011). Meibomian glands were imaged with either a custom-built high resolution OCT (Bizheva et al., 2010) or a commercial system (Hwang et al., 2013a, 2013b) allowing for three-dimensional reconstruction. Using this approach, reduced length and width of Meibomian glands was observed in patients with Meibomian gland dysfunction (Liang et al., 2015). Generally, good agreement was shown between OCT-based evaluation of Meibomian glands and classical lid transillumination (Napoli et al., 2016) as well as with two-dimensional infrared (IR) meibography (Yoo et al., 2017). Extraction of Meibomian glands from the volumetric OCT image can be further improved when using polarization sensitive detection (see section 10), which reveals age-related alterations - Fig. 19. In addition, it has been shown that

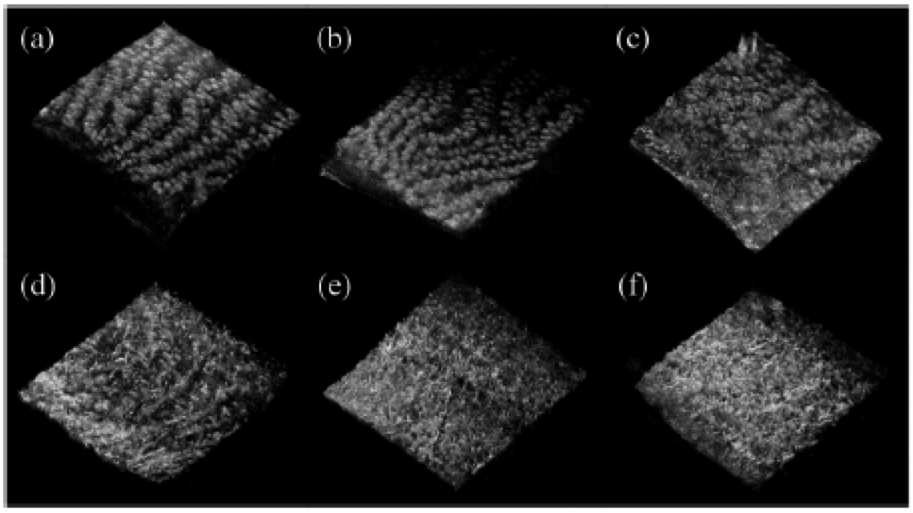

Fig. 19. Visualization of Meibomian glands using polarization-sensitive optical coherence tomography in healthy subjects at different age ((a) 28 years, (b) 32 years, (c) 56 years, (d) 63 years, (e) 72 years, and (f) 82 years (with permission from Ju and Tang, 2015).

normal punctal and vertical canalicular anatomy (Kamal et al., 2016; Timlin et al., 2016; Wawrzynski et al., 2014) as well as the anatomy of the lacrimal glands including the excretory ducts, interlobular ducts, intralobular ducts, lobules, parenchyma, and acini of the palpebral lobe (Doh et al., 2015) can be imaged with commercial OCT technology. The potential of these approaches to diagnose and follow-up DED is, however, still inadequately documented.

From a pathophysiological point of view, DED is characterized by instability of the pre-corneal TF accompanied by increased osmolarity and inflammation of the ocular surface (DEWS, 2007). One of the major challenges in the diagnosis and follow up of DED is that, up to now, the most critical component of DED, the TF itself is difficult to measure objectively with sufficient precision. Given that a stable and sufficient TF is a prerequisite for an intact ocular surface, direct imaging of the precorneal TF may have significant potential in the clinical management of DED. It may also help to obtain novel insight into the pathophysiology of the diseases (Bai and Nichols, 2017). Thus, several attempts have been made in the past to achieve measures of TF thickness (TFT) via OCT. This is, however, a challenge because the tear film changes its thickness over time after each blinking.

One approach to overcome this limitation is to use the tear meniscus as a surrogate parameter for the total tear volume – Fig. 20. Indeed, the tear meniscus can be measured with sufficient precision with OCT

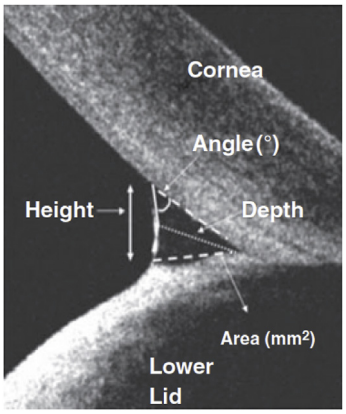

Fig. 20. An OCT image of the tear meniscus taken with s commercial Fourier-domain OCT. Lower tear meniscus is shown and meniscus height and depth as well as cornea-meniscus angle are highlighted. (with permission from Park et al., 2013).

systems, providing a resolution of approximately 10 μm (Shen et al., 2008; Wang et al., 2006a). Using continuous OCT measurements, it is possible to study the dynamics of the tear meniscus over time (Bartuzel et al., 2014). Another possibility that can allow us to gain an insight into TF dynamics is based on administration of saline solution combined with the measurement of clearance over time (Zheng et al., 2014). Data from clinical studies show that the tear meniscus decreases with age (Cui et al., 2011; Raj et al., 2016). Studies have reported that measures of tear meniscus are reduced in different dry eye populations: in patients with aqueous tear deficiency (Shen et al., 2009), in patients with thyroid-associated ophthalmopathy (Sizmaz et al., 2014) as well as in Japanese (Akiyama et al., 2015; Ibrahim et al., 2010), Chinese (Li et al., 2012a) and American DED patient populations (Nguyen et al., 2012). A study in a mixed group of DED patients shows, however, a more complex relation (Tung et al., 2014). In patients with tear dysfunction, lower tear volume correlated with severity of corneal epithelial disease. In contrast, higher tear volume was associated with corneal damage in patients with Meibomian gland disease. The finding is compatible with a separate study, which included different DED phenotypes, reported high specificity of the technique in patients with Sjögren syndrome, but little discriminative power in patients with lipid deficiency. Tear meniscus height is correlated with size of the lacrimal punctum (Sung et al., 2017).

Early approaches to measure TFT were directed towards indirect measurements using OCT technology. Employing the commercial Zeiss Stratus system, Wang and co-workers (Wang et al., 2003) took OCT measurements of subjects who were with and without contact lenses, and calculated the thickness of the tear film after measuring the thickness of the contact lens *in vitro*. The authors reported a TFT of 3.3 ± 1.5 μm. A comparable approach was used with a custom-built OCT system (Wang et al., 2006a, 2006b). Using the latter technique, central TFT was indirectly measured by calculating the difference between baseline measurements of the central corneal thickness including TF and corneal thickness obtained after instillation of artificial tears. The results for TFT obtained in healthy subject were in the same region as reported previously with a mean value of 3.3 ± 2.6 μm.

Although OCT systems with a resolution of 5 μm or less allow the visualization of the tear meniscus and other detailed structures of the cornea (Ge et al., 2013), this resolution remains inadequate to detect changes within the TF itself as they occur between blinks or in patients with DED. The further development of new light sources with a wider bandwidth has considerably improved the axial resolution of OCT systems down to a resolution of approximately 1 μm *in vivo*, which is necessary to detect clinically significant alterations in TFT (Bai and

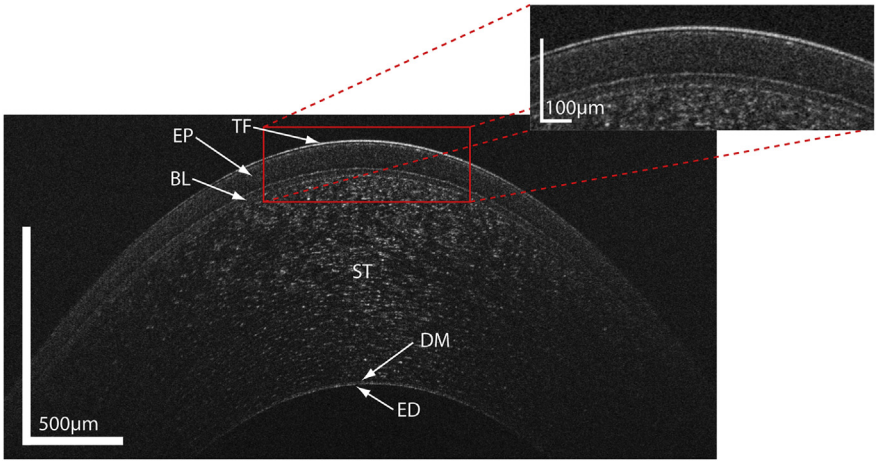

Fig. 21. Ultra high-resolution OCT image of the pre-corneal tear film as obtained in a healthy subject. (with permission from Werkmeister et al., 2013). TF: tear film; EP: epithelium; BL: Bowman's layer; ST: stroma; DM: Descemet membrane; ED: endothelium.

Nichols, 2017).

Using an ultra-high resolution spectral-domain OCT system, Chen and colleagues measured pre-corneal tear-film thickness in the range of 1.7 µm–2.0 µm *in vivo* (Chen et al., 2010). However, the interpretation of the latter result is limited by the fact that the system provides an axial resolution of approximately 3 µm only. A custom-built OCT system with a superluminescent diode providing a beam with 840 nm central wavelength and 100 nm allowed for the measurement of tear deficient DED in some patients, but reported values may not be representative because readings were most likely only obtained in those patients with thicker TFT (Cui et al., 2011).

Systems with higher resolutions report slightly different results. As such, tear film layer thickness as measured with an OCT system based on a 375 nm bandwidth supercontinuum light source, which allows for a resolution on the ocular surface of 1 µm, reports an average TFT of approximately 4 µm–5 µm in healthy subjects (Yadav et al., 2011). This is in keeping with results of other more recent studies. In a study on young healthy subjects, using a Ti: Sapphire laser OCT system with an axial resolution of 1.2 µm on the level of the ocular surface, the authors report that the average precorneal TFT was 4.79 ± 0.88 µm (Werkmeister et al., 2013). As shown in Fig. 21, the precorneal TF can be clearly delineated in this image. Further, these values are comparable to the TFT values detected by an interferometric method (King-Smith et al., 2008; Nichols et al., 2005) previously used to assess TFT. The latter study also indicates an excellent reproducibility of OCT-based measurements with an intraclass correlation coefficient of 0.97(Werkmeister et al., 2013).

One of the major challenges in DED is that the correlation between standard clinical signs such as BUT or corneal staining and the symptoms perceived by the patients is usually weak (Begley et al., 2003; Pflugfelder et al., 1998). Given that OCT is capable of directly visualizing the TF, it may be a promising alternative to the currently used clinical tests. To gain a better insight into this issue, a study investigated the correlation between symptoms, clinical signs and TFT in a group of patients with mild to moderate DED (Schmidl et al., 2015c). The study revealed that there was a significant correlation between TFT as measured with OCT and subjective symptoms in these patients, which supports a potential role of this technique in the clinical management of DED (Schmidl et al., 2015c). Moreover, TFT was positively correlated with BUT and negatively correlated with tear osmolarity. The correlations in this study were, however, relatively weak most likely because of incomplete phenotyping and with regard to tear deficiency and evaporative DED.

An important advantage of OCT based measurements of the ocular tear film is that in principle this technique has the capability to provide information not only at a single point in time but can, depending on the scanning speed, visualize TF dynamics. As such, the thinning of the TF after blinking can be quantified, which can provide valuable information regarding an important aspect of DED: tear evaporation (Werkmeister et al., 2013). Using high-speed OCT systems, these measurements are not limited to a certain point at the ocular surface but can cover larger areas of the cornea. This technique can be used to generate two dimensional thickness (enface) maps of the TF dynamics *in vivo* (Fig. 22) and has the potential of being an observer independent alternative approach to classical clinical measures such as subjective slit-lamp based BUT measurement.

Although the introduction of newly developed drugs and devices has provided additional therapeutic options for patients with severe DED (Hoy, 2017; Keating, 2017; Rodriguez-Pomar et al., 2017), the current mainstay of therapy for patients with mild to moderate DED remains the application of topical lubricants. However, a large variety of different topical lubricants with diverse chemical and physical properties are currently on the market and for the most of the agents their clinical efficacy and their behaviour on the ocular surface is only insufficiently described. Clinical trials have now shown the potential of OCT to evaluate therapeutic intervention including treatment with topical lubricants in patients with DED. In particular, it has been shown that topical application of lubricants increase TFT (Kaya et al., 2015; Schmidl et al., 2015b). Whereas topical application of physiological saline solution had only a minor effect on TFT, administration of hyaluronic acid significantly increases TFT with a maximum effect 10 min after administration (Kaya et al., 2015).

Furthermore, OCT systems are also capable of investigating differences between topical lubricants. As such, it has been shown that although both therapies, sodium hyaluronate alone as well as combination therapy between sodium hyaluronate and trehalose, lead to a significant increase in TFT, the latter led to a longer lasting effect, indicating a longer residency time of the combination product (Schmidl et al., 2015b). A long-lasting effect on TFT was also seen with topical Chitosan-N-Acetylcysteine, most likely due to the strong mucin binding of the compound (Schmidl et al., 2017). With administration of lubricant gels, there is initially a pronounced increase in TFT as shown in Fig. 23, where it as high as 3-fold in certain subjects (Wozniak et al., 2017).

Studies have also been performed focusing on tear meniscus after administration of topical eye drops. Whereas the effect of saline was only seen for 1 min, 0.1% hyaluronic acid increased tear meniscus volume for 3 min, and 0.3% hyaluronic acid provided an effect for 10 min (Akiyama-Fukuda et al., 2016). With 3% diquafosol ophthalmic solution, a significant difference when compared to saline was observed;

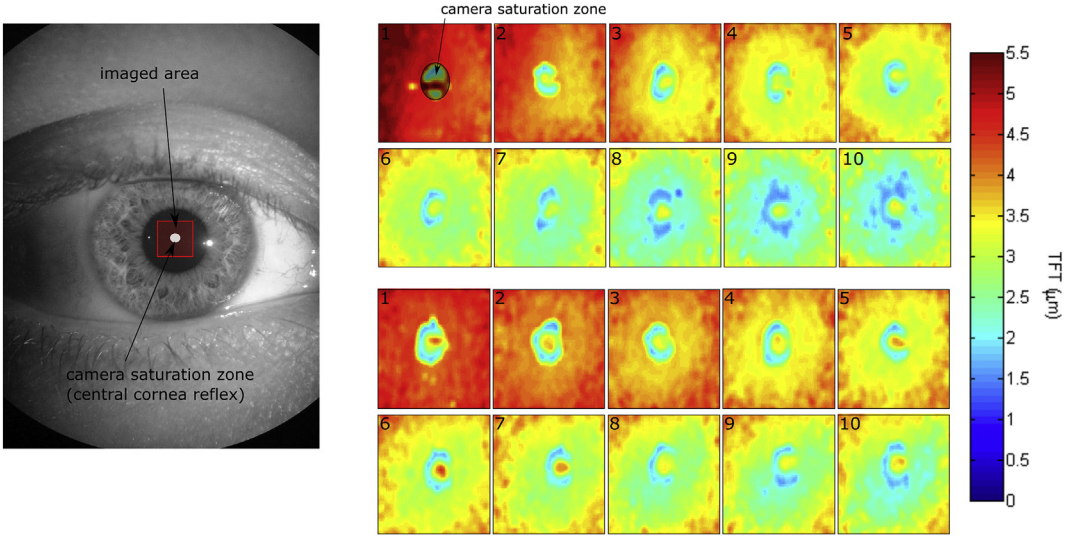

Fig. 22. Measurement of tear film dynamics using en face tear film thickness maps. Left: Slit lamp image of the front surface depicting the imaged area. Right: En face. tear film thickness maps in a healthy subject.

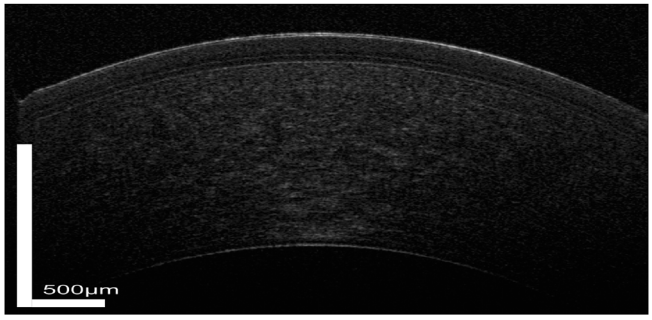

Fig. 23. Ultra high-resolution optical coherence tomography image of the pre-corneal tear film as obtained in a patient with dry eye disease before (a) and 10 min after administration of a lubricant gel (Polyethylene glycol 0.4%, propylene glycol 0.3%, hydroxypropyl guar; b). The tear film increased from a value of 4.1 mm to a value 11.7 mm.

this was as long as 30 min. A short-term increase in tear meniscus volume was also seen with carboxymethyl cellulose (Tung et al., 2012; Wang et al., 2010b), polyethylene glycol (Tung et al., 2012) as well as artificial tear formulations based on either hypromellose or a combination of polyethylene glycol 400 and sodium hyaluronate (Garcia-Lazaro et al., 2011). With the latter, an effect was seen for as long as 60 min.

Only few studies have focussed on the effects of repeated instillation of eye drops or other treatments on TFT or teat meniscus. Moreover, these studies are lacking an adequate control group and typically use a pre-post study design. A two months treatment with cyclosporine improved TFT in a small group of DED patients (Wang et al., 2012b). Measures of tear meniscus size also improved after acupuncture in patients with lipid tear deficiency and DED, but not in patients with Sjögren syndrome (Lin et al., 2015). An effect on tear meniscus in Sjögren patients was, however, observed after oral treatment with the muscarinic receptor agonist pilocarpine (Ibrahim et al., 2013). Another study that revealed increased tear meniscus volume studied the effect of botulinum toxin A injection in patients with essential blepharospasm (Park et al., 2013).

There are some limitations of the currently available OCT systems that preclude routine use in DED. First, although the OCT systems are in principle capable to measure the ocular surface at different locations, the scanning area that can be covered is currently limited to the central cornea. To measure tear film dynamics or replace standard clinical tests such as BUT, scanning of the full cornea would be necessary. This would require a modification in the illumination pathway and high-speed systems, which can also allow for a reduction of movement artefacts. Secondly, with increasing distance to the apex of the cornea, the incident angle of the laser beam is not perpendicular to the ocular surface, which leads to a decrease in the signal to noise ratio (Aranha Dos Santos et al., 2015). To overcome this hurdle, an optical setup where the incident beam is perpendicular to the ocular surface at the central cornea and also for the peripheral cornea would be required(Beer et al., 2017).

As the OCT imaging technique is rapidly evolving, efforts have been made to measure not only the tear film of the entire cornea surface, but also investigate the ultra-structure of the tear film. Among the different layers of the tear film, the outermost lipid layer is of particular interest because it is related to the stability of the pre-corneal tear film. As the lipid layer of the tear film has only a thickness of 40–80 nm, it is far beyond the optical resolution of OCT and therefore not accessible via conventional imaging. However, it has recently been shown that by super-resolved thickness measurements using an ultrahigh resolution OCT system, structures smaller than the axial resolution of the system can be visualized and *in vivo* imaging of the lipid layer is possible (Dos Santos et al., 2016). Further efforts are necessary to fully assess the potential of this technique to measure lipid layer thickness in patients with DED in a clinical setting.

Attempts have also been made to grade the quality of tear reflection and alterations with different types of lubricants (Napoli et al., 2014b). Another approach was presented by instillation of a lipid-based tracer. With this technique, enhanced OCT imaging of the lower tear meniscus was realized, given by a strongly increased reflectivity of the air-lipid interface. Based on the decay back to baseline values over time, the authors were able to estimate lipid clearance (Napoli et al., 2014a). A critical issue in all types of OCT measurements of tear film relates to the standardization of blinking before the measurement. Indeed it has been shown that normal and delayed blinking differentially affect tear meniscus (Palakuru et al., 2007). In our studies, we have used a standardized blinking pattern and started measurements one second after the opening of the eye. This means that we excluded the first tear film volume from measurement and defined tear film thickness based on the average values obtained from the volumes taken two and three seconds after opening the eye. In most of the studies, the exact blinking patterns are not provided and additional work is required to understand their impact on measures of TFT and tear meniscus. Another critical issue is in relation to temperature and humidity in the examination room. For most of our clinical studies, we try to standardize these factors in our

research clinic. However it remains unclear if this is entirely possible in a real clinical setting. In addition, the impact has not been systematically studied although it has been reported that airflow exposure has a significant impact on tear meniscus (Koh et al., 2012).

Ultrahigh-resolution OCT systems allow for the first time the visualisation and quantification of the pre-corneal tear film *in vivo*. Along with the technical improvement of the OCT systems, such as the better resolution, faster scanning speed as well as wider scanning area, further clinical applications of the OCT technique in the field of DED can be predicted in the near future. Whether measurement of tear meniscus or measurement of TFT is a more relevant sign of DED remains to be proven. Little is known about the correlation between these variables but a small study did not find any association in healthy subjects (Wang et al., 2006b). Assessment of the pre-corneal TF may, however, offer advantages such as the understanding of evaporation rate, tear break-up and thickness of the lipid layer – Fig. 23. When absolute values of TFT are measured the algorithms that are used for segmentation and estimation play an important role. Indeed, different approaches for these issues were presented (Aranha Dos Santos et al., 2015; Huang et al., 2013a, 2013b, 2014, 2016) and it is likely that they will lead to different absolute values. This is indeed the case when quantifying retinal nerve fiber layer thickness at the posterior pole of the eye (Sander et al., 2015). A comparison of different systems for measuring the tear meniscus indicates that this is also an issue for the anterior segment of the eye (Arriola-Villalobos et al., 2017).

7. Anterior segment optical coherence tomography angiography

Optical coherence tomography angiography (OCTA) essentially delineates blood vessels using OCT by comparing decorrelation between consecutive scans(Ang et al., 2018; Kashani et al., 2017; Leitgeb et al., 2014; Sharma et al., 2017; Tan et al., 2018). This can be done by comparing phase speckle contrast, changes in intensity or a variation of the full OCT signal(Chen and Wang, 2017). In the posterior segment, OCTA has become a useful rapid, non-invasive imaging modality that provides imaging of vessels(Gao et al., 2016; Zhang et al., 2015a). Currently, commercially available OCTA systems use various proprietary algorithms such as optical microangiography, full or split-spectrum amplitude-decorrelation angiography (FSADA or SSADA), and OCTA ratio analysis(Wylegala et al., 2016). However, current OCTA systems are not specifically intended for the anterior segment, but may be adapted to assess the cornea, iris or scleral vessels(Ang et al., 2015c). While the SSADA system has been most commonly described, other FD OCTA systems have also been successfully adapted for the anterior segment(Ang et al., 2016b, 2017).

Anterior segment angiography has a wide variety of clinical applications, ranging from the evaluation of ocular surface and corneoscleral inflammation (Watson, 1987; Watson and Bovey, 1985), to the assessment of corneal vascularisation (Spiteri et al., 2015). Corneal vascularisation is a pathological condition in the cornea that reduces corneal transparency, and subsequently increases rate of graft rejection (Cursiefen et al., 2003; Niederkorn, 2010). However, current assessment of the anterior segment vascular network is limited to invasive angiography techniques using fluorescein (FA) or indocyanine green (ICGA)(Kirwan et al., 2012). Thus, imaging and evaluation of corneal vascularisation is seldom performed despite its prevalence and potential sight-threatening effects(Lee et al., 1998; Resnikoff et al., 2004). As such, there is a potential increasing role for anterior segment OCTA. Moreover, it has been reported that the OCTA was comparable to ICGA for assessment of vessel density of corneal vascularisation(Ang et al., 2016a).

The main advantage of AS OCTA is that images are rapidly acquired using a non-contact technique(Ang et al., 2015c). However, there are many limitations with existing OCTA systems adapted for the anterior segment. First, motion artefacts from patient movement or saccadic eye movement are very common as current AS OCTA systems do not have in-built motion correction for ocular saccades. Second, corneal scars may cause signal blockage and artefacts – although future improvements to the software for the anterior segment may further reduce these blockages(Girard et al., 2015). Third, current AS OCTA systems do not have an eye-tracking system allowing for registration, which is required for comparisons in follow-up scans. Nonetheless, with the help of adjunct image analysis software, it has been found to be potentially useful for serial scans and follow-up for various clinical indications(Cai et al., 2017).

Despite the current limitations of AS OCTA, there are still a wide variety of potential clinical applications in the anterior segment. The ability to provide high-resolution scans of corneal pathology with accompanying information on the depth of abnormal vasculature, is useful for planning for procedures such as lamellar keratoplasty with fine-needle diathermy (Spiteri et al., 2015); or evaluation of peripheral corneal infiltrates or melts with the adjacent scleritis and occlusion of limbal vessels(Ang et al., 2016d). Other potential clinical applications include assessment of graft vascularisation with prognostication for immunological rejection (Bachmann et al., 2010), evaluation of anti-angiogenic treatments for corneal vascularisation (Chang et al., 2001), studying changes to limbal vasculature in limbal stem cell deficiency, evaluation of subconjunctival vascularity in association with bleb morphology after trabeculectomy, or even evaluation of normal iris blood supply and abnormal iris vessels in neovascular glaucoma – Fig. 24(Sng et al., 2012b).

8. Other applications of anterior segment optical coherence tomography

8.1. Imaging of extraocular muscles

In patients with strabismus AS OCT has been used for measuring the distance from the corneoscleral limbus to the insertion site of the horizontal and vertical extraocular muscles(Liu et al., 2011b; Pihlblad et al., 2016). This technique accurately measures this distance in clinical practice, but reliability decreases after reoperations(Rossetto et al., 2017). Other studies have confirmed that it is possible to determine the insertion distance from the limbus to the extraocular rectus muscles and the technique be applicable for pre-operative procedure planning in complicated strabismus patients(Pihlblad and Reynolds, 2017). The accuracy can be improved by combination of grayscale and colour modalities(Venincasa et al., 2017). Likewise, AS OCT allows for the detection of swelling at the insertion site of the extraocular muscles in patients with Graves' orbitopathy(Haner et al., 2015). During strabismus surgery live four-dimensional intraoperative imaging, is capable of visualizing suture depth during lateral rectus resection(Pasricha et al., 2017).

8.2. Imaging of limbus and sclera

The ability to assess the morphometry of the limbus *in vivo* has already been realized in the early days of AS OCT (Feng and Simpson, 2005; Sarunic et al., 2008). Changes in limbus anatomy can be observed after soft contact lens wear.{Consejo et al., 2017 #411}(Consejo et al., 2017) Using a custom built OCT operating at 1060 nm Bizehva and coworkers were able to map corneo-scleral tissue morphology including visualization of the Vogt palisades, the blood and lymph vasculature (Bizheva et al., 2011). The palisades of Vogt are radially oriented fibrovascular ridges consisting of a stem cell population that allows for regeneration of the corneal epithelium. Several groups have shown that they can be visualized using OCT (Bizheva et al., 2017b; Falke et al., 2012; Grieve et al., 2015; Haagdorens et al., 2017; Lathrop et al., 2012). Alterations in the anatomy of Vogt's palisades have been reported in patients with DED(Ghouali et al., 2017). Using either optical microangiography (Li et al., 2011), phase-variance optical coherence angiography (Poddar et al., 2015), or split-spectrum amplitude-decorrelation

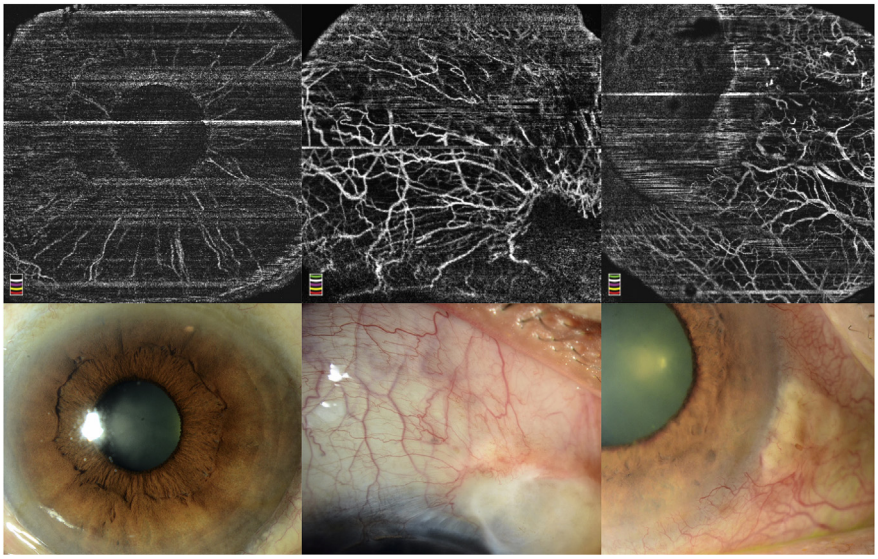

Fig. 24. (Left) Anterior segment optical coherence tomography angiography showing normal iris vasculature not obvious in pigmented irides. (Center) Avascular bleb with scarring and increased vascular network surrounding the bleb. (Right) Corneal vascularisation associated with early carcinoma in situ.

angiography (Li et al., 2015), it is possible to visualize the three-dimensional microvasculature of the limbus(Lavinsky and Lavinsky, 2016).

The sclera can also be visualized using AS OCT and values for scleral thickness between 600 μm and 800 μm have been reported for healthy subjects(Buckhurst et al., 2015; Ebneter et al., 2015). Anterior scleral curvature can be measured using mathematical modelling and has been proposed valuable for the design of scleral lenses(Choi et al., 2014). In a subgroup of elderly patients senile scleral plaques can be seen(Beck et al., 2015). These areas should be avoided as injection sites of intravitreal therapies. After repeated intravitreal injections scleral thinning can be observed(Zinkernagel et al., 2016). Subconjunctival scarring after vitrectomy can also be visualized using AS OCT and correlates well with histology(Gozawa et al., 2017). In patients with anterior scleritis hyporeflectivity within the sclera, nodules, and visible vessels can be observed that improve during treatment(Axmann et al., 2016; Levison et al., 2016).

Within the sclera and conjunctiva, AS OCT can provide detailed bleb morphology features such as bleb wall, cavity, flap, ostium patency, cysts within bleb and wall thickness(Singh et al., 2009a, 2009b). SS OCT images of the bleb can be automatically analysed to provide bleb dimensions such as area and volume. Bleb analysis with AS OCT identified features associated with functioning and failed blebs such as thickening of bleb walls and cystic spaces (Boey et al., 2011; Singh et al., 2009b). Another one of the large studies compared tumor imaging between AS OCT and UBM in 18 eyes with cystic and solid lesions of the anterior segment. Partial imaging of the solid and cystic lesions of AS OCT was providing some information on the nature of the lesions, however, it was shown that UBM was definitely superior in complete imaging of both type of lesions(Verma et al., 2017).

9. Novel developments for anterior segment optical coherence tomography

9.1. Polarization sensitive OCT

Polarization sensitive OCT (PS OCT) is an extension of OCT that analyses the polarization state of backscattered light(de Boer et al., 2017; Pircher et al., 2011). In the human eye, a variety of tissues including the cornea, the retinal nerve fibres and the sclera are birefringent and therefore contrast in PS OCT images can be improved for these tissues. Improved contrast can, however, also be obtained in other tissues such as the trabecular meshwork (Yasuno et al., 2010), and tissue discrimination between conjunctiva, sclera, trabecular meshwork, cornea, and uvea can be obtained with PS OCT. Several different systems have been proposed for PS OCT imaging of the anterior segment of the eye(Lim et al., 2011; Yamanari et al., 2008, 2015, 2016).

Already in the early days of AS OCT application of polarization-sensitive system for corneal imaging have been presented(Gotzinger et al., 2004). PS OCT has been proposed as a technique for diagnosis of keratoconus because of changes in the lamellar structure of collagen fibers leading to phase retardation (Fukuda et al., 2013; Gotzinger et al., 2007), as well as for treatment monitoring after cross-linking(Ju and Tang, 2015). A direct comparison with other techniques for keratoconus monitoring is, however, lacking. In glaucoma patients undergoing trabeculectomy the filtering bleb shows improved visibility with PS OCT because of the birefringent properties(Fukuda et al., 2014; Tsuda et al., 2015; Yasuno et al., 2009). PS-OCT has been used to measures scleral birefringence at the posterior pole of the eye to gain insight into biomechanical properties(Fialova et al., 2017). Scleral birefringence can also be measured at the anterior segment of the human eye and correlates with IOP (Yamanari et al., 2014). Currently, PS-OCT systems are not commercially available, related to the higher hardware complexity as compared to standard OCT systems.

9.2. OCT elastography

Another functional extension, OCT elastography, aims to get insight into the biomechanical properties of tissue. The technique is based on the ability of OCT to detect subtle displacement of tissue when a force is applied. This force can either be externally (Hsieh et al., 2016; Nguyen et al., 2015; Song et al., 2015), or internally from pulse related tissue changes(Dragostinoff et al., 2009; O'Hara et al., 2013). These forces are employed stepwise, transient or harmonic(Kirby et al., 2017). Independently of the source of the force the tissue response is detected by OCT by either detecting the change in position, the velocity of the tissue or a combination of both. By detecting the propagation of the tissue wave induced by the force in several directions it may also be possible to detect the anisotropic biomechanical properties of the tissue.

Since the introduction of OCT elastography, applications for the posterior and anterior segment of the eye have been reported. Early approaches used a 2-D cross-correlation algorithm to determine shear deformation and Poisson's ratio of ex vivo corneas(Ford et al., 2011). First *in vivo* results were obtained in the mouse cornea with a phase-

stabilized swept source OCT system measuring the phase response in response to a mechanical stimulus(Manapuram et al., 2012). OCT elastography has also been used to characterize the mechanical anisotropy of porcine (Singh et al., 2017a), and rabbit corneas in situ after cross-linking(Singh et al., 2017b).

For *in vivo* applications point-by-point scanning is challenging because of relatively long acquisition times and associated motion artefacts. As such ultrafast systems operating in the megahertz (MHz) range haven been realized(Singh et al., 2016; Song et al., 2016). Alternatively, line field or full-field OCT systems may be preferable because of parallel acquisition schemes. With full field OCT virtual palpation maps at the micrometer scale were obtained from the porcine cornea (Nahas et al., 2013), with a single shot line-field low coherence holography system utilizing an automatic Hilbert transform analysis based on a spatial phase shifting technique. Spatio-temporal maps of elastic wave propagation were acquired with one air-pulse excitation and used to quantify wave velocity and sample mechanical properties at a line rate of 200 kHz. The technology was successfully applied to an ex vivo porcine cornea, but *in vivo* applications have not been reported as yet.

Phase-sensitive OCT elastography has recently been used to study the dynamics of strain and tissue-shape changes during laser-induced photothermal corneal reshaping in almost real-time with 10–100 ms temporal resolution(Zaitsev et al., 2017). Using this technique ex vivo experiments demonstrate temporal plastification of the cornea and characterise strain distributions, surface displacements, and scattering.

10. Conclusions

In summary, the AS OCT currently plays an important role in many aspects of research and clinical applications in the field of Ophthalmology. These include detailed ocular surface evaluation, corneal evaluation that impact surgical outcomes, angle assessment for glaucoma diagnosis, aqueous outflow assessment as well as vascular supply of the anterior segment. These AS OCT imaging applications also extend to imaging the sclera, limbus and extraocular muscles. The main advantages of the AS OCT include the rapid, non-invasive, *in vivo* imaging of the structures within the eye – while providing quantitative measurements. Recent improvements in resolution and acquisition speed have improved image quality and reproducibility for anterior segment imaging with greater detail. The advancement of AS OCT technology has evolved from providing an overview of anterior segment structures, to details of the ocular surface and cornea with almost histological resolution - and most recently, delineating vascular flow within the anterior segment. Novel developments include polarization sensitive OCT and OCT elastography, which provide further potential clinical applications of AS OCT. Further advancement of AS OCT to ultra-high resolution, en-face image rendering and functional extensions may improve the clinical evaluation of anterior segment, corneal and ocular surface diseases.

Declaration of interests

Marcus Ang, Mani Baskaran, René M. Werkmeister, Jacqueline Chua, Doreen Schmidl, Valentin Aranha dos Santos, Gerhard Garhöfer, Jodhbir S Mehta, Leopold Schmetterer – None to declare.

Appendix A. Supplementary data

Supplementary data related to this article can be found at http://dx.doi.org/10.1016/j.preteyeres.2018.04.002.

References

Ablamowicz, A.F., Nichols, J.J., 2016. Ocular surface membrane-associated mucins. Ocul. Surf. 14, 331–341.

Akiba, M., Maeda, N., Yumikake, K., Soma, T., Nishida, K., Tano, Y., Chan, K.P., 2007. Ultrahigh-resolution imaging of human donor cornea using full-field optical coherence tomography. J. Biomed. Optic. 12 041202.

Akiyama, R., Usui, T., Yamagami, S., 2015. Diagnosis of dry eye by tear meniscus measurements using anterior segment swept source optical coherence tomography. Cornea 34 (Suppl. 11), S115–S120.

Akiyama-Fukuda, R., Usui, T., Yoshida, T., Yamagami, S., 2016. Evaluation of tear meniscus dynamics using anterior segment swept-source optical coherence tomography after topical solution instillation for dry eye. Cornea 35, 654–658.

Ang, G.S., Wells, A.P., 2011. Factors influencing laser peripheral iridotomy outcomes in white eyes: an anterior segment optical coherence tomography study. J. Glaucoma 20, 577–583.

Ang, M., Cai, Y., Shahipasand, S., Sim, D.A., Keane, P.A., Sng, C.C., Egan, C.A., Tufail, A., Wilkins, M.R., 2016a. En face optical coherence tomography angiography for corneal neovascularisation. Br. J. Ophthalmol. 100, 616–621.

Ang, M., Cai, Y., Tan, A.C., 2016b. Swept source optical coherence tomography angiography for contact lens-related corneal vascularization. J Ophthalmol 2016, 9685297.

Ang, M., Chong, W., Huang, H., Tay, W.T., Wong, T.Y., He, M.G., Aung, T., Mehta, J.S., 2013. Comparison of anterior segment optical tomography parameters measured using a semi-automatic software to standard clinical instruments. PLoS One 8 e65559.

Ang, M., Chong, W., Tay, W.T., Yuen, L., Wong, T.Y., He, M.G., Saw, S.M., Aung, T., Mehta, J.S., 2012a. Anterior segment optical coherence tomography study of the cornea and anterior segment in adult ethnic South Asian Indian eyes. Invest. Ophthalmol. Vis. Sci. 53, 120–125.

Ang, M., Devarajan, K., Das, S., Stanzel, T., Tan, A., Girard, M., Schmetterer, L., Mehta, J., 2017. Comparison of anterior segment optical coherence tomography angiography systems for corneal vascularisation. Br. J. Ophthalmol (Epub).

Ang, M., Dubis, A.M., Wilkins, M.R., 2015b. Descemet membrane endothelial keratoplasty: intraoperative and postoperative imaging spectral-domain optical coherence tomography. Case Rep Ophthalmol Med 2015, 506251.

Ang, M., Konstantopoulos, A., Goh, G., Htoon, H.M., Seah, X., Lwin, N.C., Liu, X., Chen, S., Liu, L., Mehta, J.S., 2016c. Evaluation of a micro-optical coherence tomography for the corneal endothelium in an animal model. Sci. Rep. 6, 29769.

Ang, M., Mehta, J.S., Chan, C., Htoon, H.M., Koh, J.C., Tan, D.T., 2014. Refractive lenticule extraction: transition and comparison of 3 surgical techniques. J. Cataract Refract. Surg. 40, 1415–1424.

Ang, M., Mehta, J.S., Lim, F., Bose, S., Htoon, H.M., Tan, D., 2012b. Endothelial cell loss and graft survival after Descemet's stripping automated endothelial keratoplasty and penetrating keratoplasty. Ophthalmology 119, 2239–2244.

Ang, M., Mehta, J.S., Sng, C.C., Htoon, H.M., Tan, D.T., 2012c. Indications, outcomes, and risk factors for failure in tectonic keratoplasty. Ophthalmology 119, 1311–1319.

Ang, M., Sim, D.A., Keane, P.A., Sng, C.C., Egan, C.A., Tufail, A., Wilkins, M.R., 2015c. Optical coherence tomography angiography for anterior segment vasculature imaging. Ophthalmology 122, 1740–1747.

Ang, M., Sng, C., Milea, D., 2016d. Optical coherence tomography angiography in dural carotid-cavernous sinus fistula. BMC Ophthalmol. 16, 93.

Ang, M., Tan, A.C.S., Cheung, C.M.G., Keane, P.A., Dolz-Marco, R., Sng, C.C.A., Schmetterer, L., 2018 Feb. Optical coherence tomography angiography: a review of current and future clinical applications. Graefes Arch. Clin. Exp. Ophthalmol. 256 (2), 237–245.

Ang, M., Wilkins, M.R., Mehta, J.S., Tan, D., 2016e. Descemet membrane endothelial keratoplasty. Br. J. Ophthalmol. 100, 15–21.

Aptel, F., Denis, P., 2010. Optical coherence tomography quantitative analysis of iris volume changes after pharmacologic mydriasis. Ophthalmology 117, 3–10.

Aranha Dos Santos, V., Schmetterer, L., Groschl, M., Garhofer, G., Schmidl, D., Kucera, M., Unterhuber, A., Hermand, J.P., Werkmeister, R.M., 2015. *In vivo* tear film thickness measurement and tear film dynamics visualization using spectral domain optical coherence tomography. Optic Express 23, 21043–21063.

Arriola-Villalobos, P., Fernandez-Vigo, J.I., Diaz-Valle, D., Almendral-Gomez, J., Fernandez-Perez, C., Benitez-Del-Castillo, J.M., 2017. Lower tear meniscus measurements using a new anterior segment swept-source optical coherence tomography and agreement with fourier-domain optical coherence tomography. Cornea 36, 183–188.

Au, J., Goshe, J., Dupps Jr., W.J., Srivastava, S.K., Ehlers, J.P., 2015. Intraoperative optical coherence tomography for enhanced depth visualization in deep anterior lamellar keratoplasty from the PIONEER study. Cornea 34, 1039–1043.

Axmann, S., Ebneter, A., Zinkernagel, M.S., 2016. Imaging of the sclera in patients with scleritis and episcleritis using anterior segment optical coherence tomography. Ocul. Immunol. Inflamm. 24, 29–34.

Bachmann, B., Taylor, R.S., Cursiefen, C., 2010. Corneal neovascularization as a risk factor for graft failure and rejection after keratoplasty: an evidence-based meta-analysis. Ophthalmology 117, 1300–1305 e1307.

Baek, S., Sung, K.R., Sun, J.H., Lee, J.R., Lee, K.S., Kim, C.Y., Shon, K., 2013. A hierarchical cluster analysis of primary angle closure classification using anterior segment optical coherence tomography parameters. Invest. Ophthalmol. Vis. Sci. 54, 848–853.

Bai, Y., Nichols, J.J., 2017 May. Advances in thickness measurements and dynamic visualization of the tear film using non-invasive optical approaches. Prog. Retin. Eye Res. 58, 28–44.

Bartuzel, M.M., Szczesna-Iskander, D.H., Iskander, D.R., 2014. Automatic dynamic tear meniscus measurement in optical coherence tomography. Biomed. Optic Express 5, 2759–2768.

Baskaran, M., Ho, S.W., Tun, T.A., How, A.C., Perera, S.A., Friedman, D.S., Aung, T., 2013. Assessment of circumferential angle-closure by the iris-trabecular contact index with swept-source optical coherence tomography. Ophthalmology 120,

2226–2231.
Baskaran, M., Iyer, J.V., Narayanaswamy, A.K., He, Y., Sakata, L.M., Wu, R., Liu, D., Nongpiur, M.E., Friedman, D.S., Aung, T., 2015. Anterior segment imaging predicts incident gonioscopic angle closure. Ophthalmology 122, 2380–2384.
Bata, A.M., Witkowska, K.J., Wozniak, P.A., Fondi, K., Schmidinger, G., Pircher, N., Szegedi, S., Aranha Dos Santos, V., Pantalon, A., Werkmeister, R.M., Garhofer, G., Schmetterer, L., Schmidl, D., 2016. Effect of a matrix therapy agent on corneal epithelial healing after standard collagen cross-linking in patients with keratoconus: a randomized clinical trial. JAMA Ophthalmol 134, 1169–1176.
Bechmann, M., Thiel, M.J., Neubauer, A.S., Ullrich, S., Ludwig, K., Kenyon, K.R., Ulbig, M.W., 2001. Central corneal thickness measurement with a retinal optical coherence tomography device versus standard ultrasonic pachymetry. Cornea 20, 50–54.
Beck, M., Schlatter, B., Wolf, S., Zinkernagel, M.S., 2015. Senile scleral plaques imaged with enhanced depth optical coherence tomography. Acta Ophthalmol. 93, e188–192.
Beer, F., Wartak, A., Haindl, R., Groschl, M., Baumann, B., Pircher, M., Hitzenberger, C.K., 2017. Conical scan pattern for enhanced visualization of the human cornea using polarization-sensitive OCT. Biomed. Optic Express 8, 2906–2923.
Begley, C.G., Chalmers, R.L., Abetz, L., Venkataraman, K., Mertzanis, P., Caffery, B.A., Snyder, C., Edrington, T., Nelson, D., Simpson, T., 2003. The relationship between habitual patient-reported symptoms and clinical signs among patients with dry eye of varying severity. Invest. Ophthalmol. Vis. Sci. 44, 4753–4761.
Bizheva, K., Haines, L., Mason, E., MacLellan, B., Tan, B., Hileeto, D., Sorbara, L., 2016. *In Vivo* imaging and morphometry of the human pre-descemet's layer and endothelium with ultrahigh-resolution optical coherence tomography. Invest. Ophthalmol. Vis. Sci. 57, 2782–2787.
Bizheva, K., Hutchings, N., Sorbara, L., Moayed, A.A., Simpson, T., 2011. *In vivo* volumetric imaging of the human corneo-scleral limbus with spectral domain OCT. Biomed. Optic Express 2, 1702–1794.
Bizheva, K., Lee, P., Sorbara, L., Hutchings, N., Simpson, T., 2010. *In vivo* volumetric imaging of the human upper eyelid with ultrahigh-resolution optical coherence tomography. J. Biomed. Optic. 15 040508.
Bizheva, K., Tan, B., MacLelan, B., Kralj, O., Hajialamdari, M., Hileeto, D., Sorbara, L., 2017a. Sub-micrometer axial resolution OCT for in-vivo imaging of the cellular structure of healthy and keratoconic human corneas. Biomed. Optic Express 8, 800–812.
Bizheva, K., Tan, B., MacLellan, B., Hosseinaee, Z., Mason, E., Hileeto, D., Sorbara, L., 2017b. In-vivo imaging of the palisades of Vogt and the limbal crypts with sub-micrometer axial resolution optical coherence tomography. Biomed. Optic Express 8, 4141–4151.
Boey, P.Y., Narayanaswamy, A., Zheng, C., Perera, S.A., Htoon, H.M., Tun, T.A., Seah, S.K., Wong, T.T., Aung, T., 2011. Imaging of blebs after phacotrabeculectomy with Ologen collagen matrix implants. Br. J. Ophthalmol. 95, 340–344.
Bose, S., Ang, M., Mehta, J.S., Tan, D.T., Finkelstein, E., 2013. Cost-effectiveness of Descemet's stripping endothelial keratoplasty versus penetrating keratoplasty. Ophthalmology 120, 464–470.
Braun, R.J., King-Smith, P.E., Begley, C.G., Li, L., Gewecke, N.R., 2015. Dynamics and function of the tear film in relation to the blink cycle. Prog. Retin. Eye Res. 45, 132–164.
Buckhurst, H.D., Gilmartin, B., Cubbidge, R.P., Logan, N.S., 2015. Measurement of scleral thickness in humans using anterior segment optical coherent tomography. PLoS One 10 e0132902.
Cai, Y., Alio Del Barrio, J.L., Wilkins, M.R., Ang, M., 2017. Serial optical coherence tomography angiography for corneal vascularization. Graefes Arch. Clin. Exp. Ophthalmol. 255, 135–139.
Chan, T.C., Biswas, S., Yu, M., Jhanji, V., 2015a. Longitudinal evaluation of cornea with swept-source optical coherence tomography and Scheimpflug imaging before and after lasik. Medicine (Baltim.) 94, e1219.
Chan, T.C., Liu, D., Yu, M., Jhanji, V., 2015b. Longitudinal evaluation of posterior corneal elevation after laser refractive surgery using swept-source optical coherence tomography. Ophthalmology 122, 687–692.
Chan, T.C.Y., Biswas, S., Yu, M., Jhanji, V., 2017. Comparison of corneal measurements in keratoconus using swept-source optical coherence tomography and combined Placido-Scheimpflug imaging. Acta Ophthalmol. 95, e486–e494.
Chandapura, R.S., Shetty, R., Shroff, R., Shilpy, N., Francis, M., Sinha Roy, A., 2018. OCT layered tomography of the cornea provides new insights on remodeling after photorefractive keratectomy. J. Biophot. 11.
Chang, J.H., Gabison, E.E., Kato, T., Azar, D.T., 2001. Corneal neovascularization. Curr. Opin. Ophthalmol. 12, 242–249.
Chen, C.L., Wang, R.K., 2017. Optical coherence tomography based angiography [Invited]. Biomed. Optic Express 8, 1056–1082.
Chen, J., Huang, H., Zhang, S., Chen, X., Sun, X., 2013. Expansion of Schlemm's canal by travoprost in healthy subjects determined by Fourier-domain optical coherence tomography. Invest. Ophthalmol. Vis. Sci. 54, 1127–1134.
Chen, Q., Wang, J., Tao, A., Shen, M., Jiao, S., Lu, F., 2010. Ultrahigh-resolution measurement by optical coherence tomography of dynamic tear film changes on contact lenses. Invest. Ophthalmol. Vis. Sci. 51, 1988–1993.
Cheung, C.Y., Zheng, C., Ho, C.L., Tun, T.A., Kumar, R.S., Sayyad, F.E., Wong, T.Y., Aung, T., 2011. Novel anterior-chamber angle measurements by high-definition optical coherence tomography using the Schwalbe line as the landmark. Br. J. Ophthalmol. 95, 955–959.
Choi, H.J., Lee, S.M., Lee, J.Y., Lee, S.Y., Kim, M.K., Wee, W.R., 2014. Measurement of anterior scleral curvature using anterior segment OCT. Optom. Vis. Sci. 91, 793–802.
Christopoulos, V., Kagemann, L., Wollstein, G., Ishikawa, H., Gabriele, M.L., Wojtkowski, M., Srinivasan, V., Fujimoto, J.G., Duker, J.S., Dhaliwal, D.K., Schuman, J.S., 2007. *In vivo* corneal high-speed, ultra high-resolution optical coherence tomography. Arch. Ophthalmol. 125, 1027–1035.
Consejo, A., Bartuzel, M.M., Iskander, D.R., 2017. Corneo-scleral limbal changes following short-term soft contact lens wear. Contact Lens Anterior Eye 40, 293–300.
Console, J.W., Sakata, L.M., Aung, T., Friedman, D.S., He, M., 2008. Quantitative analysis of anterior segment optical coherence tomography images: the Zhongshan Angle Assessment Program. Br. J. Ophthalmol. 92, 1612–1616.
Cui, L., Shen, M., Wang, J., Jiang, J., Li, M., Chen, D., Chen, Z., Tao, A., Lu, F., 2011. Age-related changes in tear menisci imaged by optical coherence tomography. Optom. Vis. Sci. 88, 1214–1219.
Cursiefen, C., Chen, L., Dana, M.R., Streilein, J.W., 2003. Corneal lymphangiogenesis: evidence, mechanisms, and implications for corneal transplant immunology. Cornea 22, 273–281.
Cwiklik, L., 2016. Tear film lipid layer: a molecular level view. Biochim. Biophys. Acta 1858, 2421–2430.
Dada, T., Sihota, R., Gadia, R., Aggarwal, A., Mandal, S., Gupta, V., 2007. Comparison of anterior segment optical coherence tomography and ultrasound biomicroscopy for assessment of the anterior segment. J. Cataract Refract. Surg. 33, 837–840.
Day, A.C., Garway-Heath, D.F., Broadway, D.C., Jiang, Y., Hayat, S., Dalzell, N., Khaw, K.T., Foster, P.J., 2013. Spectral domain optical coherence tomography imaging of the aqueous outflow structures in normal participants of the EPIC-Norfolk Eye Study. Br. J. Ophthalmol. 97, 189–195.
De Benito-Llopis, L., Mehta, J.S., Angunawela, R.I., Ang, M., Tan, D.T., 2014. Intraoperative anterior segment optical coherence tomography: a novel assessment tool during deep anterior lamellar keratoplasty. Am. J. Ophthalmol. 157, 334–341 e333.
de Boer, J.F., Hitzenberger, C.K., Yasuno, Y., 2017. Polarization sensitive optical coherence tomography - a review [Invited]. Biomed. Optic Express 8, 1838–1873.
DEWS, 2007. IThe definition and classification of dry eye disease: report of the definition and classification subcommittee of the international dry eye WorkShop (2007). Ocul. Surf. 5, 75–92.
Doh, S.H., Kim, E.C., Chung, S.Y., Kim, M.S., Chung, S.K., Shin, M.C., Hwang, H.S., 2015. Optical coherence tomography imaging of human lacrimal glands: an *in vivo* study. Ophthalmology 122, 2364–2366.
Dos Santos, V.A., Schmetterer, L., Triggs, G.J., Leitgeb, R.A., Groschl, M., Messner, A., Schmidl, D., Garhofer, G., Aschinger, G., Werkmeister, R.M., 2016. Super-resolved thickness maps of thin film phantoms and *in vivo* visualization of tear film lipid layer using OCT. Biomed. Optic Express 7, 2650–2670.
Dragostinoff, N., Werkmeister, R.M., Groschl, M., Schmetterer, L., 2009. Depth-resolved measurement of ocular fundus pulsations by low-coherence tissue interferometry. J. Biomed. Optic. 14 054047.
Drexler, W., Fujimoto, J., 2015. Optical Coherence Tomography, 2 ed. Springer International Publishing.
Ebneter, A., Haner, N.U., Zinkernagel, M.S., 2015. Metrics of the normal anterior sclera: imaging with optical coherence tomography. Graefes Arch. Clin. Exp. Ophthalmol. 253, 1575–1580.
Ehlers, J.P., Dupps, W.J., Kaiser, P.K., Goshe, J., Singh, R.P., Petkovsek, D., Srivastava, S.K., 2014a. The prospective intraoperative and perioperative ophthalmic ImagiNg with optical CoherEncE TomogRaphy (PIONEER) study: 2-year results. Am. J. Ophthalmol. 158, 999–1007.
Ehlers, J.P., Goshe, J., Dupps, W.J., Kaiser, P.K., Singh, R.P., Gans, R., Eisengart, J., Srivastava, S.K., 2015. Determination of feasibility and utility of microscope-integrated optical coherence tomography during ophthalmic surgery: the DISCOVER Study RESCAN Results. JAMA Ophthalmol 133, 1124–1132.
Ehlers, J.P., Kaiser, P.K., Srivastava, S.K., 2014b. Intraoperative optical coherence tomography using the RESCAN 700: preliminary results from the DISCOVER study. Br. J. Ophthalmol. 98, 1329–1332.
Ehlers, J.P., Srivastava, S.K., Feiler, D., Noonan, A.I., Rollins, A.M., Tao, Y.K., 2014c. Integrative advances for OCT-guided ophthalmic surgery and intraoperative OCT: microscope integration, surgical instrumentation, and heads-up display surgeon feedback. PLoS One 9 e105224.
Falke, K., Prakasam, R.K., Guthoff, R.F., Stachs, O., 2012. *In vivo* imaging of limbal epithelium and palisades of Vogt. Klin Monbl Augenheilkd 229, 1185–1190.
Feng, Y., Simpson, T.L., 2005. Comparison of human central cornea and limbus *in vivo* using optical coherence tomography. Optom. Vis. Sci. 82, 416–419.
Feng, Y., Varikooty, J., Simpson, T.L., 2001. Diurnal variation of corneal and corneal epithelial thickness measured using optical coherence tomography. Cornea 20, 480–483.
Fialova, S., Augustin, M., Fischak, C., Schmetterer, L., Handschuh, S., Glosmann, M., Pircher, M., Hitzenberger, C.K., Baumann, B., 2017. Posterior rat eye during acute intraocular pressure elevation studied using polarization sensitive optical coherence tomography. Biomed. Optic Express 8, 298–314.
Ford, M.R., Dupps Jr., W.J., Rollins, A.M., Sinha, R.A., Hu, Z., 2011. Method for optical coherence elastography of the cornea. J. Biomed. Optic. 16 016005.
Francis, A.W., Kagemann, L., Wollstein, G., Ishikawa, H., Folz, S., Overby, D.R., Sigal, I.A., Wang, B., Schuman, J.S., 2012. Morphometric analysis of aqueous humor outflow structures with spectral-domain optical coherence tomography. Invest. Ophthalmol. Vis. Sci. 53, 5198–5207.
Friedman, D.S., He, M., 2008. Anterior chamber angle assessment techniques. Surv. Ophthalmol. 53, 250–273.
Fu, H., Xu, Y., Lin, S., Zhang, X., Wong, D.W.K., Liu, J., Frangi, A., Baskaran, M., Aung, T., 2017. Segmentation and quantification for angle-closure glaucoma assessment in anterior segment OCT. IEEE Trans. Med. Imag. 36, 1930–1938.
Fuentes, E., Sandali, O., El Sanharawi, M., Basli, E., Hamiche, T., Goemaere, I., Borderie, V., Bouheraoua, N., Laroche, L., 2015. Anatomic predictive factors of acute corneal hydrops in keratoconus: an optical coherence tomography study. Ophthalmology 122, 1653–1659.

Fuest, M., Ang, M., Htoon, H.M., Tan, D., Mehta, J.S., 2017. Long-term visual outcomes comparing descemet stripping automated endothelial keratoplasty and penetrating keratoplasty. Am. J. Ophthalmol. 182, 62–71.
Fuest, M., Kuerten, D., Koch, E., Becker, J., Hirsch, T., Walter, P., Plange, N., 2016. Evaluation of early anatomical changes following canaloplasty with anterior segment spectral-domain optical coherence tomography and ultrasound biomicroscopy. Acta Ophthalmol. 94, e287–292.
Fujimoto, H., Maeda, N., Shintani, A., Nakagawa, T., Fuchihata, M., Higashiura, R., Nishida, K., 2016. Quantitative evaluation of the natural progression of keratoconus using three-dimensional optical coherence tomography. Invest. Ophthalmol. Vis. Sci. 57, OCT169–175.
Fukuda, S., Beheregaray, S., Kasaragod, D., Hoshi, S., Kishino, G., Ishii, K., Yasuno, Y., Oshika, T., 2014. Noninvasive evaluation of phase retardation in blebs after glaucoma surgery using anterior segment polarization-sensitive optical coherence tomography. Invest. Ophthalmol. Vis. Sci. 55, 5200–5206.
Fukuda, S., Yamanari, M., Lim, Y., Hoshi, S., Beheregaray, S., Oshika, T., Yasuno, Y., 2013. Keratoconus diagnosis using anterior segment polarization-sensitive optical coherence tomography. Invest. Ophthalmol. Vis. Sci. 54, 1384–1391.
Gao, S.S., Jia, Y., Zhang, M., Su, J.P., Liu, G., Hwang, T.S., Bailey, S.T., Huang, D., 2016. Optical coherence tomography angiography. Invest. Ophthalmol. Vis. Sci. 57, OCT27–36.
Garcia-De la Rosa, G., Olivo-Payne, A., Serna-Ojeda, J.C., Salazar-Ramos, M.S., Lichtinger, A., Gomez-Bastar, A., Ramirez-Miranda, A., Navas, A., Graue-Hernandez, E.O., 2018 Apr. Anterior segment optical coherence tomography angle and vault analysis after toric and non-toric implantable collamer lens V4c implantation in patients with high myopia. Br. J. Ophthalmol. 102 (4), 544–548.
Garcia-Lazaro, S., Belda-Salmeron, L., Ferrer-Blasco, T., Cervino, A., Montes-Mico, R., 2011. Comparison of two artificial tear formulations for dry eye through high-resolution optical coherence tomography. Clin. Exp. Optom. 94, 549–556.
Gasser, T., Romano, V., Seifarth, C., Bechrakis, N.E., Kaye, S.B., Steger, B., 2017. Morphometric characterisation of pterygium associated with corneal stromal scarring using high-resolution anterior segment optical coherence tomography. Br. J. Ophthalmol. 101, 660–664.
Ge, L., Yuan, Y., Shen, M., Tao, A., Wang, J., Lu, F., 2013. The role of axial resolution of optical coherence tomography on the measurement of corneal and epithelial thicknesses. Invest. Ophthalmol. Vis. Sci. 54, 746–755.
Ghouali, W., Tahiri Joutei Hassani, R., Djerada, Z., Liang, H., El Sanharawi, M., Labbe, A., Baudouin, C., 2017. *In vivo* imaging of palisades of Vogt in dry eye versus normal subjects using en-face spectral-domain optical coherence tomography. PLoS One 12 e0187864.
Girard, M.J., Ang, M., Chung, C.W., Farook, M., Strouthidis, N., Mehta, J.S., Mari, J.M., 2015. Enhancement of corneal visibility in optical coherence tomography images using corneal adaptive compensation. Transl Vis Sci Technol 4, 3.
Gora, M., Karnowski, K., Szkulmowski, M., Kaluzny, B.J., Huber, R., Kowalczyk, A., Wojtkowski, M., 2009. Ultra high-speed swept source OCT imaging of the anterior segment of human eye at 200 kHz with adjustable imaging range. Optic Express 17, 14880–14894.
Gotzinger, E., Pircher, M., Dejaco-Ruhswurm, I., Kaminski, S., Skorpik, C., Hitzenberger, C.K., 2007. Imaging of birefringent properties of keratoconus corneas by polarization-sensitive optical coherence tomography. Invest. Ophthalmol. Vis. Sci. 48, 3551–3558.
Gotzinger, E., Pircher, M., Sticker, M., Fercher, A.F., Hitzenberger, C.K., 2004. Measurement and imaging of birefringent properties of the human cornea with phase-resolved, polarization-sensitive optical coherence tomography. J. Biomed. Optic. 9, 94–102.
Gozawa, M., Takamura, Y., Miyake, S., Iwasaki, K., Arimura, S., Takihara, Y., Inatani, M., 2017. Comparison of subconjunctival scarring after microincision vitrectomy surgery using 20-, 23-, 25- and 27-gauge systems in rabbits. Acta Ophthalmol. 95, e602–e609.
Grewal, D.S., Schultz, T., Basti, S., Dick, H.B., 2016. Femtosecond laser-assisted cataract surgery–current status and future directions. Surv. Ophthalmol. 61, 103–131.
Grieve, K., Ghoubay, D., Georgeon, C., Thouvenin, O., Bouheraoua, N., Paques, M., Borderie, V.M., 2015. Three-dimensional structure of the mammalian limbal stem cell niche. Exp. Eye Res. 140, 75–84.
Haagdorens, M., Behaegel, J., Rozema, J., Van Gerwen, V., Michiels, S., Ni Dhubhghaill, S., Tassignon, M.J., Zakaria, N., 2017. A method for quantifying limbal stem cell niches using OCT imaging. Br. J. Ophthalmol. 101, 1250–1255.
Haner, N.U., Dysli, M., Abegg, M., Zinkernagel, M.S., 2015. Enhanced-depth optical coherence tomography for imaging horizontal rectus muscles in Graves' orbitopathy. Graefes Arch. Clin. Exp. Ophthalmol. 253, 1569–1573.
Hirano, K., Ito, Y., Suzuki, T., Kojima, T., Kachi, S., Miyake, Y., 2001. Optical coherence tomography for the noninvasive evaluation of the cornea. Cornea 20, 281–289.
Hirnschall, N., Buehren, T., Bajramovic, F., Trost, M., Teuber, T., Findl, O., 2017. Prediction of postoperative intraocular lens tilt using swept-source optical coherence tomography. J. Cataract Refract. Surg. 43, 732–736.
Hoffmann, P.C., Abraham, M., Hirnschall, N., Findl, O., 2014. Prediction of residual astigmatism after cataract surgery using swept source fourier domain optical coherence tomography. Curr. Eye Res. 39, 1178–1186.
Hong, J., Xu, J., Wei, A., Wen, W., Chen, J., Yu, X., Sun, X., 2013. Spectral-domain optical coherence tomographic assessment of Schlemm's canal in Chinese subjects with primary open-angle glaucoma. Ophthalmology 120, 709–715.
Hong, J., Yang, Y., Wei, A., Deng, S.X., Kong, X., Chen, J., Girard, M.J., Mari, J.M., Xu, J., Sun, X., 2014. Schlemm's canal expands after trabeculectomy in patients with primary angle-closure glaucoma. Invest. Ophthalmol. Vis. Sci. 55, 5637–5642.
Hoy, S.M., 2017. Ciclosporin ophthalmic emulsion 0.1%: a review in severe dry eye disease. Drugs 77, 1909–1916.
Hsieh, B.Y., Song, S., Nguyen, T.M., Yoon, S.J., Shen, T.T., Wang, R.K., O'Donnell, M., 2016. Moving-source elastic wave reconstruction for high-resolution optical coherence elastography. J. Biomed. Optic. 21, 116006.
Huang, A.S., Belghith, A., Dastiridou, A., Chopra, V., Zangwill, L.M., Weinreb, R.N., 2017. Automated circumferential construction of first-order aqueous humor outflow pathways using spectral-domain optical coherence tomography. J. Biomed. Optic. 22, 66010.
Huang, D., Swanson, E.A., Lin, C.P., Schuman, J.S., Stinson, W.G., Chang, W., Hee, M.R., Flotte, T., Gregory, K., Puliafito, C.A., et al., 1991. Optical coherence tomography. Science 254, 1178–1181.
Huang, J., Clarkson, E., Kupinski, M., Lee, K.S., Maki, K.L., Ross, D.S., Aquavella, J.V., Rolland, J.P., 2013a. Maximum-likelihood estimation in Optical Coherence Tomography in the context of the tear film dynamics. Biomed. Optic Express 4, 1806–1816.
Huang, J., Hindman, H.B., Rolland, J.P., 2016. *In vivo* thickness dynamics measurement of tear film lipid and aqueous layers with optical coherence tomography and maximum-likelihood estimation. Opt. Lett. 41, 1981–1984.
Huang, J., Lee, K.S., Clarkson, E., Kupinski, M., Maki, K.L., Ross, D.S., Aquavella, J.V., Rolland, J.P., 2013b. Phantom study of tear film dynamics with optical coherence tomography and maximum-likelihood estimation. Opt. Lett. 38, 1721–1723.
Huang, J., Yuan, Q., Zhang, B., Xu, K., Tankam, P., Clarkson, E., Kupinski, M.A., Hindman, H.B., Aquavella, J.V., Suleski, T.J., Rolland, J.P., 2014. Measurement of a multi-layered tear film phantom using optical coherence tomography and statistical decision theory. Biomed. Optic Express 5, 4374–4386.
Huo, T., Wang, C., Zhang, X., Chen, T., Liao, W., Zhang, W., Ai, S., Hsieh, J.C., Xue, P., 2015. Ultrahigh-speed optical coherence tomography utilizing all-optical 40 MHz swept-source. J. Biomed. Optic. 20 030503.
Hutchings, N., Simpson, T.L., Hyun, C., Moayed, A.A., Hariri, S., Sorbara, L., Bizheva, K., 2010. Swelling of the human cornea revealed by high-speed, ultrahigh-resolution optical coherence tomography. Invest. Ophthalmol. Vis. Sci. 51, 4579–4584.
Hwang, H.S., Park, C.W., Joo, C.K., 2013a. Novel noncontact meibography with anterior segment optical coherence tomography: hosik meibography. Cornea 32, 40–43.
Hwang, H.S., Shin, J.G., Lee, B.H., Eom, T.J., Joo, C.K., 2013b. *In vivo* 3D meibography of the human eyelid using real time imaging fourier-domain OCT. PLoS One 8 e67143.
Ibrahim, O.M., Dogru, M., Kawashima, S., Wakamatsu, T.H., Tsubota, K., Fujishima, H., 2013. Visante optical coherence tomography and tear function test evaluation of cholinergic treatment response in patients with sjogren syndrome. Cornea 32, 653–657.
Ibrahim, O.M., Dogru, M., Takano, Y., Satake, Y., Wakamatsu, T.H., Fukagawa, K., Tsubota, K., Fujishima, H., 2010. Application of visante optical coherence tomography tear meniscus height measurement in the diagnosis of dry eye disease. Ophthalmology 117, 1923–1929.
Imamoglu, S., Sevim, M.S., Alpogan, O., Ercalik, N.Y., Kumral, E.T., Pekel, G., Bardak, H., 2016. *In vivo* biometric evaluation of Schlemm's canal with spectral-domain optical coherence tomography in pseuduexfoliation glaucoma. Acta Ophthalmol. 94, e688–e692.
Ishida, S., Nishizawa, N., 2012. Quantitative comparison of contrast and imaging depth of ultrahigh-resolution optical coherence tomography images in 800-1700 nm wavelength region. Biomed. Optic Express 3, 282–294.
Izatt, J.A., Hee, M.R., Swanson, E.A., Lin, C.P., Huang, D., Schuman, J.S., Puliafito, C.A., Fujimoto, J.G., 1994. Micrometer-scale resolution imaging of the anterior eye *in vivo* with optical coherence tomography. Arch. Ophthalmol. 112, 1584–1589.
Jiang, Y., Chang, D.S., Zhu, H., Khawaja, A.P., Aung, T., Huang, S., Chen, Q., Munoz, B., Grossi, C.M., He, M., Friedman, D.S., Foster, P.J., 2014. Longitudinal changes of angle configuration in primary angle-closure suspects: the Zhongshan angle-closure prevention trial. Ophthalmology 121, 1699–1705.
Johnstone, M.A., 2004. The aqueous outflow system as a mechanical pump: evidence from examination of tissue and aqueous movement in human and non-human primates. J. Glaucoma 13, 421–438.
Jonnal, R.S., Kocaoglu, O.P., Zawadzki, R.J., Liu, Z., Miller, D.T., Werner, J.S., 2016. A review of adaptive optics optical coherence tomography: technical advances, scientific applications, and the future. Invest. Ophthalmol. Vis. Sci. 57, OCT51–68.
Ju, M.J., Tang, S., 2015. Usage of polarization-sensitive optical coherence tomography for investigation of collagen cross-linking. J. Biomed. Optic. 20 046001.
Kagemann, L., Wang, B., Wollstein, G., Ishikawa, H., Nevins, J.E., Nadler, Z., Sigal, I.A., Bilonick, R.A., Schuman, J.S., 2014. IOP elevation reduces Schlemm's canal cross-sectional area. Invest. Ophthalmol. Vis. Sci. 55, 1805–1809.
Kagemann, L., Wollstein, G., Ishikawa, H., Bilonick, R.A., Brennen, P.M., Folio, L.S., Gabriele, M.L., Schuman, J.S., 2010. Identification and assessment of Schlemm's canal by spectral-domain optical coherence tomography. Invest. Ophthalmol. Vis. Sci. 51, 4054–4059.
Kagemann, L., Wollstein, G., Ishikawa, H., Nadler, Z., Sigal, I.A., Folio, L.S., Schuman, J.S., 2012. Visualization of the conventional outflow pathway in the living human eye. Ophthalmology 119, 1563–1568.
Kalev-Landoy, M., Day, A.C., Cordeiro, M.F., Migdal, C., 2007. Optical coherence tomography in anterior segment imaging. Acta Ophthalmol. 85, 427–430.
Kaluzny, B.J., Kaluzny, J.J., Szkulmowska, A., Gorczynska, I., Szkulmowski, M., Bajraszewski, T., Wojtkowski, M., Targowski, P., 2006. Spectral optical coherence tomography: a novel technique for cornea imaging. Cornea 25, 960–965.
Kamal, S., Ali, M.J., Ali, M.H., Naik, M.N., 2016. Fourier domain optical coherence tomography with 3D and en face imaging of the punctum and vertical canaliculus: a step toward establishing a normative database. Ophthalmic Plast. Reconstr. Surg. 32, 170–173.
Karimi, A.H., Wong, A., Bizheva, K., 2011. Automated detection and cell density assessment of keratocytes in the human corneal stroma from ultrahigh resolution optical coherence tomograms. Biomed. Optic Express 2, 2905–2916.
Kashani, A.H., Chen, C.L., Gahm, J.K., Zheng, F., Richter, G.M., Rosenfeld, P.J., Shi, Y., Wang, R.K., 2017. Optical coherence tomography angiography: a comprehensive

review of current methods and clinical applications. Prog. Retin. Eye Res. 60, 66–100.
Kaya, S., Schmidl, D., Schmetterer, L., Witkowska, K.J., Unterhuber, A., Aranha Dos Santos, V., Baar, C., Garhofer, G., Werkmeister, R.M., 2015. Effect of hyaluronic acid on tear film thickness as assessed with ultra-high resolution optical coherence tomography. Acta Ophthalmol. 93, 439–443.
Keating, G.M., 2017. Lifitegrast ophthalmic solution 5%: a review in dry eye disease. Drugs 77, 201–208.
Kim, T.I., Hong, J.P., Ha, B.J., Stulting, R.D., Kim, E.K., 2010. Determination of treatment strategies for granular corneal dystrophy type 2 using Fourier-domain optical coherence tomography. Br. J. Ophthalmol. 94, 341–345.
King-Smith, P.E., Nichols, J.J., Nichols, K.K., Fink, B.A., Braun, R.J., 2008. Contributions of evaporation and other mechanisms to tear film thinning and break-up. Optom. Vis. Sci. 85, 623–630.
Kirby, M.A., Pelivanov, I., Song, S., Ambrozinski, L., Yoon, S.J., Gao, L., Li, D., Shen, T.T., Wang, R.K., O'Donnell, M., 2017. Optical coherence elastography in ophthalmology. J. Biomed. Optic. 22, 1–28.
Kirwan, R.P., Zheng, Y., Tey, A., Anijeet, D., Sueke, H., Kaye, S.B., 2012. Quantifying changes in corneal neovascularization using fluorescein and indocyanine green angiography. Am. J. Ophthalmol. 154, 850–858 e852.
Koh, S., Tung, C., Kottaiyan, R., Zavislan, J., Yoon, G., Aquavella, J., 2012. Effect of airflow exposure on the tear meniscus. Journal of ophthalmology 2012, 983182.
Kolb, J.P., Klein, T., Kufner, C.L., Wieser, W., Neubauer, A.S., Huber, R., 2015. Ultra-widefield retinal MHz-OCT imaging with up to 100 degrees viewing angle. Biomed. Optic Express 6, 1534–1552.
Konstantopoulos, A., Kuo, J., Anderson, D., Hossain, P., 2008. Assessment of the use of anterior segment optical coherence tomography in microbial keratitis. Am. J. Ophthalmol. 146, 534–542.
Lai, I., Mak, H., Lai, G., Yu, M., Lam, D.S., Leung, C.K., 2013. Anterior chamber angle imaging with swept-source optical coherence tomography: measuring peripheral anterior synechia in glaucoma. Ophthalmology 120, 1144–1149.
Lathrop, K.L., Gupta, D., Kagemann, L., Schuman, J.S., Sundarraj, N., 2012. Optical coherence tomography as a rapid, accurate, noncontact method of visualizing the palisades of Vogt. Invest. Ophthalmol. Vis. Sci. 53, 1381–1387.
Lavanya, R., Foster, P.J., Sakata, L.M., Friedman, D.S., Kashiwagi, K., Wong, T.Y., Aung, H.T., Alfred, T., Gao, H., Ee, A.G., Seah, S.K., Aung, T., 2008. Screening for narrow angles in the Singapore population: evaluation of new noncontact screening methods. Ophthalmology 115, 1720–1727 1727.e1721-1722.
Lavinsky, F., Lavinsky, D., 2016. Novel perspectives on swept-source optical coherence tomography. Int J Retina Vitreous 2, 25.
Lawman, S., Dong, Y., Williams, B.M., Romano, V., Kaye, S., Harding, S.P., Willoughby, C., Shen, Y.C., Zheng, Y., 2016. High resolution corneal and single pulse imaging with line field spectral domain optical coherence tomography. Optic Express 24, 12395–12405.
Lee, K.S., Sung, K.R., Shon, K., Sun, J.H., Lee, J.R., 2013. Longitudinal changes in anterior segment parameters after laser peripheral iridotomy assessed by anterior segment optical coherence tomography. Invest. Ophthalmol. Vis. Sci. 54, 3166–3170.
Lee, P., Wang, C.C., Adamis, A.P., 1998. Ocular neovascularization: an epidemiologic review. Surv. Ophthalmol. 43, 245–269.
Lee, R.Y., Huang, G., Cui, Q.N., He, M., Porco, T.C., Lin, S.C., 2012. Association of lens vault with narrow angles among different ethnic groups. Curr. Eye Res. 37, 486–491.
Leitgeb, R., Hitzenberger, C., Fercher, A., 2003. Performance of fourier domain vs. time domain optical coherence tomography. Optic Express 11, 889–894.
Leitgeb, R.A., Werkmeister, R.M., Blatter, C., Schmetterer, L., 2014. Doppler optical coherence tomography. Prog. Retin. Eye Res. 41, 26–43.
Leung, C.K., Chan, W.M., Ko, C.Y., Chui, S.I., Woo, J., Tsang, M.K., Tse, R.K., 2005. Visualization of anterior chamber angle dynamics using optical coherence tomography. Ophthalmology 112, 980–984.
Leung, C.K., Cheung, C.Y., Li, H., Dorairaj, S., Yiu, C.K., Wong, A.L., Liebmann, J., Ritch, R., Weinreb, R., Lam, D.S., 2007. Dynamic analysis of dark-light changes of the anterior chamber angle with anterior segment OCT. Invest. Ophthalmol. Vis. Sci. 48, 4116–4122.
Leung, C.K., Li, H., Weinreb, R.N., Liu, J., Cheung, C.Y., Lai, R.Y., Pang, C.P., Lam, D.S., 2008. Anterior chamber angle measurement with anterior segment optical coherence tomography: a comparison between slit lamp OCT and Visante OCT. Invest. Ophthalmol. Vis. Sci. 49, 3469–3474.
Leung, C.K., Yung, W.H., Yiu, C.K., Lam, S.W., Leung, D.Y., Tse, R.K., Tham, C.C., Chan, W.M., Lam, D.S., 2006. Novel approach for anterior chamber angle analysis: anterior chamber angle detection with edge measurement and identification algorithm (ACADEMIA). Arch. Ophthalmol. 124, 1395–1401.
Levison, A.L., Lowder, C.Y., Baynes, K.M., Kaiser, P.K., Srivastava, S.K., 2016. Anterior segment spectral domain optical coherence tomography imaging of patients with anterior scleritis. Int. Ophthalmol. 36, 499–508.
Li, G., Farsiu, S., Chiu, S.J., Gonzalez, P., Lutjen-Drecoll, E., Overby, D.R., Stamer, W.D., 2014a. Pilocarpine-induced dilation of Schlemm's canal and prevention of lumen collapse at elevated intraocular pressures in living mice visualized by OCT. Invest. Ophthalmol. Vis. Sci. 55, 3737–3746.
Li, G., Mukherjee, D., Navarro, I., Ashpole, N.E., Sherwood, J.M., Chang, J., Overby, D.R., Yuan, F., Gonzalez, P., Kopczynski, C.C., Farsiu, S., Stamer, W.D., 2016a. Visualization of conventional outflow tissue responses to netarsudil in living mouse eyes. Eur. J. Pharmacol. 787, 20–31.
Li, J., Shen, M., Wang, J., Ma, H., Tao, A., Xu, S., Lu, F., 2012a. Clinical significance of tear menisci in dry eye. Eye Contact Lens 38, 183–187.
Li, P., An, L., Reif, R., Shen, T.T., Johnstone, M., Wang, R.K., 2011. *In vivo* microstructural and microvascular imaging of the human corneo-scleral limbus using optical coherence tomography. Biomed. Optic Express 2, 3109–3118.
Li, P., Butt, A., Chien, J.L., Ghassibi, M.P., Furlanetto, R.L., Netto, C.F., Liu, Y., Kirkland, W., Liebmann, J.M., Ritch, R., Park, S.C., 2017. Characteristics and variations of *in vivo* Schlemm's canal and collector channel microstructures in enhanced-depth imaging optical coherence tomography. Br. J. Ophthalmol. 101, 808–813.
Li, P., Reif, R., Zhi, Z., Martin, E., Shen, T.T., Johnstone, M., Wang, R.K., 2012b. Phase-sensitive optical coherence tomography characterization of pulse-induced trabecular meshwork displacement in ex vivo nonhuman primate eyes. J. Biomed. Optic. 17 076026.
Li, Y., Chamberlain, W., Tan, O., Brass, R., Weiss, J.L., Huang, D., 2016c. Subclinical keratoconus detection by pattern analysis of corneal and epithelial thickness maps with optical coherence tomography. J. Cataract Refract. Surg. 42, 284–295.
Li, Y., Lu, C.D., Jia, Y., 2015. Anterior segment angiography with 1050 nm swept-source optical coherence tomography. Invest. Ophthalmol. Vis. Sci. 56, 4512.
Li, Y., Netto, M.V., Shekhar, R., Krueger, R.R., Huang, D., 2007. A longitudinal study of LASIK flap and stromal thickness with high-speed optical coherence tomography. Ophthalmology 114, 1124–1132.
Li, Y., Tan, O., Brass, R., Weiss, J.L., Huang, D., 2012c. Corneal epithelial thickness mapping by Fourier-domain optical coherence tomography in normal and keratoconic eyes. Ophthalmology 119, 2425–2433.
Li, Y., Wang, Y.E., Huang, G., Wang, D., He, M., Qiu, M., Lin, S., 2014b. Prevalence and characteristics of plateau iris configuration among American Caucasian, American Chinese and mainland Chinese subjects. Br. J. Ophthalmol. 98, 474–478.
Liang, Q., Pan, Z., Zhou, M., Zhang, Y., Wang, N., Li, B., Baudouin, C., Labbe, A., 2015. Evaluation of optical coherence tomography meibography in patients with obstructive meibomian gland dysfunction. Cornea 34, 1193–1199.
Lim, H., Jiang, Y., Wang, Y., Huang, Y.C., Chen, Z., Wise, F.W., 2005. Ultrahigh-resolution optical coherence tomography with a fiber laser source at 1 microm. Opt. Lett. 30, 1171–1173.
Lim, L.S., Aung, H.T., Aung, T., Tan, D.T., 2008. Corneal imaging with anterior segment optical coherence tomography for lamellar keratoplasty procedures. Am. J. Ophthalmol. 145, 81–90.
Lim, Y., Yamanari, M., Fukuda, S., Kaji, Y., Kiuchi, T., Miura, M., Oshika, T., Yasuno, Y., 2011. Birefringence measurement of cornea and anterior segment by office-based polarization-sensitive optical coherence tomography. Biomed. Optic Express 2, 2392–2402.
Lin, T., Gong, L., Liu, X., Ma, X., 2015. Fourier-domain optical coherence tomography for monitoring the lower tear meniscus in dry eye after acupuncture treatment. Evid Based Complement Alternat Med 2015, 492150.
Liu, L., Gardecki, J.A., Nadkarni, S.K., Toussaint, J.D., Yagi, Y., Bouma, B.E., Tearney, G.J., 2011a. Imaging the subcellular structure of human coronary atherosclerosis using micro-optical coherence tomography. Nat. Med. 17, 1010–1014.
Liu, Y.C., Lwin, N.C., Chan, N.S., Mehta, J.S., 2014. Use of anterior segment optical coherence tomography to predict corneal graft rejection in small animal models. Invest. Ophthalmol. Vis. Sci. 55, 6736–6741.
Liu, X., Wang, F., Xiao, Y., Ye, X., Hou, L., 2011b. Measurement of the limbus-insertion distance in adult strabismus patients with anterior segment optical coherence tomography. Invest. Ophthalmol. Vis. Sci. 52, 8370–8373.
Lluch, S., Julio, G., Pujol, P., Merindano, D., 2016. What biomarkers explain about pterygium OCT pattern. Graefes Arch. Clin. Exp. Ophthalmol. 254, 143–148.
Lucisano, A., Ferrise, M., Balestrieri, M., Busin, M., Scorcia, V., 2017. Evaluation of postoperative toric intraocular lens alignment with anterior segment optical coherence tomography. J. Cataract Refract. Surg. 43, 1007–1009.
Manapuram, R.K., Aglyamov, S.R., Monediado, F.M., Mashiatulla, M., Li, J., Emelianov, S.Y., Larin, K.V., 2012. *In vivo* estimation of elastic wave parameters using phase-stabilized swept source optical coherence elastography. J. Biomed. Optic. 17, 100501.
Matalia, H., Francis, M., Gangil, T., Chandapura, R.S., Kurian, M., Shetty, R., Nelson, E.J.R., Sinha Roy, A., 2017. Noncontact quantification of topography of anterior corneal surface and Bowman's layer with high-speed OCT. J. Refract. Surg. 33, 330–336.
McNabb, R.P., Farsiu, S., Stinnett, S.S., Izatt, J.A., Kuo, A.N., 2015. Optical coherence tomography accurately measures corneal power change from laser refractive surgery. Ophthalmology 122, 677–686.
Mi, H., Tan, N., Ang, M., Htoon, H.M., Mehta, J.S., 2015. Comparison of anterior and posterior topographic analysis between 3 imaging systems. J. Cataract Refract. Surg. 41, 2533–2545.
Moon, S., Kim, D.Y., 2006. Ultra-high-speed optical coherence tomography with a stretched pulse supercontinuum source. Optic Express 14, 11575–11584.
Moutsouris, K., Dapena, I., Ham, L., Balachandran, C., Oellerich, S., Melles, G.R., 2011. Optical coherence tomography, Scheimpflug imaging, and slit-lamp biomicroscopy in the early detection of graft detachment after Descemet membrane endothelial keratoplasty. Cornea 30, 1369–1375.
Nahas, A., Bauer, M., Roux, S., Boccara, A.C., 2013. 3D static elastography at the micrometer scale using full field OCT. Biomed. Optic Express 4, 2138–2149.
Nanji, A.A., Sayyad, F.E., Galor, A., Dubovy, S., Karp, C.L., 2015. High-resolution optical coherence tomography as an adjunctive tool in the diagnosis of corneal and conjunctival pathology. Ocul. Surf. 13, 226–235.
Napoli, P.E., Coronella, F., Satta, G.M., Fossarello, M., 2014a. A novel technique of contrast-enhanced optical coherence tomography imaging in evaluation of clearance of lipids in human tears. PLoS One 9 e109843.
Napoli, P.E., Coronella, F., Satta, G.M., Iovino, C., Sanna, R., Fossarello, M., 2016. A simple novel technique of infrared meibography by means of spectral-domain optical coherence tomography: a cross-sectional clinical study. PLoS One 11 e0165558.
Napoli, P.E., Satta, G.M., Coronella, F., Fossarello, M., 2014b. Spectral-domain optical coherence tomography study on dynamic changes of human tears after instillation of artificial tears. Invest. Ophthalmol. Vis. Sci. 55, 4533–4540.
Narayanaswamy, A., Sakata, L.M., He, M.G., Friedman, D.S., Chan, Y.H., Lavanya, R.,

Baskaran, M., Foster, P.J., Aung, T., 2010. Diagnostic performance of anterior chamber angle measurements for detecting eyes with narrow angles: an anterior segment OCT study. Arch. Ophthalmol. 128, 1321–1327.
Nguyen, P., Chopra, V., 2013. Applications of optical coherence tomography in cataract surgery. Curr. Opin. Ophthalmol. 24, 47–52.
Nguyen, P., Huang, D., Li, Y., Sadda, S.R., Ramos, S., Pappuru, R.R., Yiu, S.C., 2012. Correlation between optical coherence tomography-derived assessments of lower tear meniscus parameters and clinical features of dry eye disease. Cornea 31, 680–685.
Nguyen, T.M., Arnal, B., Song, S., Huang, Z., Wang, R.K., O'Donnell, M., 2015. Shear wave elastography using amplitude-modulated acoustic radiation force and phase-sensitive optical coherence tomography. J. Biomed. Optic. 20 016001.
Nichols, J.J., Mitchell, G.L., King-Smith, P.E., 2005. Thinning rate of the precorneal and prelens tear films. Invest. Ophthalmol. Vis. Sci. 46, 2353–2361.
Niederkorn, J.Y., 2010. High-risk corneal allografts and why they lose their immune privilege. Curr. Opin. Allergy Clin. Immunol. 10, 493–497.
Nishizawa, N., Chen, Y., Hsiung, P., Ippen, E.P., Fujimoto, J.G., 2004. Real-time, ultra-high-resolution, optical coherence tomography with an all-fiber, femtosecond fiber laser continuum at 1.5 microm. Opt. Lett. 29, 2846–2848.
Niwas, S.I., Lin, W., Bai, X., Kwoh, C.K., Jay Kuo, C.C., Sng, C.C., Aquino, M.C., Chew, P.T., 2016. Automated anterior segment OCT image analysis for Angle Closure Glaucoma mechanisms classification. Comput. Meth. Progr. Biomed. 130, 65–75.
Nolan, W.P., See, J.L., Chew, P.T., Friedman, D.S., Smith, S.D., Radhakrishnan, S., Zheng, C., Foster, P.J., Aung, T., 2007. Detection of primary angle closure using anterior segment optical coherence tomography in Asian eyes. Ophthalmology 114, 33–39.
Nongpiur, M.E., Gong, T., Lee, H.K., Perera, S.A., Cheng, L., Foo, L.L., He, M., Friedman, D.S., Aung, T., 2013a. Subgrouping of primary angle-closure suspects based on anterior segment optical coherence tomography parameters. Ophthalmology 120, 2525–2531.
Nongpiur, M.E., Haaland, B.A., Friedman, D.S., Perera, S.A., He, M., Foo, L.L., Baskaran, M., Sakata, L.M., Wong, T.Y., Aung, T., 2013b. Classification algorithms based on anterior segment optical coherence tomography measurements for detection of angle closure. Ophthalmology 120, 48–54.
Nongpiur, M.E., He, M., Amerasinghe, N., Friedman, D.S., Tay, W.T., Baskaran, M., Smith, S.D., Wong, T.Y., Aung, T., 2011. Lens vault, thickness, and position in Chinese subjects with angle closure. Ophthalmology 118, 474–479.
Nongpiur, M.E., Sakata, L.M., Friedman, D.S., He, M., Chan, Y.H., Lavanya, R., Wong, T.Y., Aung, T., 2010. Novel association of smaller anterior chamber width with angle closure in Singaporeans. Ophthalmology 117, 1967–1973.
Nozaki, M., Kimura, H., Kojima, M., Ogura, Y., 2002. Optical coherence tomographic findings of the anterior segment after nonpenetrating deep sclerectomy. Am. J. Ophthalmol. 133, 837–839.
O'Hara, K.E., Schmoll, T., Vass, C., Leitgeb, R.A., 2013. Measuring pulse-induced natural relative motions within human ocular tissue *in vivo* using phase-sensitive optical coherence tomography. J. Biomed. Optic. 18, 121506.
Ong, S.S., Vora, G.K., Gupta, P.K., 2016. Anterior segment imaging in ocular surface squamous neoplasia. J Ophthalmol 2016, 5435092.
Ortiz, S., Perez-Merino, P., Alejandre, N., Gambra, E., Jimenez-Alfaro, I., Marcos, S., 2012. Quantitative OCT-based corneal topography in keratoconus with intracorneal ring segments. Biomed. Optic Express 3, 814–824.
Pahuja, N., Shroff, R., Pahanpate, P., Francis, M., Veeboy, L., Shetty, R., Nuijts, R., Roy, A.S., 2017. Application of high resolution OCT to evaluate irregularity of Bowman's layer in asymmetric keratoconus. J. Biophot. 10, 701–707.
Palakuru, J.R., Wang, J., Aquavella, J.V., 2007. Effect of blinking on tear dynamics. Invest. Ophthalmol. Vis. Sci. 48, 3032–3037.
Park, D.I., Shin, H.M., Lee, S.Y., Lew, H., 2013. Tear production and drainage after botulinum toxin A injection in patients with essential blepharospasm. Acta Ophthalmol. 91, e108–112.
Pasricha, N.D., Bhullar, P.K., Shieh, C., Carrasco-Zevallos, O.M., Keller, B., Izatt, J.A., Toth, C.A., Freedman, S.F., Kuo, A.N., 2017. Four-dimensional microscope-integrated optical coherence tomography to visualize suture depth in strabismus surgery. J. Pediatr. Ophthalmol. Strabismus 54, e1–e5.
Paulaviciute-Baikstiene, D., Vaiciuliene, R., Jasinskas, V., Januleviciene, I., 2016. Evaluation of outflow structures *in vivo* after the phacocanaloplasty. J Ophthalmol 2016, 4519846.
Pflugfelder, S.C., Tseng, S.C., Sanabria, O., Kell, H., Garcia, C.G., Felix, C., Feuer, W., Reis, B.L., 1998. Evaluation of subjective assessments and objective diagnostic tests for diagnosing tear-film disorders known to cause ocular irritation. Cornea 17, 38–56.
Pihlblad, M.S., Erenler, F., Sharma, A., Manchandia, A., Reynolds, J.D., 2016. Anterior segment optical coherence tomography of the horizontal and vertical extraocular muscles with measurement of the insertion to limbus distance. J. Pediatr. Ophthalmol. Strabismus 53, 141–145.
Pihlblad, M.S., Reynolds, J.D., 2017. Anterior segment optical coherence tomography of previously operated extraocular muscles. Am. Orthopt. J. 67, 61–66.
Pircher, M., Hitzenberger, C.K., Schmidt-Erfurth, U., 2011. Polarization sensitive optical coherence tomography in the human eye. Prog. Retin. Eye Res. 30, 431–451.
Poddar, R., Zawadzki, R.J., Cortes, D.E., Mannis, M.J., Werner, J.S., 2015. *In vivo* volumetric depth-resolved vasculature imaging of human limbus and sclera with 1mum swept source phase-variance optical coherence angiography. J. Optic. 17.
Polans, J., Keller, B., Carrasco-Zevallos, O.M., LaRocca, F., Cole, E., Whitson, H.E., Lad, E.M., Farsiu, S., Izatt, J.A., 2017. Wide-field retinal optical coherence tomography with wavefront sensorless adaptive optics for enhanced imaging of targeted regions. Biomed. Optic Express 8, 16–37.
Potsaid, B., Gorczynska, I., Srinivasan, V.J., Chen, Y., Jiang, J., Cable, A., Fujimoto, J.G., 2008 Sep 15. Ultrahigh speed spectral / Fourier domain OCT ophthalmic imaging at 70,000 to 312,500 axial scans per second. Opt. Express 16 (19), 15149–15169.
Quigley, H.A., Silver, D.M., Friedman, D.S., He, M., Plyler, R.J., Eberhart, C.G., Jampel, H.D., Ramulu, P., 2009. Iris cross-sectional area decreases with pupil dilation and its dynamic behavior is a risk factor in angle closure. J. Glaucoma 18, 173–179.
Radhakrishnan, S., Rollins, A.M., Roth, J.E., Yazdanfar, S., Westphal, V., Bardenstein, D.S., Izatt, J.A., 2001. Real-time optical coherence tomography of the anterior segment at 1310 nm. Arch. Ophthalmol. 119, 1179–1185.
Raj, A., Dhasmana, R., Nagpal, R.C., 2016. Anterior segment optical coherence tomography for tear meniscus evaluation and its correlation with other tear variables in healthy individuals. J. Clin. Diagn. Res. 10, NC01–04.
Reddy, H.S., Li, Y., Yiu, S.C., Irvine, J.A., Huang, D., 2007. Optical coherence tomography of corneal and scleral melts. Ophthalmic Surg. Laser. Imag. 38, 514–517.
Resnikoff, S., Pascolini, D., Etya'ale, D., Kocur, I., Pararajasegaram, R., Pokharel, G.P., Mariotti, S.P., 2004. Global data on visual impairment in the year 2002. Bull. World Health Organ. 82, 844–851.
Rocha, K.M., Perez-Straziota, C.E., Stulting, R.D., Randleman, J.B., 2014. Epithelial and stromal remodeling after corneal collagen cross-linking evaluated by spectral-domain OCT. J. Refract. Surg. 30, 122–127.
Rodriguez-Pomar, C., Pintor, J., Colligris, B., Carracedo, G., 2017. Therapeutic inhibitors for the treatment of dry eye syndrome. Expet Opin. Pharmacother. 18, 1855–1865.
Rosas Salaroli, C.H., Li, Y., Huang, D., 2009. High-resolution optical coherence tomography visualization of LASIK flap displacement. J. Cataract Refract. Surg. 35, 1640–1642.
Rossetto, J.D., Cavuoto, K.M., Allemann, N., McKeown, C.A., Capo, H., 2017. Accuracy of optical coherence tomography measurements of rectus muscle insertions in adult patients undergoing strabismus surgery. Am. J. Ophthalmol. 176, 236–243.
Sakata, L.M., Lavanya, R., Friedman, D.S., Aung, H.T., Seah, S.K., Foster, P.J., Aung, T., 2008. Assessment of the scleral spur in anterior segment optical coherence tomography images. Arch. Ophthalmol. 126, 181–185.
Sandali, O., El Sanharawi, M., Temstet, C., Hamiche, T., Galan, A., Ghouali, W., Goemaere, I., Basli, E., Borderie, V., Laroche, L., 2013. Fourier-domain optical coherence tomography imaging in keratoconus: a corneal structural classification. Ophthalmology 120, 2403–2412.
Sander, B., Al-Abiji, H.A., Kofod, M., Jorgensen, T.M., 2015. Do different spectral domain OCT hardwares measure the same? Comparison of retinal thickness using third-party software. Graefes Arch. Clin. Exp. Ophthalmol. 253, 1915–1921.
Sarunic, M.V., Asrani, S., Izatt, J.A., 2008. Imaging the ocular anterior segment with real-time, full-range Fourier-domain optical coherence tomography. Arch. Ophthalmol. 126, 537–542.
Sayed-Ahmed, I.O., Palioura, S., Galor, A., Karp, C.L., 2017. Diagnosis and medical management of ocular surface squamous neoplasia. Expet Rev. Ophthalmol. 12, 11–19.
Schmidl, D., Schmetterer, L., Garhofer, G., Popa-Cherecheanu, A., 2015a. Pharmacotherapy of glaucoma. J. Ocul. Pharmacol. Therapeut. 31, 63–77.
Schmidl, D., Schmetterer, L., Witkowska, K.J., Unterhuber, A., Aranha Dos Santos, V., Kaya, S., Nepp, J., Baar, C., Rosner, P., Werkmeister, R.M., Garhofer, G., 2015b. Tear film thickness after treatment with artificial tears in patients with moderate dry eye disease. Cornea 34, 421–426.
Schmidl, D., Werkmeister, R., Kaya, S., Unterhuber, A., Witkowska, K.J., Baumgartner, R., Holler, S., O'Rourke, M., Peterson, W., Wolter, A., Prinz, M., Schmetterer, L., Garhofer, G., 2017. A controlled, randomized double-blind study to evaluate the safety and efficacy of chitosan-N-acetylcysteine for the treatment of dry eye syndrome. J. Ocul. Pharmacol. Therapeut. 33, 375–382.
Schmidl, D., Witkowska, K.J., Kaya, S., Baar, C., Faatz, H., Nepp, J., Unterhuber, A., Werkmeister, R.M., Garhofer, G., Schmetterer, L., 2015c. The association between subjective and objective parameters for the assessment of dry-eye syndrome. Invest. Ophthalmol. Vis. Sci. 56, 1467–1472.
Scorcia, V., Busin, M., Lucisano, A., Beltz, J., Carta, A., Scorcia, G., 2013. Anterior segment optical coherence tomography-guided big-bubble technique. Ophthalmology 120, 471–476.
Sharma, S., Ang, M., Najjar, R.P., Sng, C., Cheung, C.Y., Rukmini, A.V., Schmetterer, L., Milea, D., 2017. Optical coherence tomography angiography in acute non-arteritic anterior ischaemic optic neuropathy. Br. J. Ophthalmol. 101, 1045–1051.
Shen, M., Li, J., Wang, J., Ma, H., Cai, C., Tao, A., Yuan, Y., Lu, F., 2009. Upper and lower tear menisci in the diagnosis of dry eye. Invest. Ophthalmol. Vis. Sci. 50, 2722–2726.
Shen, M., Wang, J., Tao, A., Chen, Q., Lin, S., Qu, J., Lu, F., 2008. Diurnal variation of upper and lower tear menisci. Am. J. Ophthalmol. 145, 801–806.
Shi, G., Wang, F., Li, X., Lu, J., Ding, Z., Sun, X., Jiang, C., Zhang, Y., 2012. Morphometric measurement of Schlemm's canal in normal human eye using anterior segment swept source optical coherence tomography. J. Biomed. Optic. 17 016016.
Shin, J.G., Hwang, H.S., Eom, T.J., Lee, B.H., 2017. *In vivo* three-dimensional imaging of human corneal nerves using Fourier-domain optical coherence tomography. J. Biomed. Optic. 22, 10501.
Shousha, M.A., Karp, C.L., Perez, V.L., Hoffmann, R., Ventura, R., Chang, V., Dubovy, S.R., Wang, J., 2011. Diagnosis and management of conjunctival and corneal intraepithelial neoplasia using ultra high-resolution optical coherence tomography. Ophthalmology 118, 1531–1537.
Siebelmann, S., Scholz, P., Sonnenschein, S., Bachmann, B., Matthaei, M., Cursiefen, C., Heindl, L.M., 2017. Anterior segment optical coherence tomography for the diagnosis of corneal dystrophies according to the IC3D classification. Surv. Ophthalmol (Epub).
Singh, M., Aung, T., Aquino, M.C., Chew, P.T., 2009a. Utility of bleb imaging with anterior segment optical coherence tomography in clinical decision-making after trabeculectomy. J. Glaucoma 18, 492–495.
Singh, M., Li, J., Han, Z., Raghunathan, R., Nair, A., Wu, C., Liu, C.H., Aglyamov, S., Twa, M.D., Larin, K.V., 2017a. Assessing the effects of riboflavin/UV-A crosslinking on porcine corneal mechanical anisotropy with optical coherence elastography. Biomed. Optic Express 8, 349–366.
Singh, M., Li, J., Han, Z., Wu, C., Aglyamov, S.R., Twa, M.D., Larin, K.V., 2016.

Investigating elastic anisotropy of the porcine cornea as a function of intraocular pressure with optical coherence elastography. J. Refract. Surg. 32, 562–567.
Singh, M., Li, J., Vantipalli, S., Han, Z., Larin, K.V., Twa, M.D., 2017b. Optical coherence elastography for evaluating customized riboflavin/UV-A corneal collagen cross-linking. J. Biomed. Optic. 22, 91504.
Singh, M., See, J.L., Aquino, M.C., Thean, L.S., Chew, P.T., 2009b. High-definition imaging of trabeculectomy blebs using spectral domain optical coherence tomography adapted for the anterior segment. Clin. Exp. Ophthalmol. 37, 345–351.
Sizmaz, S., Altan-Yaycioglu, R., Bakiner, O.S., Bozkirli, E., Coban-Karatas, M., Ulas, B., 2014. Assessment of tear meniscus with optical coherence tomography in thyroid-associated ophtalmopathy. Curr. Eye Res. 39, 323–328.
Skaat, A., Rosman, M.S., Chien, J.L., Ghassibi, M.P., Liebmann, J.M., Ritch, R., Park, S.C., 2017. Microarchitecture of Schlemm canal before and after selective laser trabeculoplasty in enhanced depth imaging optical coherence tomography. J. Glaucoma 26, 361–366.
Skaat, A., Rosman, M.S., Chien, J.L., Mogil, R.S., Ren, R., Liebmann, J.M., Ritch, R., Park, S.C., 2016. Effect of pilocarpine hydrochloride on the Schlemm canal in healthy eyes and eyes with open-angle glaucoma. JAMA Ophthalmol 134, 976–981.
Smith, S.D., Singh, K., Lin, S.C., Chen, P.P., Chen, T.C., Francis, B.A., Jampel, H.D., 2013. Evaluation of the anterior chamber angle in glaucoma: a report by the american academy of ophthalmology. Ophthalmology 120, 1985–1997.
Sng, C.C., Aquino, M.C., Liao, J., Ang, M., Zheng, C., Loon, S.C., Chew, P.T., 2014. Pretreatment anterior segment imaging during acute primary angle closure: insights into angle closure mechanisms in the acute phase. Ophthalmology 121, 119–125.
Sng, C.C., Aquino, M.C., Liao, J., Zheng, C., Ang, M., Chew, P.T., 2016. Anterior segment morphology after acute primary angle closure treatment: a randomised study comparing iridoplasty and medical therapy. Br. J. Ophthalmol. 100, 542–548.
Sng, C.C., Luengo Gimeno, F., Mehta, J.S., Htoon, H.M., Tan, D.T., 2012a. Intraoperative use of spectral-domain optical coherence tomography during Descemet's stripping automated endothelial keratoplasty. Clin. Ophthalmol. 6, 479–486.
Sng, C.C., Singh, M., Chew, P.T., Ngo, C.S., Zheng, C., Tun, T.A., See, J.L., Ang, M., Loon, S.C., Aung, T., 2012b. Quantitative assessment of changes in trabeculectomy blebs after laser suture lysis using anterior segment coherence tomography. J. Glaucoma 21, 313–317.
Song, S., Le, N.M., Huang, Z., Shen, T., Wang, R.K., 2015. Quantitative shear-wave optical coherence elastography with a programmable phased array ultrasound as the wave source. Opt. Lett. 40, 5007–5010.
Song, S., Wei, W., Hsieh, B.Y., Pelivanov, I., Shen, T.T., O'Donnell, M., Wang, R.K., 2016. Strategies to improve phase-stability of ultrafast swept source optical coherence tomography for single shot imaging of transient mechanical waves at 16 kHz frame rate. Appl. Phys. Lett. 108, 191104.
Spiteri, N., Romano, V., Zheng, Y., Yadav, S., Dwivedi, R., Chen, J., Ahmad, S., Willoughby, C.E., Kaye, S.B., 2015. Corneal angiography for guiding and evaluating fine-needle diathermy treatment of corneal neovascularization. Ophthalmology 122, 1079–1084.
Stamer, W.D., Acott, T.S., 2012. Current understanding of conventional outflow dysfunction in glaucoma. Curr. Opin. Ophthalmol. 23, 135–143.
Steven, P., Le Blanc, C., Lankenau, E., Krug, M., Oelckers, S., Heindl, L.M., Gehlsen, U., Huettmann, G., Cursiefen, C., 2014. Optimising deep anterior lamellar keratoplasty (DALK) using intraoperative online optical coherence tomography (iOCT). Br. J. Ophthalmol. 98, 900–904.
Steven, P., Le Blanc, C., Velten, K., Lankenau, E., Krug, M., Oelckers, S., Heindl, L.M., Gehlsen, U., Huttmann, G., Cursiefen, C., 2013. Optimizing descemet membrane endothelial keratoplasty using intraoperative optical coherence tomography. JAMA Ophthalmol 131, 1135–1142.
Su, J.P., Li, Y., Tang, M., Liu, L., Pechauer, A.D., Huang, D., Liu, G., 2015. Imaging the anterior eye with dynamic-focus swept-source optical coherence tomography. J. Biomed. Optic. 20, 126002.
Sung, Y., Park, J.S., Lew, H., 2017. Measurement of lacrimal punctum using spectralis domain anterior optical coherence tomography. Acta Ophthalmol. 95, e619–e624.
Szalai, E., Nemeth, G., Hassan, Z., Modis Jr., L., 2017. Noncontact evaluation of corneal grafts: swept-source fourier domain OCT versus high-resolution Scheimpflug imaging. Cornea 36, 434–439.
Tamm, E.R., 2009. The trabecular meshwork outflow pathways: structural and functional aspects. Exp. Eye Res. 88, 648–655.
Tan, A.C.S., Tan, G.S., Denniston, A.K., Keane, P.A., Ang, M., Milea, D., Chakravarthy, U., Cheung, C.M.G., 2018. An overview of the clinical applications of optical coherence tomography angiography. Eye 32, 262–286.
Tan, D.T., Dart, J.K., Holland, E.J., Kinoshita, S., 2012. Corneal transplantation. Lancet 379, 1749–1761.
Tay, E., Li, X., Chan, C., Tan, D.T., Mehta, J.S., 2012. Refractive lenticule extraction flap and stromal bed morphology assessment with anterior segment optical coherence tomography. J. Cataract Refract. Surg. 38, 1544–1551.
Timlin, H.M., Keane, P.A., Day, A.C., Salam, T., Abdullah, M., Rose, G.E., Ezra, D.G., 2016. Characterizing the lacrimal punctal region using anterior segment optical coherence tomography. Acta Ophthalmol. 94, 154–159.
Titiyal, J.S., Kaur, M., Falera, R., Jose, C.P., Sharma, N., 2016. Evaluation of time to donor lenticule apposition using intraoperative optical coherence tomography in descemet stripping automated endothelial keratoplasty. Cornea 35, 477–481.
Tsuda, S., Kunikata, H., Yamanari, M., Nakazawa, T., 2015. Association between histological findings and polarization-sensitive optical coherence tomography analysis of a post-trabeculectomy human eye. Clin. Exp. Ophthalmol. 43, 685–688.
Tun, T.A., Baskaran, M., Perera, S.A., Htoon, H.M., Aung, T., Husain, R., 2015. Swept-source optical coherence tomography assessment of iris-trabecular contact after phacoemulsification with or without goniosynechialysis in eyes with primary angle closure glaucoma. Br. J. Ophthalmol. 99, 927–931.
Tun, T.A., Baskaran, M., Tan, S.S., Perera, S.A., Aung, T., Husain, R., 2017. Evaluation of the anterior segment angle-to-angle scan of Cirrus high-definition optical coherence tomography and comparison with gonioscopy and with the visante OCT. Invest. Ophthalmol. Vis. Sci. 58, 59–64.
Tung, C.I., Kottaiyan, R., Koh, S., Wang, Q., Yoon, G., Zavislan, J.M., Davio, S.R., Aquavella, J.V., 2012. Noninvasive, objective, multimodal tear dynamics evaluation of 5 over-the-counter tear drops in a randomized controlled trial. Cornea 31, 108–114.
Tung, C.I., Perin, A.F., Gumus, K., Pflugfelder, S.C., 2014. Tear meniscus dimensions in tear dysfunction and their correlation with clinical parameters. Am. J. Ophthalmol. 157, 301–310 e301.
Uji, A., Muraoka, Y., Yoshimura, N., 2016. *In vivo* identification of the posttrabecular aqueous outflow pathway using swept-source optical coherence tomography. Invest. Ophthalmol. Vis. Sci. 57, 4162–4169.
Usui, T., Tomidokoro, A., Mishima, K., Mataki, N., Mayama, C., Honda, N., Amano, S., Araie, M., 2011. Identification of Schlemm's canal and its surrounding tissues by anterior segment fourier domain optical coherence tomography. Invest. Ophthalmol. Vis. Sci. 52, 6934–6939.
Venincasa, M.J., Osigian, C.J., Cavuoto, K.M., Rossetto, J.D., Capo, H., 2017. Combination of anterior segment optical coherence tomography modalities to improve accuracy of rectus muscle insertion location. J AAPOS 21, 243–246.
Veres, A., Tapaszto, B., Kosina-Hagyo, K., Somfai, G.M., Nemeth, J., 2011. Imaging lid-parallel conjunctival folds with OCT and comparing its grading with the slit lamp classification in dry eye patients and normal subjects. Invest. Ophthalmol. Vis. Sci. 52, 2945–2951.
Verma, S., Nongpiur, M.E., Oo, H.H., Atalay, E., Goh, D., Wong, T.T., Perera, S.A., Aung, T., 2017. Plateau Iris distribution across anterior segment optical coherence tomography defined subgroups of subjects with primary angle closure glaucoma. Invest. Ophthalmol. Vis. Sci. 58, 5093–5097.
Wang, B., Sakata, L.M., Friedman, D.S., Chan, Y.H., He, M., Lavanya, R., Wong, T.Y., Aung, T., 2010a. Quantitative iris parameters and association with narrow angles. Ophthalmology 117, 11–17.
Wang, F., Shi, G., Li, X., Lu, J., Ding, Z., Sun, X., Jiang, C., Zhang, Y., 2012a. Comparison of Schlemm's canal's biological parameters in primary open-angle glaucoma and normal human eyes with swept source optical. J. Biomed. Optic. 17, 116008.
Wang, J., Abou Shousha, M., Perez, V.L., Karp, C.L., Yoo, S.H., Shen, M., Cui, L., Hurmeric, V., Du, C., Zhu, D., Chen, Q., Li, M., 2011. Ultra-high resolution optical coherence tomography for imaging the anterior segment of the eye. Ophthalmic Surg. Laser. Imag. 42 (Suppl. l), S15–S27.
Wang, J., Aquavella, J., Palakuru, J., Chung, S., 2006a. Repeated measurements of dynamic tear distribution on the ocular surface after instillation of artificial tears. Invest. Ophthalmol. Vis. Sci. 47, 3325–3329.
Wang, J., Aquavella, J., Palakuru, J., Chung, S., Feng, C., 2006b. Relationships between central tear film thickness and tear menisci of the upper and lower eyelids. Invest. Ophthalmol. Vis. Sci. 47, 4349–4355.
Wang, J., Cui, L., Shen, M., Perez, V.L., Wang, M.R., 2012b. Ultra-high resolution optical coherence tomography for monitoring tear meniscus volume in dry eye after topical cyclosporine treatment. Clin. Ophthalmol. 6, 933–938.
Wang, J., Fonn, D., Simpson, T.L., Jones, L., 2003. Precorneal and pre- and postlens tear film thickness measured indirectly with optical coherence tomography. Invest. Ophthalmol. Vis. Sci. 44, 2524–2528.
Wang, Y., Zhuang, H., Xu, J., Wang, X., Jiang, C., Sun, X., 2010b. Dynamic changes in the lower tear meniscus after instillation of artificial tears. Cornea 29, 404–408.
Watson, P.G., 1987. Anterior segment fluorescein angiography in the surgery of immunologically induced corneal and scleral destructive disorders. Ophthalmology 94, 1452–1464.
Watson, P.G., Bovey, E., 1985. Anterior segment fluorescein angiography in the diagnosis of scleral inflammation. Ophthalmology 92, 1–11.
Wawrzynski, J.R., Smith, J., Sharma, A., Saleh, G.M., 2014. Optical coherence tomography imaging of the proximal lacrimal system. Orbit 33, 428–432.
Wecker, T., Anton, A., Neuburger, M., Jordan, J.F., van Oterendorp, C., 2017. Trabeculotomy opening size and IOP reduction after Trabectome(R) surgery. Graefes Arch. Clin. Exp. Ophthalmol. 255, 1643–1650.
Werkmeister, R.M. (Ed.), 2016. Uhr-oct in Glaucoma and PEX, European Association for Vision and Eye Research Annual Meeting, Nice, France.
Werkmeister, R.M., Alex, A., Kaya, S., Unterhuber, A., Hofer, B., Riedl, J., Bronhagl, M., Vietauer, M., Schmidl, D., Schmoll, T., Garhofer, G., Drexler, W., Leitgeb, R.A., Groeschl, M., Schmetterer, L., 2013. Measurement of tear film thickness using ultrahigh-resolution optical coherence tomography. Invest. Ophthalmol. Vis. Sci. 54, 5578–5583.
Werkmeister, R.M., Sapeta, S., Schmidl, D., Garhöfer, G., Schmetterer, L., 2017a. Ultrahigh-resolution OCT imaging of the anterior eye segment. In: ARVO 2017 Annual Meeting, Baltimore, Maryland.
Werkmeister, R.M., Sapeta, S., Schmidl, D., Garhofer, G., Schmidinger, G., Aranha Dos Santos, V., Aschinger, G.C., Baumgartner, I., Pircher, N., Schwarzhans, F., Pantalon, A., Dua, H., Schmetterer, L., 2017b. Ultrahigh-resolution OCT imaging of the human cornea. Biomed. Optic Express 8, 1221–1239.
Whitcher, J.P., Srinivasan, M., Upadhyay, M.P., 2001. Corneal blindness: a global perspective. Bull. World Health Organ. 79, 214–221.
Wozniak, P.A., Schmidl, D., Bata, A.M., Fondi, K., Witkowska, K.J., Aranha Dos Santos, V., Baar, C., Room, K.I., Nepp, J., Baumgartner, I., Popa-Cherecheanu, A., Garhofer, G., Werkmeister, R.M., Schmetterer, L., 2017. Effect of different lubricant eye gels on tear film thickness as measured with ultrahigh-resolution optical coherence tomography. Acta Ophthalmol. 95, e307–e313.
Wu, S., Tao, A., Jiang, H., Xu, Z., Perez, V., Wang, J., 2014. Vertical and horizontal corneal epithelial thickness profile using ultra-high resolution and long scan depth

optical coherence tomography. PLoS One 9 e97962.
Wylegala, A., Teper, S., Dobrowolski, D., Wylegala, E., 2016. Optical coherence angiography: a review. Medicine (Baltim.) 95 e4907.
Xin, C., Chen, X., Li, M., Shi, Y., Wang, H., Wang, R., Wang, N., 2017. Imaging collector channel entrance with a new intraocular micro-probe swept-source optical coherence tomography. Acta Ophthalmol. 95, 602–607.
Xin, C., Johnstone, M., Wang, N., Wang, R.K., 2016. OCT study of mechanical properties associated with trabecular meshwork and collector channel motion in human eyes. PLoS One 11 e0162048.
Xu, B.Y., Israelsen, P., Pan, B.X., Wang, D., Jiang, X., Varma, R., 2016. Benefit of measuring anterior segment structures using an increased number of optical coherence tomography images: the Chinese american eye study. Invest. Ophthalmol. Vis. Sci. 57, 6313–6319.
Xu, Y., Liu, J., Cheng, J., Lee, B.H., Wong, D.W., Baskaran, M., Perera, S., Aung, T., 2013. Automated anterior chamber angle localization and glaucoma type classification in OCT images. Conf Proc IEEE Eng Med Biol Soc 2013, 7380–7383.
Yadav, R., Lee, K.S., Rolland, J.P., Zavislan, J.M., Aquavella, J.V., Yoon, G., 2011. Micrometer axial resolution OCT for corneal imaging. Biomed. Optic Express 2, 3037–3046.
Yamanari, M., Makita, S., Yasuno, Y., 2008. Polarization-sensitive swept-source optical coherence tomography with continuous source polarization modulation. Optic Express 16, 5892–5906.
Yamanari, M., Nagase, S., Fukuda, S., Ishii, K., Tanaka, R., Yasui, T., Oshika, T., Miura, M., Yasuno, Y., 2014. Scleral birefringence as measured by polarization-sensitive optical coherence tomography and ocular biometric parameters of human eyes *in vivo*. Biomed. Optic Express 5, 1391–1402.
Yamanari, M., Tsuda, S., Kokubun, T., Shiga, Y., Omodaka, K., Aizawa, N., Yokoyama, Y., Himori, N., Kunimatsu-Sanuki, S., Maruyama, K., Kunikata, H., Nakazawa, T., 2016. Estimation of Jones matrix, birefringence and entropy using Cloude-Pottier decomposition in polarization-sensitive optical coherence tomography. Biomed. Optic Express 7, 3551–3573.
Yamanari, M., Tsuda, S., Kokubun, T., Shiga, Y., Omodaka, K., Yokoyama, Y., Himori, N., Ryu, M., Kunimatsu-Sanuki, S., Takahashi, H., Maruyama, K., Kunikata, H., Nakazawa, T., 2015. Fiber-based polarization-sensitive OCT for birefringence imaging of the anterior eye segment. Biomed. Optic Express 6, 369–389.
Yasuno, Y., Yamanari, M., Kawana, K., Miura, M., Fukuda, S., Makita, S., Sakai, S., Oshika, T., 2010. Visibility of trabecular meshwork by standard and polarization-sensitive optical coherence tomography. J. Biomed. Optic. 15 061705.
Yasuno, Y., Yamanari, M., Kawana, K., Oshika, T., Miura, M., 2009. Investigation of post-glaucoma-surgery structures by three-dimensional and polarization sensitive anterior eye segment optical coherence tomography. Optic Express 17, 3980–3996.
Yeh, R.Y., Quilendrino, R., Musa, F.U., Liarakos, V.S., Dapena, I., Melles, G.R., 2013. Predictive value of optical coherence tomography in graft attachment after Descemet's membrane endothelial keratoplasty. Ophthalmology 120, 240–245.
Yoo, Y.S., Na, K.S., Byun, Y.S., Shin, J.G., Lee, B.H., Yoon, G., Eom, T.J., Joo, C.K., 2017. Examination of gland dropout detected on infrared meibography by using optical coherence tomography meibography. Ocul. Surf. 15, 130–138 e131.
Zaitsev, V.Y., Matveyev, A.L., Matveev, L.A., Gelikonov, G.V., Omelchenko, A.I., Baum, O.I., Avetisov, S.E., Bolshunov, A.V., Siplivy, V.I., Shabanov, D.V., Vitkin, A., Sobol, E.N., 2017. Optical coherence elastography for strain dynamics measurements in laser correction of cornea shape. J. Biophot. 10, 1450–1463.
Zarei-Ghanavati, S., Betancurt, C., Mas, A.M., Wang, J., Perez, V.L., 2015. Ultra high resolution optical coherence tomography in Boston type I keratoprosthesis. J. Ophthalmic Vis. Res. 10, 26–32.
Zhang, A., Zhang, Q., Chen, C.L., Wang, R.K., 2015a. Methods and algorithms for optical coherence tomography-based angiography: a review and comparison. J. Biomed. Optic. 20, 100901.
Zhang, Y., Li, S.Z., Li, L., He, M.G., Thomas, R., Wang, N.L., 2015b. Quantitative analysis of iris changes following mydriasis in subjects with different mechanisms of angle closure. Invest. Ophthalmol. Vis. Sci. 56, 563–570.
Zhao, Z., Zhu, X., He, W., Jiang, C., Lu, Y., 2016. Schlemm's canal expansion after uncomplicated phacoemulsification surgery: an optical coherence tomography study. Invest. Ophthalmol. Vis. Sci. 57, 6507–6512.
Zheng, X., Kamao, T., Yamaguchi, M., Sakane, Y., Goto, T., Inoue, Y., Shiraishi, A., Ohashi, Y., 2014. New method for evaluation of early phase tear clearance by anterior segment optical coherence tomography. Acta Ophthalmol. 92, e105–111.
Zhi, Z., Qin, W., Wang, J., Wei, W., Wang, R.K., 2015. 4D optical coherence tomography-based micro-angiography achieved by 1.6-MHz FDML swept source. Opt. Lett. 40, 1779–1782.
Zinkernagel, M.S., Wolf, S., Ebneter, A., 2016. Fluctuations in pigment epithelial detachment and retinal fluid using a bimonthly treatment regimen with aflibercept for neovascular age-related macular degeneration. Ophthalmologica 235, 42–48.